Master's thesis

NTNU
Norwegian University of Science and Technology
Faculty of Natural Sciences
Department of Materials Science and Engineering

Frederick Andre Wessel

Modeling of Galvanic Corrosion - in Presence of External Direct and Alternating Currents

Master's thesis in Materials Science and Engineering
Supervisor: Andreas Erbe
Co-supervisor: Martin Høyer-Hansen and Ivana Jevremovic
June 2022

NTNU
Norwegian University of
Science and Technology

Frederick Andre Wessel

Modeling of Galvanic Corrosion - in Presence of External Direct and Alternating Currents

Master's thesis in Materials Science and Engineering
Supervisor: Andreas Erbe
Co-supervisor: Martin Høyer-Hansen and Ivana Jevremovic
June 2022

Norwegian University of Science and Technology
Faculty of Natural Sciences
Department of Materials Science and Engineering

NTNU
Norwegian University of
Science and Technology

Preface

This master's thesis has been written as part of the course "TMT4905 - Materials Technology, Master's Thesis" at the Department of Materials Science and Engineering, NTNU. In this work, the modeling has been performed at KII, and the supplementary experimental work has been carried out at the corrosion lab in KII, both during the spring of 2022.

I would like to thank my supervisor Professor Andreas Erbe at the Department of Materials Science and Engineering (NTNU) for good guidance and interesting discussions, and for always answering my questions. Thank you to my co-supervisors, Martin Høyer-Hansen at Sintef Energy and Ivana Jevremovic at Sintef Industry, for helpful meetings and for giving me inspiration on how to approach the modeling. They also contributed with relevant reports and articles on the subject, which I am thankful for.

My gratitude goes to Staff Engineers Anita Storsve and Marthe Folstad for technical assistance at the laboratory. A special thanks goes to Iman Taji for allowing me to use the modeling software (COMSOL Multiphysics®), which was only available at his office. Without his flexibility, I would not have been able to finish the modeling work.

Finally, I would like to thank Yuan Lin at COMSOL for helping with the modeling issues I encountered. She has been a reliable source for me when the model solution would not converge, or when I got counter-intuitive results.

Abstract

Field observations have shown that the corrosion rates of ships connected to onshore power increases. One possible explanation is the formation of a galvanic couple between the coating defects in the ship's hull (carbon steel) and the ground electrode (copper) in seawater. Since large ships and cruise-liners are usually protected by an impressed current cathodic protection (ICCP) system, the steel-copper couple is supplied with external currents to avoid corrosion. Because of the presence of electric power systems and high-voltage AC power transmission lines near the docked ship, alternating currents (AC) can interfere with both the ICCP system and the steel-copper couple. This results in the risk of AC-assisted galvanic corrosion, which is the subject of this thesis.

A model was developed in COMSOL Multiphysics® to study AC corrosion on a steel-copper couple by solving the Nernst-Planck equation in two dimensions (2D) using the finite element method (FEM). Two different inert anodes were investigated: platinum (for use in validation experiments) and a mixed metal oxide (MMO) anode (typical for ICCP systems). Modeling was performed on a simple 2D geometry, and a current distribution that accounts for continuous changes in a water-based electrolyte was utilized. Supplemental laboratory work were performed to obtain relevant parameters that were used as inputs to the model, such as exchange current densities and Tafel slopes. When gathering the model results, parametric sweeps were performed by varying the double layer capacitance, frequency, and steel/copper area ratio, in addition to varying the AC and DC magnitudes. Initially, the double layer capacitance, frequency, and steel/copper area ratio were set to 0.1 F/m^2 at each electrode, 50 Hz and 1, respectively.

The computational results revealed that by applying AC to a galvanic couple of steel and copper, both the potential and the corrosion rate of the steel generally increased. It was found that application of a current AC_{rms} = 20 mA to the cathodically protected steel-copper pair was acceptable, corresponding to an AC current density of 12.5 A/m^2. However, it was found that an AC of 50 mA (31.25 A/m^2) was unacceptable, resulting in a corrosion rate of about 4 mm/year. The considerably higher corrosion rates at elevated AC levels were attributed to oversimplified dissolution reactions and a lack of chemical reactions (e.g., formation of corrosion products and precipitates) in the modeling.

In particular, the double layer capacitance significantly affected the corrosion of carbon steel. It was found that increasing the double layer capacitance also increased the protection of carbon steel. At a capacitance value of 0.2 F/m^2, the steel was protected from corrosion at an AC_{rms} = 50 mA. Further increasing the double layer capacitance, up to 0.7 F/m^2, showed that the steel was protected at an AC_{rms} = 200 mA (125 A/m^2). The strong influence of the double layer capacitance on the protection of carbon steel was supported by the literature and explained by increased capacitive charge storage induced by AC. The steel corrosion rate at high ACs increased when the copper was isolated from the system, as the AC current density on the steel increased because of the halving of the total surface area.

Sammendrag

Det har blitt observert økte korrosjonsrater på skip koblet til landstrøm. En mulig forklaring er dannelsen av en galvanisk kobling mellom defekter i malingsbelegget på skipsskroget (karbonstål) og jordingsanlegget på land (kobber) i sjøvann. Ettersom store skip typisk er beskyttet av et ICCP-anlegg, vil ytre strømmer kunne påvirke koblingen mellom stål og kobber. I nærvær av kraftsystemer og høyspentlinjer på land vil det i tillegg kunne oppstå interferens, slik at AC blir tilført stål-kobber koblingen. Dette vil kunne føre til AC-assistert galvanisk korrosjon på skroget, noe som er temaet i denne oppgaven.

En modell har blitt utviklet i COMSOL Multiphysics® for å undersøke AC korrosjon på en stål-kobber kobling ved å løse Nernst-Planck likningen i to dimensjoner ved hjelp av FEM. To ulike inerte anoder ble undersøkt: platina (for å validere modellen eksperimentelt) og MMO anode (typisk for ICCP-anlegg). Modelleringen ble gjennomført på en enkel 2D geometri, og det ble brukt en strømfordeling som tar høyde for kontinuerlige endringer i sjøvannet. Laboratoriearbeid ble gjennomført for å innhente data for bruk i modellen, slik som utviklingsstrømtettheter og Tafel-helninger. Resultatene fra modellen ble innhentet ved hjelp av parametersveip, der kapasitansen (til det elektriske dobbeltlaget), frekvensen, og arealforholdet mellom stål og kobber ble variert, i tillegg til å variere størrelsen på AC og DC som ble påført systemet. Innledningsvis ble henholdsvis kapasitansen, frekvensen og arealforholdet satt lik 0.1 $\mathrm{F/m^2}$, 50 Hz og 1.

Resultatene fra modellen viste at både potensialet og korrosjonsraten til stålet økte når AC ble påført stål-kobber koblingen. Det ble funnet at en $\mathrm{AC_{rms}}$ på 20 mA sendt til den katodisk beskyttede koblingen medførte at stålet ble tilstrekkelig beskytta. Dette tilsvarte en AC strømtetthet på 12.5 $\mathrm{A/m^2}$. Å øke $\mathrm{AC_{rms}}$ til 50 mA (31.25 $\mathrm{A/m^2}$) var derimot ikke akseptabelt, ettersom dette medførte en korrosjonsrate på omtrent 4 mm/år. De vesentlig høye korrosjonsratene ved høy AC ble forklart ved at oppløsningsreaksjonen i modellen var noe forenklet, samt at modellen manglet relevante kjemiske reaksjoner (slik som dannelse av korrosjonsprodukter og presipitater).

Det ble funnet at særlig kapasitansen til det elektriske dobbeltlaget påvirket korrosjonsraten på karbonstålet. En økende kapasitans medførte at stålet ble bedre beskyttet mot korrosjon. Ved en kapasitansverdi på 0.2 $\mathrm{F/m^2}$ ble det funnet at stålet var beskyttet ved 50 mA $\mathrm{AC_{rms}}$. Ytterligere økning av kapasitansen, opp til 0.7 $\mathrm{F/m^2}$, medførte at stålet ble beskyttet helt opp til en $\mathrm{AC_{rms}}$ på 200 mA (125 $\mathrm{A/m^2}$). Den kraftige innflytelsen kapasitansen hadde på beskyttelsen av stålet ble bekreftet ved hjelp av litteratur, samt forklart ved at kapasitansens lagringskapasitet økte. Korrosjonsraten til stål (ved høy AC) økte dersom kobber ble isolert fra systemet, ettersom AC strømtettheten på stålet økte siden totalarealet ble halvert.

List of Abbreviations

α	Charge-transfer coefficient
η	Overpotential
b_a	Anodic Tafel slope
b_c	Cathodic Tafel slope
C_{dl}	Double layer capacitance
D	Diffusion coefficient
E_0	Standard reduction potential
E_{rev}	Reversible potential
f	Frequency
i	Current density
i_0	Exchange current density
i_{lim}	Limiting current density
s	Standard deviation
z	Number of electrons transferred per mole of reaction
AC	Alternating current
$\mathbf{AC_{rms}}$	Root mean square value of AC
Ag/AgCl	Silver/silver chloride reference electrode
B-V	Butler-Volmer equation
BEM	Boundary element method
CER	Chlorine evolution reaction
Cu	Copper
DC	Direct current
EDL	Electrical double layer
HER	Hydrogen evolution reaction
ICCP	Impressed current cathodic protection
MMO	Mixed metal oxide
OCP	Open circuit potential
OER	Oxygen evolution reaction
ORR	Oxygen reduction reaction
Pt	Platinum

Table of Contents

List of Figures

List of Tables

1 Introduction

1.1 Background and motivation

This work is inspired from the ongoing "ElMar"-project at SINTEF. It involves the use of onshore power for supplying ships with electricity when docked. By connecting the ships to onshore power, energy efficiency can be increased and emissions can be reduced, as compared to the use of diesel generators on board [1]. According to Parise et al. [2], supplying ships with onshore power when docked could reduce the emissions of NO_x and CO_2 by 50%, and SO_x by 90%. Reduction of greenhouse gas (GHG) emissions in the transport sector is of great importance, both internationally and nationally. The European Union intends to reduce GHG emissions in the European transport sector by at least 60% by 2050 compared with 1990 levels [3]. Similarly, the Norwegian government is targeting zero GHG emissions in the Norwegian transport and maritime sector by 2050 [4].

Field observations have suggested that the corrosion rate on hull of ships increases when ships are supplied with onshore power. When a ship is supplied with onshore power, there will be an electrical connection between the ship and the grounding system on land. As they are exposed to the same electrolyte (seawater), this creates a galvanic couple between the ground electrode and the ship hull. A typical ship hull material is carbon steel, and by considering the ground electrode as a copper electrode [5], a steel-copper galvanic couple will be formed. Since copper is more noble than steel, the steel will sacrifice itself to protect the copper, meaning the corrosion rate on the steel increases.

Today, the majority of ships worldwide have a cathodic protection system installed, in addition to being coated. For large ships and cruise-liners, the most common form of protection system is impressed current cathodic protection (ICCP) [5]. Despite being coated initially, some parts of the coating could break down or deteriorate, exposing the carbon steel to seawater. These parts are susceptible to corrosion. When connected to onshore power, the ship ICCP system has to protect both the exposed carbon steel as well as the copper in the grounding system. Hence, a possible explanation for the observed increase in corrosion could be that the needed protection current exceeds the supply limit for the ICCP system. Furthermore, the connection between the ship and the ground network could cause unwanted interference with the electric power systems near the quay. The interference could mean that alternating currents from high-voltage AC power transmission lines interfere with the ICCP system on the ship, affecting the overall protection of the ship [6].

1.2 Aim and scope of the work

The goal of this work is to investigate the effect of direct and alternating currents impressed to a steel-copper galvanic couple in seawater. As the effect of direct currents has been studied previously [7], the effect of alternating currents on the galvanic couple will be emphasized in this work. The effect of different inert anodes will also be investigated.

Finite element modeling in COMSOL Multiphysics® will be carried out for this purpose [8]. For simplicity reasons, the model will be limited to a simple geometry in two dimensions. Kinetics, diffusion, and migration will be included in the model, where the goal is to solve the Nernst-Planck equation. Furthermore, the effect of parameters such as double layer capacitance, frequency, and the steel/copper area ratio on the AC corrosion of steel in the galvanic couple will be investigated. Laboratory work will supplement the modeling, by obtaining relevant parameters and by verifying the trends of the modeling results.

2 Theory and literature

2.1 Electrochemical reactions and kinetics

A reaction between chemical species involving electron-transfer is called an electrochemical reaction. The reduction potential of an electrochemical reaction or half-reaction, sometimes referred to as the reversible potential E_{rev}, can be calculated using the Nernst equation:

$$E_{\text{rev}} = E_0 - \frac{\text{R}T}{z\text{F}} \ln\left(\frac{\prod^i (a_i^{\nu_i})}{\prod^j (a_j^{\nu_j})}\right). \tag{1}$$

Here, E_0 is the standard reduction potential of the reaction, R is the gas constant, T is the temperature, z is the number of electrons per reaction or half-reaction, and F is the Faraday constant. The activities a of the products i and reactants j are raised to the power of their stoichiometric coefficient, ν_i and ν_j respectively. Assuming an activity coefficient equal to 1, the activity of aqueous species is equal to its concentration divided by the reference concentration of 1 mol/L. For dissolution of gases in water, the reference concentration is its solubility. This can be further clarified by considering the oxygen reduction reaction (ORR) in alkaline solution:

$$\text{O}_2 + 2\text{H}_2\text{O} + 4\text{e}^- \longrightarrow 4\text{OH}^-. \tag{2}$$

By assuming that the activities equal the concentrations, and stating the concentrations c in mol/L, the reversible reduction potential can be expressed as

$$E_{\text{rev}} = E_0 - \frac{\text{R}T}{4\text{F}} \ln\left(\frac{c_{\text{OH}^-}^4}{(c_{\text{O}_2}/c_{\text{O}_2,\text{sol}})}\right), \tag{3}$$

with E_0 of this reaction equal to 0.401 V vs. the standard hydrogen electrode (SHE), or 0.204 V vs. Ag/AgCl/saturated KCl at $T = 298$K. The solubility of oxygen in water is denoted as $c_{\text{O}_2,\text{sol}}$. For the hydrogen evolution reaction (HER) in alkaline solution,

$$2\text{H}_2\text{O} + 2\text{e}^- \longrightarrow \text{H}_2 + 2\text{OH}^-, \tag{4}$$

the reduction potential is

$$E_{\text{rev}} = E_0 - \frac{\text{R}T}{2\text{F}} \ln\left(c_{\text{OH}^-}^2 \cdot (c_{\text{H}_2}/c_{\text{H}_2,\text{sol}})\right). \tag{5}$$

E_0 for HER in alkaline solution is equal to -1.025 V vs. Ag/AgCl/saturated KCl. The activation overpotential η for a half-reaction is a measure on the potential difference between the experimental reduction potential E and the theoretical reduction potential E_{rev} [9]:

$$\eta = E - E_{\text{rev}}. \tag{6}$$

This is equivalent to the activation energy of the electrode reaction, and is non-zero for reactions at polarizable electrodes due to the reaction occurring at a finite rate. Ideal non-polarizable electrodes yield an activation potential of zero, meaning that the electrode reaction is infinitely fast. However, this is difficult in practice [10]. The Butler-Volmer (B-V) equation relates the overpotential η to the electrolyte current density i_l:

$$i_l = i_0 \left[\exp\left(\frac{\alpha_a z\text{F}}{\text{R}T}\eta\right) - \exp\left(-\frac{\alpha_c z\text{F}}{\text{R}T}\eta\right)\right], \tag{7}$$

neglecting the concentration difference between the electrode surface and the bulk. α_a and α_c represent the anodic and cathodic charge-transfer coefficient, respectively. i_0 denotes the

exchange current density, which can be found explicitly for each reaction at an electrode. i_0 is dependent on other parameters such as the electrolyte composition and temperature. For a general, one-electron transfer,

$$O + \mathrm{e}^- \rightleftharpoons R, \tag{8}$$

the concentration dependence of the exchange current density can be expressed as [9]:

$$i_0 = \mathrm{F}k_0(c_O^{\alpha_a} c_R^{\alpha_c}). \tag{9}$$

Here, c_O and c_R are the bulk concentrations of the species O and R, respectively. The equation also shows that i_0 is proportional to the rate constant k_0. Thus, if i_0 is found experimentally in a given environment with concentrations c_{ref} for species O and R, the i_0 corresponding to the new concentrations c_{new} can be expressed:

$$i_{0,rd}(c_{\mathrm{new}}) = \left(\frac{c_{O,\mathrm{new}}}{c_{O,\mathrm{ref}}}\right)^{\Omega_{O,rd}} \left(\frac{c_{R,\mathrm{new}}}{c_{R,\mathrm{ref}}}\right)^{\Omega_{R,rd}} i_{0,rd}(c_{\mathrm{ref}}) \tag{10}$$

for a reduction reaction. The exponents $\Omega_{O,rd}$ and $\Omega_{R,rd}$ refer to the reaction order of the reactant O and product R, respectively. The same concept applies for an oxidation reaction as well, denoting the reaction orders as $\Omega_{O,ox}$ and $\Omega_{R,ox}$:

$$i_{0,ox}(c_{\mathrm{new}}) = \left(\frac{c_{O,\mathrm{new}}}{c_{O,\mathrm{ref}}}\right)^{\Omega_{O,ox}} \left(\frac{c_{R,\mathrm{new}}}{c_{R,\mathrm{ref}}}\right)^{\Omega_{R,ox}} i_{0,ox}(c_{\mathrm{ref}}). \tag{11}$$

For the general, one-electron transfer reaction (8), the reaction orders are equal to the charge transfer coefficients [11]:

$$\Omega_{R,rd} = \frac{\partial \ln(|i_{l,rd}|)}{\partial \ln(c_R)} = \alpha_c, \tag{12}$$

$$\Omega_{O,rd} = \frac{\partial \ln(|i_{l,rd}|)}{\partial \ln(c_O)} = \alpha_a. \tag{13}$$

However, if the reaction mechanism is unknown, and perhaps more than one electron is transferred, the reaction order must be determined experimentally.

For sufficiently large and positive overpotentials, $\eta \gg 0$, the second term of the Butler-Volmer equation becomes insignificant, giving

$$i_l = i_0 \cdot \exp\left(\frac{\alpha z \mathrm{F}}{\mathrm{R}T}\eta\right). \tag{14}$$

Rewritten, this gives the anodic Tafel equation:

$$\eta = b_a \cdot \log_{10}\left(\frac{i_l}{i_0}\right). \tag{15}$$

Tafel predicts, for large positive η, a positive linear relationship between the overpotential and the logarithm of the current density i. The slope, often referred to as the anodic Tafel slope, denoted b_a, can be expressed as

$$b_a = \frac{\mathrm{R}T\ln(10)}{\alpha_a z \mathrm{F}}. \tag{16}$$

Similarly, for sufficiently large and negative overpotentials, $\eta \ll 0$, the first term of the Butler-Volmer equation can be neglected. This gives the cathodic Tafel equation

$$\eta = b_c \cdot \log_{10}\left(\frac{|i_l|}{i_0}\right), \tag{17}$$

with a slope b_c, referred to as the cathodic Tafel slope, equal to

$$b_c = -\frac{\mathrm{R}T\ln(10)}{\alpha_c z\mathrm{F}}. \tag{18}$$

The anodic and cathodic Tafel equations provide a simple relationship between current and potential. Thus, these equations are commonly utilized when working with current distribution problems [12]. Some reactions have mass-transfer limitations, which causes an upper limit for the current density. The ORR is an example, where the supply of reactant (O_2) could be inadequate [13]. Generally, the diffusion-limiting current density can be described as

$$i_{\mathrm{lim}} = \frac{z\mathrm{F}Dc_\infty}{\delta}. \tag{19}$$

Here, D is the diffusion coefficient of the specie, c_∞ is the bulk concentration of the specie and δ is the Nernst diffusion layer thickness. It should be noted that this only holds when the diffusion is the dominant mass-transport mechanism. For an oxidation reaction occurring at a high overpotential, $\eta \gg 0$, the partial current density of a reaction at an electrode surface can be expressed as

$$i_l = \frac{i_{\mathrm{Tafel}}}{1 + \frac{i_{\mathrm{Tafel}}}{i_{\mathrm{lim}}}}, \tag{20}$$

where i_{Tafel} is the current density according to the anodic Tafel equation, stated in equation (14). When the partial current density calculated from equation (14) is much lower than the limiting current density, the term $i_{\mathrm{Tafel}}/i_{\mathrm{lim}}$ approaches 0, such that the anodic Tafel equation holds:

$$i_l = \frac{i_{\mathrm{Tafel}}}{1 + \frac{i_{\mathrm{Tafel}}}{i_{\mathrm{lim}}}} \approx i_{\mathrm{Tafel}} = i_0 \cdot \exp\left(\frac{\alpha z\mathrm{F}}{\mathrm{R}T}\eta\right). \tag{21}$$

2.2 Transport

In electrochemistry, transport of species due to concentration gradients in the solution is referred to as diffusion. According to Fick's first law, species will diffuse from a high-concentration region to a low-concentration region:

$$N_{i,\mathrm{dif}} = -D_i \cdot \nabla c_i. \tag{22}$$

Here, $N_{i,\mathrm{dif}}$ is the diffusion-flux density of specie i, D is the diffusion coefficient and ∇c is the concentration gradient. The diffusion coefficients of different species can be found in literature, and depend on factors such as temperature and type of solvent. Due to electrochemical reactions, there will also be a potential gradient in the solution. When an electric field is present, the negatively charged species will move to the positive side of the electric field, and vice versa. The motion of charged species due to an electric field is called migration:

$$N_{i,\mathrm{mig}} = -z_i u_i \mathrm{F} c_i \nabla \Phi_l, \tag{23}$$

where $N_{i,\mathrm{mig}}$ is the migration-flux density of specie i. Φ_l is here the electrolyte potential, and the gradient, $\nabla\Phi_l$, is the negative of the electric field. The migration-flux density is also dependent on the parameter u, called the mobility, which relates the velocity of the specie in response to an electric field. Mobility relates migration to diffusion, through the Nernst-Einstein relation [12]:

$$u_i = \frac{D_i}{\mathrm{k_B}T}. \tag{24}$$

In this equation, $\mathrm{k_B}$ is the Boltzmann constant. There is also transport by convection, which is due to bulk motion of the fluid in the solution. The convection can be expressed as

$$N_{i,\mathrm{con}} = c_i v, \tag{25}$$

with v being the bulk velocity of the fluid. By neglecting convection, the total flux density of specie i can be described by the Nernst-Planck equation for infinitely dilute solutions:

$$N_i = N_{i,\text{mig}} + N_{i,\text{dif}} = -z_i u_i \text{F} c_i \nabla \Phi_l - D_i \nabla c_i. \tag{26}$$

For a time-dependent study, the continuity equation can be expressed as

$$\frac{\partial c_i}{\partial t} + \nabla N_i = R_i, \tag{27}$$

where the first term considers the change in concentration of specie i with time. R_i represents the net volumetric source for the concentration c_i. Equation (27) can also be viewed as a material balance for a small-volume element. In most electrochemical systems, R_i is zero, except at the electrode surfaces [12]. The motion of charged species gives rise to an electrolyte current density, which is equal to the sum of the flux density times the charge for each specie:

$$i_l = \text{F} \sum_i z_i N_i. \tag{28}$$

For a secondary current distribution, it is assumed that there are no concentration variances in the solution, i.e. a constant electrolyte composition. This assumption suggests there are no concentration gradients, and therefore no diffusion either. In this case, only the migration-term is left of the overall flux density, and one ends up with

$$i_l = -\kappa \nabla \Phi_l, \tag{29}$$

with the electrolyte conductivity κ defined as

$$\kappa = \text{F}^2 \sum_i z_i^2 u_i c_i. \tag{30}$$

However, if there are concentration variances in the solution, the result gets slightly more complicated:

$$i_l = i_{l,\text{dif}} + i_{l,\text{mig}} = \text{F} \sum_i z_i (-D_i \nabla c_i - z_i u_i \text{F} c_i \nabla \Phi_l). \tag{31}$$

Here, the diffusion-term cannot be neglected when inserting the overall flux density into equation (28). Given that the electroneutrality condition,

$$\sum_i z_i c_i = 0, \tag{32}$$

is obeyed, it can be seen that equation (31) holds for all systems, even if convection is present:

$$i_{l,\text{con}} = \text{F} \sum_i z_i N_{i,\text{con}} = \text{F} v \sum_i z_i c_i = 0. \tag{33}$$

Similarly as the electrolyte current density i_l, the electrode current density i_s can be expressed:

$$i_s = -\sigma \nabla \Phi_s, \tag{34}$$

where σ is the conductivity of the electrode, typically some orders of magnitude greater than the electrolyte conductivity κ. Φ_s is the electric potential of the solid phase. Thus, the potential E is the difference between Φ_s and Φ_l, which can be used to define the overpotential η as

$$\eta = \Phi_s - \Phi_l - E_{\text{rev}}. \tag{35}$$

In a problem involving cathodic protection, it is desired to solve the Laplace equation

$$\nabla^2 \Phi_l = 0, \tag{36}$$

which is obeyed for an uniform, isotropic electrolyte.

2.3 Galvanic corrosion

If two dissimilar metals are in electrical contact, both submerged in the same electrolyte, a galvanic couple will be formed. In the galvanic couple, the more noble metal will be protected by the more active (i.e. less noble) metal, increasing the corrosion rate of the active metal. Assuming no potential drop in the electrolyte, the potential of the two metals will be equal to the couple potential, E_{couple}. When carbon steel and copper form a galvanic couple in seawater, copper will be protected by the carbon steel [14]. Then, the corrosion rates on carbon steel and copper will increase greatly and decrease to almost zero, respectively.

Electrode reactions on the metals can be divided into two main parts, according to the mixed potential theory; oxidations and reductions. The mixed potential theory states that

$$\sum I_{ox} = \sum |I_{red}| \tag{37}$$

at a potential $E = E_{couple}$. This means that at the couple potential, the total rate of oxidation and the total rate of reduction are equal [15]. By denoting carbon steel as Fe and copper as Cu, equation (37) can be written more explicitly:

$$\sum I_{ox(\underline{Fe}-Cu)} + \sum I_{ox(Fe-\underline{Cu})} - \sum |I_{red(Fe)}| - \sum |I_{red(Cu)}| = 0. \tag{38}$$

Here, the first term is the corrosion on steel when in contact with copper, and the second term the corrosion on copper when in contact with steel. Typical reduction reactions in seawater are ORR and HER on the respective electrodes.

Due to the coupling of the metals, there will be a net flow of current, from the anode (Fe) to the cathode (Cu) through the electrolyte. The net current I_{net} can be measured by the use of an ammeter. If the resistance in electrolyte, cables and ammeter is negligible, the measured net current is equal to

$$I_{net} = \sum I_{ox(\underline{Fe}-Cu)} - \sum |I_{red(Fe)}| = \sum |I_{red(Cu)}| - \sum |I_{ox(Fe-\underline{Cu})}|. \tag{39}$$

Thus, if the rates of the reduction reactions on steel are negligible compared to the corrosion on steel, the measured net current is equal to the corrosion current.

2.4 ICCP - Impressed current cathodic protection

2.4.1 Mode of operation

One way of protecting metals or structures from corroding is by use of impressed current cathodic protection (ICCP). The ICCP-system consists of reference electrodes and inert anodes placed around on the structure, as well as a control unit able to supply direct current (DC). An ICCP-system works by measuring the potential of the metal to be protected versus the reference electrodes. Furthermore, the control unit will drain current from this metal, and pass the current to the inert anodes. By doing this, the metal gets polarized to a lower potential until it is protected from corrosion. The current drain is automatically regulated by the control unit of the ICCP-system, by comparing the actual potential with the wanted (i.e. protection) potential. The so-called protection potential will vary depending on both type of metal and environment. For carbon steel in seawater, the protection potential is typically -800 mV vs. Ag/AgCl (seawater) reference electrode [5, 16] - or about -731 mV vs. Ag/AgCl/saturated KCl. However, if the potential of the steel gets lower than -1150 mV vs. Ag/AgCl (seawater), the steel will be over-protected [17]. Over-protection should be avoided, as it makes HER the dominant cathodic

reaction - the hydrogen gas formed could diffuse into the metal matrix, causing hydrogen embrittlement of the steel. Also, the potential of a metal will often vary locally on the structure, due to placement of anodes and reference electrodes. This is especially important when an ICCP-system is used for cathodic protection of large structures [18]. It is therefore necessary to have a potential range which is acceptable. For carbon steel in seawater, a protection potential range could be between -900 mV and -1050 mV vs. Ag/AgCl/saturated KCl [16], ensuring that the metal is neither under-protected nor over-protected. By using inert anodes, the anodes will ideally not be consumed. However, some anodes are preferred over others.

2.4.2 Anodes for ICCP

The choice of anodes for ICCP protection systems is dependent on several factors, such as type of electrolyte, pH, temperature and cathode material. Still, there are some requirements that always need to be fulfilled. First of all, the anodes need to have a low consumption rate, high stability, and the service life must be long to avoid having to replace them. The anodes should have good electrochemical properties, such that the output current density is large. The anodes should have good mechanical properties and high reliability, as these are important aspects when manufacturing and installing the anodes. As with everything, costs and ease of manufacturing and installation are also important criteria that must be taken into consideration [19].

In seawater, there are typically two competing reactions occurring at the anode; oxygen evolution and chlorine evolution, respectively:

$$4OH^- \longrightarrow O_2 + 2H_2O + 4e^- \tag{40}$$

$$2Cl^- \longrightarrow Cl_2 + 2e^-. \tag{41}$$

Both reactions are thermodynamically possible, meaning the kinetics of the anode will determine the dominating reaction. Selection of anode material is of great importance, as different anodes have different kinetics with regards to gas evolution. For example, some anodes promote evolution of oxygen gas rather than chlorine. This can be described by the anodes' oxygen efficiency. It is defined as the ratio of oxygen to chlorine gas production. Thus, for an anode with a high oxygen efficiency, reaction (40) will be the main reaction at the anode. One example of such an anode is magnetite [20].

If an anode with low oxygen efficiency is desired, a mixed metal oxide (MMO) anode is a possibility. Such anodes promote evolution of chlorine gas, by the reaction stated in (41). MMO anodes are essentially mixed metal oxides coated onto a titanium substrate. The coating is usually made from oxides of noble metals, such as ruthenium and iridium. Modification of the coated layer is also possible, optimizing it for its application. Generally, MMO anodes provide a high current density output, in addition to having a long service life and low maintenance requirements. Hence, MMO anodes are commonly used in the industry where cathodic protection is desired [21, 22].

2.5 Electrical double layer

When an electrode is exposed to a fluid, an electrical double layer (EDL) is formed at the electrode-solution interface. The EDL is formed mainly due to the species in the solution having different preferences with regards to placement, as some species want to sit near the electrode surface. There are several ways to describe the EDL; the Helmholtz model is the most simplified. According to the Helmholtz model, a plane cut through the centers of the specifically adsorbed ions or molecules gives the inner Helmholtz plane, denoted IHP in Figure 2.1. For a metal-solution interface in seawater, which mostly consists of Na^+ and Cl^- in addition to water molecules, the IHP could consist of Na^+, Cl^-, water, or other species that are present in the solution. This depends on several factors, with the type of electrode being one of them. If the metal in contact with seawater is negatively charged, the ions (called counter-ions) in the outer Helmholtz plane (OHP) will be positively charged. This means that mainly Na^+ will be prominent in the OHP, leading to a charge build-up near the electrode surface. The OHP goes through the centers of the nearest counter-ions, located at position y_2 in Figure 2.1. Since the charges at the metal surface and in the OHP are separated, this gives the EDL capacitive properties, meaning it can act as a parallel plate capacitor [11, 12].

Due to thermal agitation in the solution, the counter-ions are spread out into the diffuse layer as well, extending from the OHP and to the diffusion layer. Because of these charged ions, the solution is not electrically neutral at the Helmholtz planes, nor in the diffuse part of the double layer. From the diffusion layer and beyond, the electrolytic solution is again electrically neutral [9, 11].

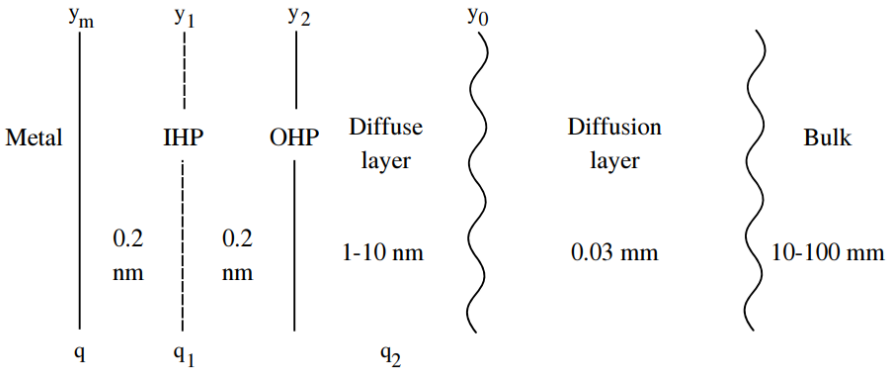

Figure 2.1: A sketch of a general EDL structure at an electrode-solution interface. Adapted from Newman [12].

At the electrode, two types of processes can occur. The process where charges, such as electrons, are transferred across the EDL, is referred to as a Faradaic process. If the charges transferred in fact are electrons, an oxidation or a reduction will occur at the electrode surface, depending on the direction of the flow of electrons. For some electrode-solution interfaces at specific potentials, no charge-transfer reactions can occur as they are unfavorable, either thermodynamically or kinetically. Then, non-Faradaic processes will occur, such as adsorption or desorption of species at the electrode surface. In this case, charge will not flow across the interface, but instead participate in charging of the double layer. An electrode in which no charge-transfer can occur is in literature referred to as an ideal polarizable electrode, meaning that the only process occurring at the electrode-solution interface is non-Faradaic. On the contrary, an ideal non-polarizable electrode is an electrode where only Faradaic processes occur. This prevents the electrode from being polarized, and the electrode potential is therefore unchanged. The Ag/AgCl electrode is one example of an electrode that is close to being an ideal non-polarizable electrode [9].

2.6 Alternating currents (AC) in electrochemical systems

2.6.1 System response

When an alternating current is applied to an electrochemical system, its excitation signal has the form

$$I(t) = I_a \sin(2\pi f t), \tag{42}$$

where I_a is the amplitude of the current, f the frequency of the signal and t the time. For small amplitudes, the corresponding potential signal will also be sinusoidal, but shifted in phase:

$$E(t) = E_a \sin(2\pi f t + \phi). \tag{43}$$

In this formula, $E(t)$ is the time-dependent potential, and E_a the potential amplitude. Sometimes, it can be useful to state I_{rms} rather than the current amplitude, where rms means root mean square. They are related through the following equation for sinusoidal current signals:

$$I_{rms} = \frac{I_a}{\sqrt{2}}. \tag{44}$$

Depending on the phase shift ϕ, the alternating currents could act as capacitive currents, i.e. contribute to charging of the electrical double layer. For $\phi = 0°$, i.e. no phase shift, the electrical circuit element is equivalent to a resistor, meaning only Faradaic processes will occur. However, if ϕ = -90°, the electrical circuit element is equivalent to a capacitor, implying that all currents are capacitive. A phase shift between 0° and -90° suggest that there is a combination of Faradaic and capacitive currents. As explained in Section 2.5, the charging of the double layer is a non-Faradaic process, and the current density associated with this can be denoted as i_{nf}. The total current density i_t is equal to the sum of the Faradaic and non-Faradaic current densities:

$$i_t = i_f + i_{nf} = i_f + C_{dl}\left(\frac{\partial(\Phi_s - \Phi_l)}{\partial t}\right). \tag{45}$$

Here, the surface charge density stored by the capacitor is $Q = C_{dl}(\Phi_s - \Phi_l)$, with C_{dl} being the double layer capacitance. Assuming that the double layer capacitor is equal to a parallel plate capacitor, the capacitance can be related by the area A, the permittivity of the solution ϵ, and the separation distance d:

$$C = \epsilon\frac{A}{d}. \tag{46}$$

For an electrode in contact with an electrolytic solution, an equivalent electrical circuit can be introduced to model the electrode-solution interface. A simple model that fairly accurately describes this is the Randles circuit. Figure 2.2 shows this, where the Warburg element (W) due to mass transfer is included as well. In the figure, R_{ct} is the charge transfer resistance and R_s is the solution resistance. The current can be visualized as having two options when flowing through the system - it can either contribute to Faradaic current (bottom) or to charging of the double layer (top). Note that this simplified model suggests that all capacitive currents contribute to charging of the electrical double layer. In other words, the dielectric capacitance due to a stable oxide layer on the metal surface is not included here.

The impedance of the double layer capacitance can be stated as

$$Z_{C_{dl}} = \frac{1}{(j \cdot 2\pi f)^{\mathrm{n}} \cdot C_{dl}}, \tag{47}$$

where j is the imaginary unit, and n is a positive constant. For an ideal capacitor, n is equal to 1. From equation (47), it is clear that a high frequency signal reduces the capacitive impedance. For the charge-transfer resistance (resistor), the impedance is independent of the frequency of the AC signal.

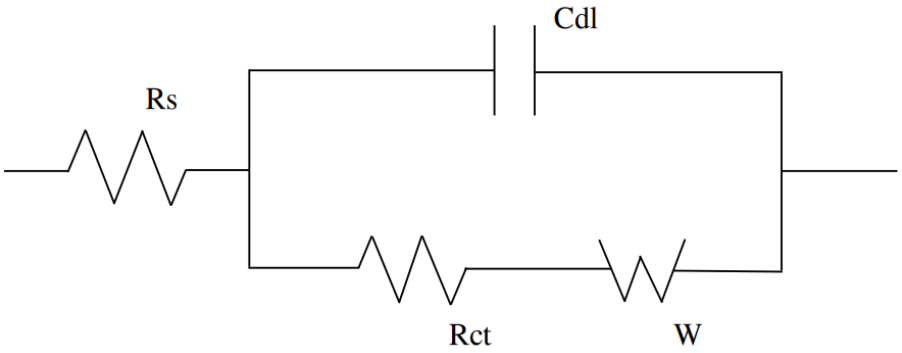

Figure 2.2: A model of the electrode-solution interface for a simple electrochemical reaction, including diffusion. The equivalent electrical circuit is referred to as a Randles circuit. In the figure, which is adapted from Randles [23], the electrode is on the right side, with the solution being on the left.

2.6.2 Effect on electrochemical behavior

By applying an AC signal, there will be a shift in potential given by equation (43). Since the relationship between potential and current is non-linear at $|\eta| \gg 0$, this affects the corrosion process. Bosch and Bogaerts [24] found that the parameter $r = b_a/b_c$, i.e. the ratio between the anodic and cathodic Tafel slopes, could be used to determine the change in open circuit potential of a corroding system. They concluded that a large r increased the OCP level, whereas a small r reduced the OCP when influenced by AC. Another interesting find by Bosch and Bogaerts is that the corrosion rate increases exponentially with the applied AC voltage. They concluded that the larger the difference between b_a and b_c, the quicker the corrosion rate increased. One exception is when b_a or $b_c \to \infty$, i.e. when the anodic reaction is completely passivated or when the cathodic reaction is completely under diffusion control, respectively. Here, the corrosion rate was independent of the applied AC.

These results were under the assumption of constant kinetics parameters. Experimental work by Goidanich et al. [25] contradicts this - they found that the kinetics of the electrode reactions are influenced by application of AC. For carbon steel in 35 g/L NaCl, it was found that an increase in AC, generally, leads to an increase in i_0 and decrease in absolute value for b_c. The anodic Tafel slope b_a, however, showed no clear trend.

2.7 Finite element method modeling using COMSOL Multiphysics®

COMSOL Multiphysics® is a modeling software that is able to solve multiphysics problems by the use of numerical methods. There are a variety of physics to choose from, and these are, unlike in programming languages such as Matlab or Python, already implemented in the software. The predefined physics makes it easy to start building a model, because the relevant equations are already included in the COMSOL software. Later, the model can be extended to solve more complex problems.

In the real world, problems are often complex and difficult to solve. Typically, partial differential equations can be used to describe the laws of physics in problems that are dependent on both space and time. As these differential equations are difficult or impossible to solve analytically, other methods must be utilized. One option is to use the finite element method (FEM) to gain a numerical approximation of the solution.

When using FEM, the geometry is first divided into several smaller parts, or finite elements,

that could vary in space and time. This process is typically referred to as meshing. Then, a set of linear equations are formed by the partial differential equations in each finite element. By combining all equations at all points, a global system of equations is formed. These can in turn be solved by numerical methods, such as the implicit Euler method or the Runge-Kutta method.

For some problems with high complexity, a high number of finite elements are required to solve the problem. This increases the number of equations to be solved, which also increases the computational time of the model. An advantage of FEM is that the size of the mesh can be altered along the geometry, meaning some parts can be more finely meshed than others. For example, a partial differential equation to be solved might depend on the temperature. The temperature change could be due to the heat of an electrochemical reaction occurring at a particular surface. In that case, a fine mesh near that surface would be advantageous because the temperature gradient is large here. Further away from this surface, the mesh could be coarser since the temperature gradient is small. The results of the modeling are still quite accurate, and an unnecessarily long computational time is avoided [26, 27].

3 Materials and method

3.1 COMSOL model

3.1.1 Geometry and mesh

In COMSOL, a simple 2D geometry was created as shown in Figure 3.1. The geometry consisted of one 28cm x 20cm domain representing the electrolyte, i.e. seawater. At the top of the seawater, three electrodes were defined as line segments, having a length of 4 cm each. Similarly, the electrodes were separated by 4 cm as well. All the electrodes were in contact with the seawater. In addition, COMSOL ensured electrical connection between the copper (left), anode (middle) and carbon steel (right).

Since the geometry was created in two dimensions, it was necessary to define an "out of plane thickness", which is essentially the length of the domain and boundaries in the third dimension. This was set to 4 cm. Hence, the surface areas of the electrodes were 16 cm^2 each. In the model, the active surface area was set equal to the total surface area. This implied that no coating was included in the model. Unless specified, this geometry was utilized in all computations of the model.

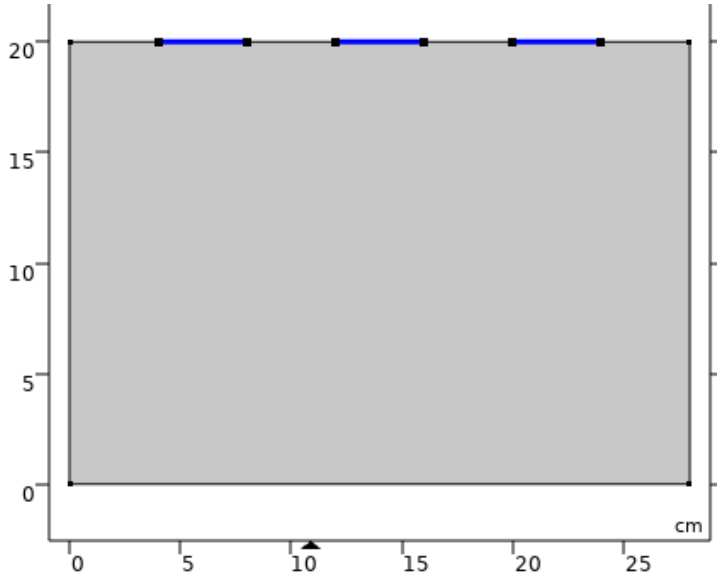

Figure 3.1: Geometry used in COMSOL. The three blue lines indicate (from left to right) copper, anode and carbon steel. The grey domain represents the electrolyte - seawater.

Use of FEM implies that the geometry must be divided into several smaller sub-domains, called meshing. To be able to cope with such a complex and non-linear problem, as emphasized in Section 2, it was necessary to create a fine mesh. This was especially important at the electrode surfaces, where the main reactions occurred. Otherwise, the solution would not converge. The full mesh is shown in Figure 3.2. At the electrode surfaces, the sizes of the triangles were between $5.6{\cdot}10^{-4}$ cm and 0.28 cm, visualized in Figure 3.3. To reduce the computational time of the model, other parts of the geometry were meshed more roughly. Between the electrode surfaces, the triangle sizes were about 0.05 cm. A quite coarse mesh was used near the bottom of the electrolyte, i.e. the furthest away from the electrode surfaces. Here, the sizes of the triangles were about 1.04 cm.

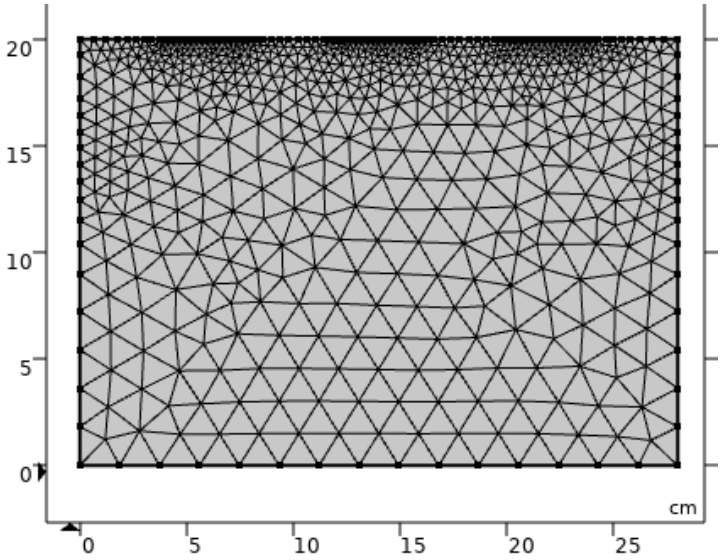

Figure 3.2: Overview of the mesh used in COMSOL.

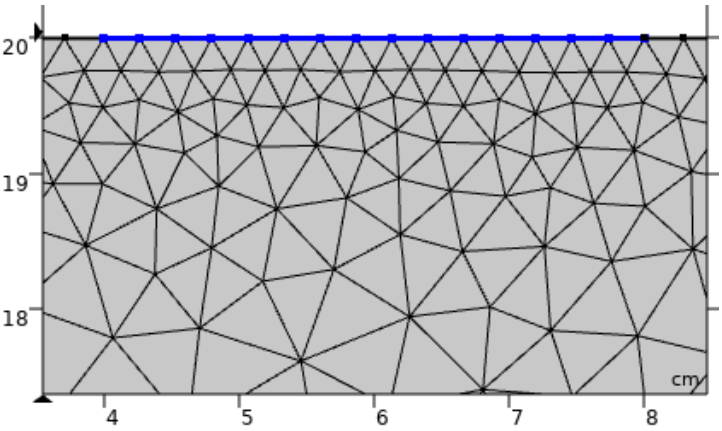

Figure 3.3: The mesh used in COMSOL, zoomed in on the leftmost electrode surface. The electrode surface is marked in blue.

3.1.2 Physics and implementation

There are a variety of different physics to choose from in COMSOL Multiphysics. In this case, it was necessary to choose a physics that deals with the distribution of current in aqueous solutions. As the modeled system had a finite volume, the electrochemical reactions taking place at the electrodes would change the composition of the electrolyte to some extent. Hence, the secondary current distribution was insufficient, and the tertiary current distribution was instead chosen. "Water-based with electroneutrality" was chosen as the type of electrolyte charge conservation, which made sure that the electroneutrality condition stated in equation (32) was obeyed. It also related the concentration of H^+ to the concentration of OH^-:

$$c_{H^+} \cdot c_{OH^-} = 10^{-14} \tag{48}$$

at 298K. At the different electrode surfaces, several electrochemical reactions competed. These were implemented in the model using the "Electrode reaction" node under "Electrode surface". For the two cathodes, carbon steel and copper, simple oxidation reactions were included in order to calculate the corrosion rate:

$$Fe \longrightarrow Fe^{2+} + 2e^- \tag{49}$$

$$\mathrm{Cu} \longrightarrow \mathrm{Cu}^{2+} + 2\mathrm{e}^{-}. \tag{50}$$

However, it was necessary to also define the possible reduction reactions on these electrodes, given that they both were cathodically protected. In slightly alkaline seawater, the oxygen reduction (ORR) and hydrogen evolution (HER) reactions are the most common:

$$\mathrm{O_2} + 2\mathrm{H_2O} + 4\mathrm{e}^{-} \longrightarrow 4\mathrm{OH}^{-} \tag{51}$$

$$2\mathrm{H_2O} + 2\mathrm{e}^{-} \longrightarrow \mathrm{H_2} + 2\mathrm{OH}^{-}. \tag{52}$$

Assuming that the anode is inert, no metal-dissolution will occur here. Then, the possible oxidation reactions are, as stated in Section 2.4.2, oxygen evolution (OER) and chlorine evolution (CER):

$$4\mathrm{OH}^{-} \longrightarrow \mathrm{O_2} + 2\mathrm{H_2O} + 4\mathrm{e}^{-} \tag{53}$$

$$2\mathrm{Cl}^{-} \longrightarrow \mathrm{Cl_2} + 2\mathrm{e}^{-}. \tag{54}$$

To make sure that the model properly solved at times where the impressed current was small or even negative due to the AC magnitude, oxygen reduction (ORR) and hydrogen evolution (HER) were also included as possible reactions on the inert anode. In the system, two different anodes were utilized - platinum and MMO. When switching anode from Pt to MMO, the electrode reactions were modified. MMO has a low oxygen efficiency, as explained in Section 2.4.2, meaning the rate of OER is low. The OER was therefore excluded from the modeling when MMO was used as the inert anode. In addition, the kinetics of CER varied on the two anodes, so the Tafel slope b_a and exchange current density i_0 were modified when changing anode material in the model.

At the inert anode, a "total current" node was used to define the current impressed to the system. In order to replicate the scenario of impressed direct current (DC) from ICCP, together with unwanted alternating currents (AC), the total current was defined as the sum of two terms:

$$I = I_{\mathrm{DC}} + I_{\mathrm{AC,rms}} \cdot \sqrt{2} \cdot \sin(2\pi f t). \tag{55}$$

Here, the relationship stated in equation (44) was utilized. Since the problem is related to alternating currents, which can lead to a mix of Faradaic and non-Faradaic currents, it was necessary to include double layer capacitance in the model. The double layer capacitance was defined for each electrode surface. Lastly, the concentration of $\mathrm{O_2}$ was set constant at the electrolyte-air interface, i.e. next to the electrode surfaces in Figure 3.1. This was due to the assumption of the electrolyte being freely exposed to oxygen in the air. An overview of all the different nodes is shown in Figure 3.4.

3.1.3 Model inputs and assumptions

It is impossible to consider every aspect of a complex problem in fine detail. Therefore, some assumptions must be made. Because of the impressed currents, the carbon steel and copper electrodes are, ideally, protected from corrosion. This implies that the concentration changes of these metal ions are minimal. By applying a constant reversible potential for reaction (49) and (50), the problem is reduced by at least two variables. This assumption also facilitates the comparison of the computed solution with laboratory results, since $c_{\mathrm{Fe}^{2+}}$ and $c_{\mathrm{Cu}^{2+}}$ are unknown in the laboratory system. The open circuit potentials (OCP) for carbon steel and copper were defined in the model and set equal to -618 and -155 mV vs. Ag/AgCl/saturated KCl, respectively. These values were determined experimentally as part of the author's specialization project [7].

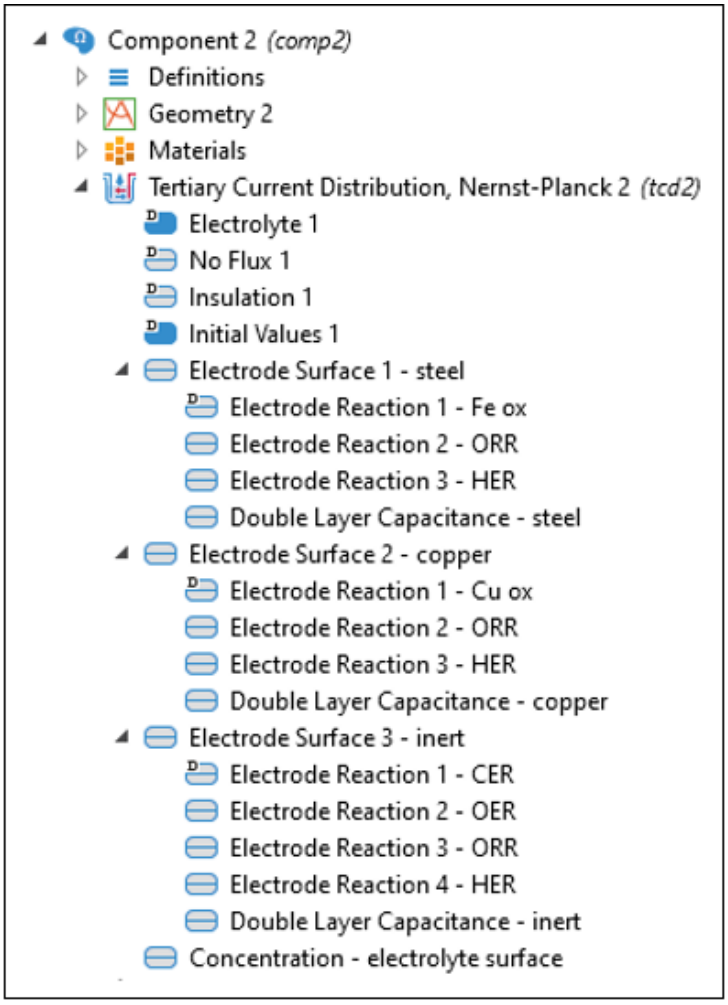

Figure 3.4: A model tree, showing the different nodes utilized in the COMSOL model.

The transport of oxygen in aqueous solution is limited by diffusion and could lead to an upper limit for the current density. Therefore, a limiting current density was implemented for the ORR reactions. In seawater, $i_{\text{lim, ORR}}$ is about 5 A/m^2 on steel [28]. For the other two electrode surfaces, the limiting current density for ORR was also assumed to be 5 A/m^2.

Several input parameters are required to actually solve the model. The initial concentration and diffusion coefficient of the relevant species are given in Table 3.1. For the gas species, the concentration is limited by their solubility in water. These are also given in the table, assuming that the electrolyte is in equilibrium with air. To avoid species exceeding their concentration (solubility) limit, a reverse reaction rate was implemented for each reaction. The rate of this reaction was positive if $c_i > c_{i,sol}$. Otherwise, the rate of the reverse reaction was 0.

Also, parameters related to the kinetics of the electrodes had to be defined. In the model, the anodic and cathodic Tafel equations, stated in equation (15) and (17), were used to relate the electrode potential to the partial current density and the reversible potential for each reaction. Hence, the exchange current density i_0 and the Tafel slope b_a or b_c for each reaction at each electrode were needed as inputs in the model. Some of the parameters were found experimentally, either in a previous work [7], or in this work. The latter will be accounted for later, in Section 4.3. However, some of the kinetics-parameters were difficult to obtain experimentally, meaning literature search was necessary. No literature was found on the kinetics of ORR and HER on MMO, since MMO normally acts as an anode. Therefore, it was assumed that the

Table 3.1: Initial concentration and diffusion coefficient of different species used as input parameters in the model. The solubilities of the gases are stated in parenthesis [29].

Specie	Initial conc. (solubility) [mol/dm^3]	Diff. coeff. [m^2/s]	Ref.
OH^-(aq)	$1.0{\cdot}10^{-6}$	$5.3{\cdot}10^{-9}$	[30]
H^+(aq)	$1.0{\cdot}10^{-8}$	$9.3{\cdot}10^{-9}$	[30]
Cl^-(aq)	$6.0{\cdot}10^{-1}$	$2.0{\cdot}10^{-9}$	[30]
O_2(aq)	$2.3{\cdot}10^{-4}$ ($2.5{\cdot}10^{-4}$)	$2.3{\cdot}10^{-9}$	[31]
H_2(aq)	$1.0{\cdot}10^{-7}$ ($7.6{\cdot}10^{-4}$)	$5.0{\cdot}10^{-9}$	[31]
Cl_2(aq)	$1.4{\cdot}10^{-6}$ ($9.2{\cdot}10^{-2}$)	$1.9{\cdot}10^{-9}$	[32]

kinetics of HER and ORR on MMO would be similar to that of Pt, although Pt is known to be a good catalyst. Nevertheless, it is clear that the exchange current densities of ORR and HER are lower than that of CER, which is desirable for the MMO electrode. All the parameters used as input in the COMSOL model are stated in Table 3.2.

Table 3.2: The kinetics of the reactions at different electrodes used in the model: exchange current density i_0 and (anodic or cathodic) Tafel slope b.

Reaction @Electrode	i_0 [A/m^2]	Ref.	b [mV/dec]	Ref.
$Fe \longrightarrow Fe^{2+}$ @Steel	$2.3{\cdot}10^{-2}$	[7]	143	[7]
$Cu \longrightarrow Cu^{+}$ @Copper	$1.7{\cdot}10^{-2}$	[7]	60	[7]
ORR @Steel	$4.6{\cdot}10^{-6}$	[7]	-313	[7]
HER @Steel	$7.4{\cdot}10^{-4}$	[7]	-125	[7]
ORR @Copper	$1.1{\cdot}10^{-5}$	this work	-285	this work
HER @Copper	$1.9{\cdot}10^{-4}$	this work	-143	this work
ORR @Platinum	$1.4{\cdot}10^{-3}$	this work	-374	this work
HER @Platinum	$2.3{\cdot}10^{-2}$	this work	-187	this work
OER @Platinum	$3.4{\cdot}10^{-5}$	this work	146	this work
CER @Platinum	$1.4{\cdot}10^{-2}$	this work	98	this work
ORR @MMO	$1.4{\cdot}10^{-3}$*	-	-374*	-
HER @MMO	$2.3{\cdot}10^{-2}$*	-	-187*	-
CER @MMO	1.0†	[33]	30†	[33]

* No data found - platinum data used.
† In 0.5 M NaCl. i_0 was estimated from the reference data.

Double layer capacitances needed to be defined on each electrode participating in the system. These were assumed equal and set to 0.1 F/m^2. However, the double layer capacitances were varied when the effect of C_{dl} was investigated. Similarly, the frequency of the AC perturbation was set to 50 Hz, but this was also varied.

It was also desired to scale the exchange current density with concentration of the relevant species, based on the equations (10) and (11). These were set to +1 for the reactants (i.e. $\Omega_{O,rd}$ = $\Omega_{R,ox}$ = 1), and -1 for the products (i.e. $\Omega_{R,rd}$ = $\Omega_{O,ox}$ = -1).

To get a measure of the uncertainty in the computations, the input parameters were varied randomly within a ± 10% range. A total of three computations were carried out for each combination of parameters.

3.1.4 Study steps

The goal of the model was to obtain a relatively stable potential due to the impressed DC (1), and then include an AC-term on top of the DC-signal for a short amount of time (2). When DC was impressed, it was found that the system needed about 10 000 seconds to obtain a stable potential. This solution will later be referred to as the quasi-stationary solution. As the frequency of the AC-signal was set to 50 Hz, this gave a spatial period of 20 ms for the sinusoidal wave. In order to obtain about 15 periods, the total time for the AC-signal was set to 300 ms. For other frequencies, which will be discussed later, the total time of this step was altered to obtain 15 periods. To summarize, a study with two steps was desired:

- Study 1
  - Time-dependent (0 to 10 000 seconds), only DC.
  - Time-dependent (10 000 to 10 000.3 seconds), DC+AC.

Initially, these studies were combined by switching the AC-term on/off, such that $\mathrm{AC}_{\mathrm{switch}} = 0$ when only DC was applied, and $\mathrm{AC}_{\mathrm{switch}} = 1$ when the AC-term was included as well. This led to a modified version of equation (55):

$$I = I_{\mathrm{DC}} + I_{\mathrm{AC,rms}} \cdot \sqrt{2} \cdot \sin\left(2\pi f t\right) \cdot \mathrm{AC}_{\mathrm{switch}}. \tag{56}$$

However, obtaining a quasi-stationary solution for the impressed DC proved time-consuming. It was found that it would be better to separate (1) and (2) into two studies; denoted in the model as "study 1" and "study 2". The solution of study 1 at the last time step was used as initial conditions in study 2. Then, if only $I_{\mathrm{AC,rms}}$ or the double layer capacitance were altered, only the solution of study 2 had to be updated, as the solution of study 1 was independent of these parameters. Since study 2 had a much shorter computational time, the separation into two studies reduced the overall computational time by a large factor.

Prior to the two studies, a study step called "Current distribution initialization" was used, where a secondary current distribution type was used to obtain a stationary solution (i.e. at t=0). This reduced the overall computational time, as the electrode and electrolyte potential from this step was used as initial conditions in study 1. In the end, these study steps were used in the model:

- Study 1
  - Current distribution initialization (0 seconds)
  - Time-dependent (0 to 10 000 seconds), only DC
- Study 2
  - Time-dependent (0 to 0.3 seconds), DC+AC

3.2 Experimental

3.2.1 Preparation of samples and electrolyte

In the laboratory experiments, synthetic seawater was used as the electrolyte. The synthetic seawater was prepared based on the ASTM International Standard for preparation of substitute ocean water [34]. Since there are many different compounds included in the standard, only the most prominent were included in the preparation. These are stated in Table 3.3 along with their respective concentrations. The preparation was made by adding these salts to a large Erlenmeyer flask containing deionized water, while stirring the solution at the same time. By the use of a pH indicator, the pH of the synthetic seawater was found to be about 8. Since the prepared synthetic seawater was freely exposed to laboratory air, its temperature was close to room temperature.

A total of four electrodes were used across all experiments. These were carbon steel, copper, platinum, and an Ag/AgCl/saturated KCl reference electrode. The preparation of the carbon steel and copper samples was similar; they were both cut into small circular shapes with a diameter of 2.90 cm. In this way, they fit into the sample holders in the laboratory. Although the area of each sample was 6.61 cm^2 each, the active area was only 1.29 cm^2 due to the type of sample holder. A carbon steel sample before and after it was placed in the sample holder is shown in Figure 3.5.

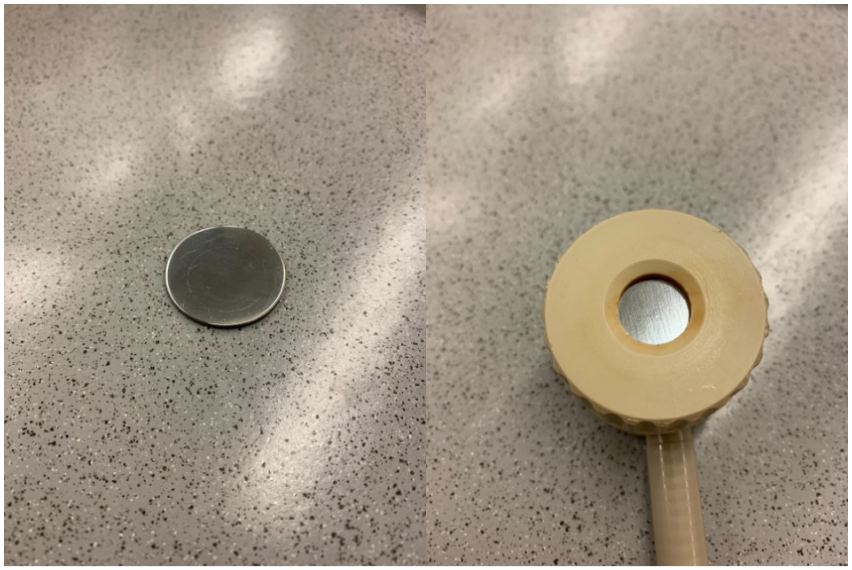

Figure 3.5: One of the carbon steel samples used in the lab experiments. The image on the right shows the steel sample when inserted into the sample holder.

Table 3.3: The concentration of the different salts used to prepare the synthetic seawater used experimentally [34].

Salt	**Concentration [g/L]**
NaCl	24.5
$MgCl_2$	5.2
Na_2SO_4	4.1
$CaCl_2$	1.2
KCl	0.7

A commercial Ag/AgCl electrode immersed in a saturated KCl solution acted as the reference electrode in the experiments. This was in turn connected to the system via a salt bridge. To ensure contact between synthetic seawater and the KCl solution, the salt bridge was in one end filled with synthetic seawater, and in the other end filled with agar. The agar ensured that the KCl solution did not mix with the synthetic seawater in the system, while still allowing the charged particles to flow. All potentials reported in this work are with respect to the Ag/AgCl/saturated KCl electrode, which has a potential of about +0.197 V vs. the standard hydrogen electrode at room temperature. As for the platinum electrode, no further preparation was needed after receiving it. The dimensions of the platinum electrode were 2 x 2 cm.

3.2.2 Laboratory setup

For the main laboratory experiments, a cylindrical beaker was filled with about 800 mL of synthetic seawater. Carbon steel and copper samples were inserted in sample holders, and submerged in the seawater together with the platinum electrode. In the setup, carbon steel and copper both faced the platinum electrode. In addition, the tip of the salt bridge that contained synthetic seawater was submerged into the electrolyte. The tip was placed near the carbon steel surface to prevent any potential drop. Carbon steel, copper, platinum and the salt bridge tip were all positioned at a similar height as well. Figure 3.6 shows the setup.

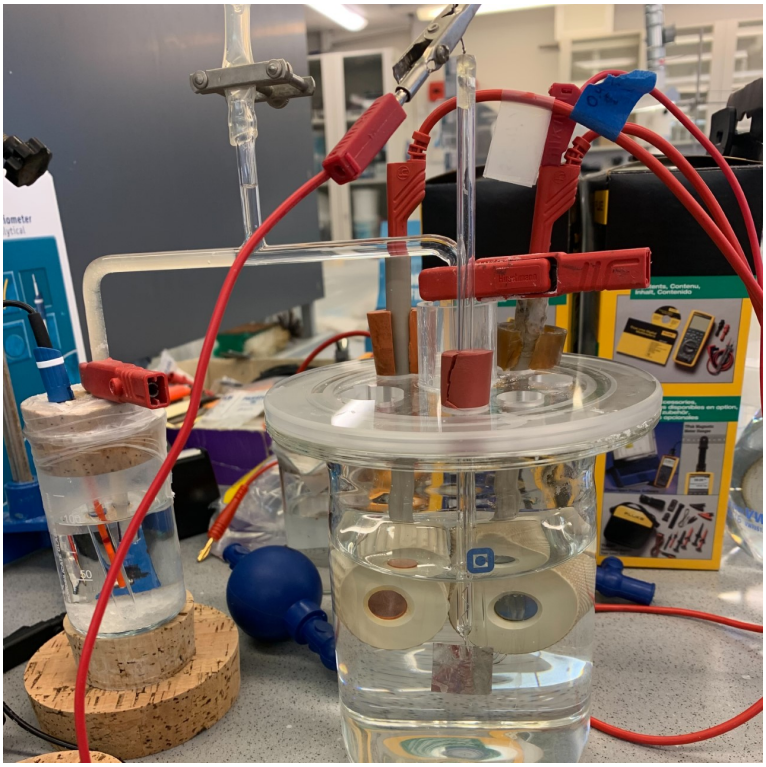

Figure 3.6: The laboratory setup. In the beaker, the copper (left), carbon steel (right) and platinum (in front) are all electrically connected via the Gamry software. On the left, an Ag/AgCl reference electrode (in red) is connected to the system through a salt bridge.

A Gamry software was utilized when the measurements were carried out. Between the carbon steel and copper electrodes, a cable was introduced to obtain electrical contact. Hence, when a current was impressed, it had two possible paths - towards either carbon steel or copper. The carbon steel was chosen as the working electrode, but as there was electrical contact between the carbon steel and copper, both these metals were essentially the working electrode. Platinum was the counter electrode of the system, with Ag/AgCl as the reference electrode.

3.2.3 Measurements at lab

Before doing the main experiments, polarization curves for copper and platinum were obtained through cyclic polarization scans. The goal was to obtain the Tafel slopes and exchange current densities for various reactions at these electrodes. Scans were performed in the cathodic direction for copper, and in both cathodic and anodic direction for platinum. For the cyclic polarization scan of copper, the copper was chosen as the working electrode, and platinum as the counter electrode. When cyclic polarization scans of platinum were carried out, however, the roles were switched, meaning that platinum acted as the working electrode and copper as the counter electrode. In both cases, the carbon steel electrode was removed from the system.

Then, the carbon steel was again included, which gave the setup shown in Figure 3.6. Firstly, galvanostatic scans were performed, where direct currents (DC) of various magnitudes were set, and the corresponding potentials were measured. The current ranged between -60 and -200 µA. As the only option in Gamry is to pass current to the working electrode, the currents were given with a negative sign. Three scans were done for each of the different currents in this range, and each scan lasted for 1000 seconds. Both electrolyte and metal samples were changed frequently between the scans to reduce the likelihood of e.g. corrosion products or unwanted electrochemical reactions affecting the results.

Following the galvanostatic scans, galvanostatic EIS (Electrochemical Impedance Spectroscopy) scans were performed for different combinations of DC and AC. For each DC, four different magnitudes of AC_{rms} were used: 0.1, 1, 5 and 10 mA. Three scans were carried out for each AC, resulting in a total of twelve scans at each DC. As the goal of the scans was to obtain the potentials associated with the different DC+AC combinations at a frequency of 50 Hz, the initial and final frequencies were set to 51 and 49 Hz respectively. Obtaining a stable potential prior to the measurements was necessary, so a potential conditioning was included before each measurement. The potential set in the conditioning step was equal to the potential obtained from the galvanostatic scan at the specific DC magnitude. Directly after the potential conditioning, the galvanostatic EIS scan was carried out. An example of the procedure is shown below, for -60 µA DC and 0.1 mA AC_{rms}, in chronological order:

1. Galvanostatic scan (x3)
    - DC = -60 µA
    - Time = 1000 seconds
2. (Median potential calculated)
3. Potential conditioning
    - Potential = Median potential calculated
    - Time = 600 seconds
4. Galvanostatic EIS scan (x3)
    - DC = -60 µA
    - AC_{rms} = 0.1 mA
    - Frequency range = [51,49] Hz
    - Points/dec = 10 000

4 Results

4.1 Direct and alternating currents impressed to platinum

A system consisting of carbon steel, copper and platinum was studied by applying external direct and alternating currents. Varying the magnitude of the currents gave the corresponding potential of the carbon steel electrode. Different combinations of AC and DC were investigated, and the results from both modeling and experimental work are presented here. For the modeling, three computations were made for each case by varying the input parameters within a ± 10% range. Presented values are the mean of these three computations.

4.1.1 Computational results

In the COMSOL model, the effect of AC and DC on the steel-copper-platinum couple in seawater was investigated by defining a total current on the platinum electrode. Firstly, only DC was impressed to the system to ensure a quasi-stationary solution, i.e. a stable potential on the carbon steel. After 10 000 seconds, AC was applied in combination with DC for 300 ms. How the potential varied with time in these two steps is presented in Figure 4.1 for DC = 1 mA and AC_{rms} = 5 mA, at f = 50 Hz and C_{dl} = 0.1 F/m^2 on each electrode. For this specific case, the potential of carbon steel was converging towards -1009 mV vs. Ag/AgCl when only DC was applied, and the mean potential after applying AC was reduced to -1014 mV vs. Ag/AgCl. Similar curves were observed for each combination of AC and DC.

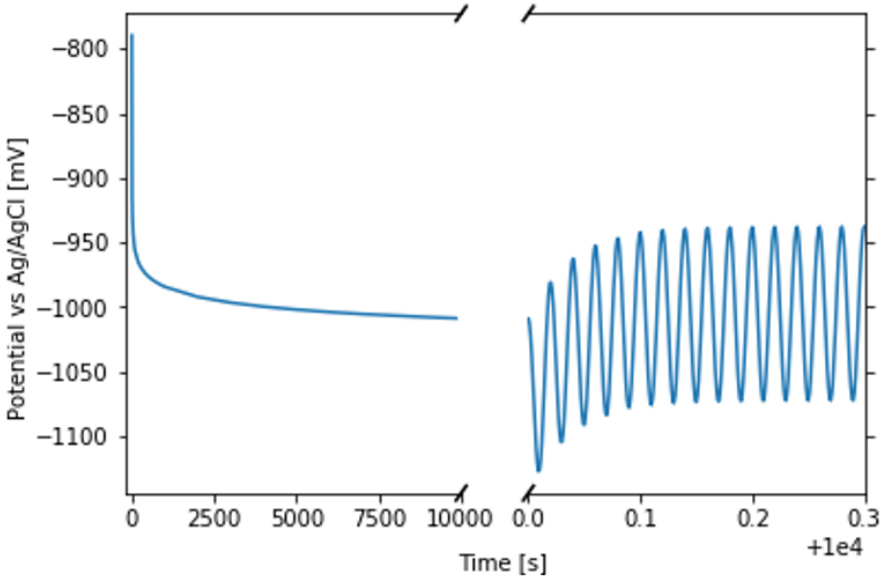

Figure 4.1: The potential of carbon steel after impressing 1 mA DC for 10 000 seconds, followed by impressing 1 mA DC and 5 mA AC_{rms} for 300 ms. Could be interpreted as turning on an AC-switch at t=10 000 s. The frequency of the AC signal was 50 Hz, and the double layer capacitance C_{dl} was set to 0.1 F/m^2 on each electrode.

For the case where platinum acted as the inert anode, four different AC_{rms} were studied for each DC. The computed mean potentials of the carbon steel electrode are presented in Figure 4.2. The frequency f of the AC-signal was set to 50 Hz, and the double layer capacitance C_{dl} was assumed constant and equal to 0.1 F/m ^{2} for each electrode. The computed potentials stated with two standard deviations ($2s$) are given in Table C.1.

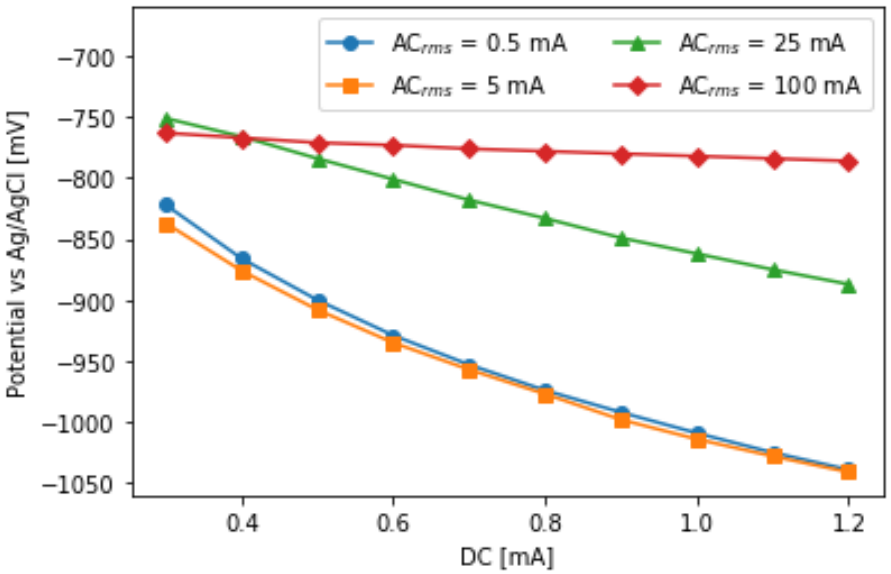

Figure 4.2: Model: Mean potential of carbon steel at various combinations of DC and AC impressed to the platinum electrode. The double layer capacitance was set equal to 0.1 F/m^2 on each electrode, and the frequency of the AC signal was 50 Hz.

With small AC magnitudes impressed to the system, the electrode potential of carbon steel does not change much. In fact, it can be observed that the potential decreases when the AC_{rms} increases from 0.5 mA to 5 mA. However, when the AC magnitude exceeds a certain limit, the potential increases greatly. The protection potential for carbon steel in seawater is in the range [-1050, -900] mV vs. Ag/AgCl [16]. Hence, in the modeled system, a DC in the range [0.5, 1.2] mA sufficiently protects the carbon steel when the AC_{rms} is small and negligible. By imposing a large AC_{rms}, the potential generally increases. Figure 4.2 shows that an AC_{rms} of 25 mA and 100 mA polarizes the carbon steel above the protection potential limit of -900 mV vs. Ag/AgCl when DC $\leq$ 1.2 mA.

Similar computations were performed for a larger double layer capacitance. C_{dl} on each electrode was increased from 0.1 F/m^2 to 0.5 F/m^2, and the results are presented in Figure 4.3. Results from this computation are tabulated in Table C.2, stated with $2s$ uncertainty. It can be seen that for all combinations of DC and AC, with a few exceptions, the potential of carbon steel is within the protection potential range. Carbon steel is not protected when the DC impressed is lower than 0.5 mA and the applied AC is low. However, increasing the AC_{rms} up to 100 mA at 0.3 mA and 0.4 mA DC protects the carbon steel, as the potential is reduced below -900 mV vs. Ag/AgCl here.

Comparing Figure 4.2 with Figure 4.3 shows that the increase in C_{dl} does not affect the potential much at small AC magnitudes. At elevated AC-levels, however, there is a clear deviation. An AC_{rms} of 25 mA decreases the potential of carbon steel when the double layer capacitance is large (C_{dl} = 0.5 F/m^2), while the opposite is true for the smaller capacitance value (C_{dl} = 0.1 F/m^2).

For the case where C_{dl} = 0.5 F/m^2, an AC_{rms} of 100 mA affects the potential rather strangely. Although the potential decreases with increasing DC, the slope of the red curve in Figure 4.3 is significantly lower than the others. This implies that an increase in AC_{rms} from 0.5 mA to 100 mA increases the potential of carbon steel at high DCs, but decreases the potential at low DCs.

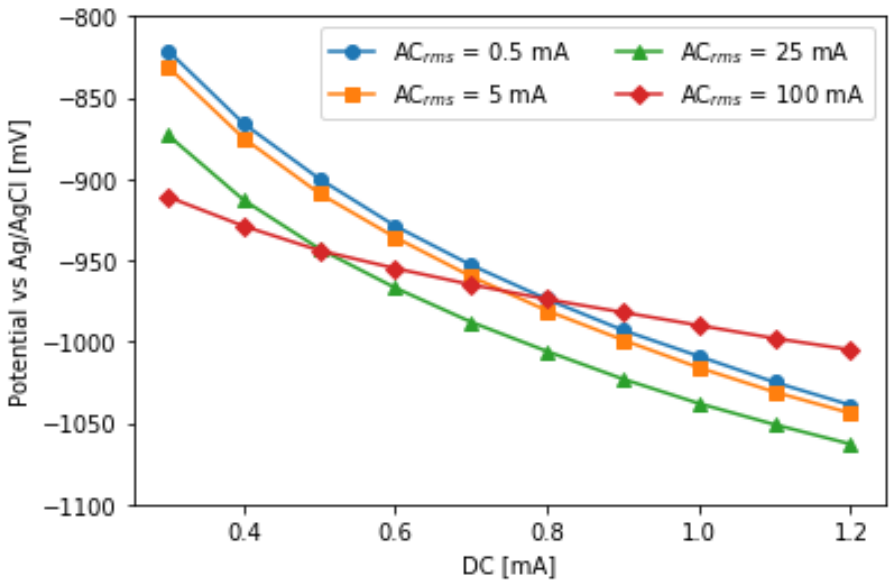

Figure 4.3: Model: Mean potential of carbon steel at various combinations of DC and AC impressed to the platinum electrode. Here, the double layer capacitance was set equal to 0.5 F/m^2 on each electrode. The frequency of the AC signal was 50 Hz.

4.1.2 Laboratory results

Similar to the modeling, different combinations of direct and alternating currents were impressed at the laboratory. With the procedure described in Section 3.2.3, the mean potentials were calculated. These are plotted in Figure 4.4. For each scattered point, the uncertainty of the measurement is stated as two standard deviations ($2s$). To avoid too much information in one figure, the error bars are excluded in Figure 4.4, but they can be observed in Section B.1 for each combination of DC and AC. Calculation of the mean and the standard deviation is showcased in Section A.2, for DC = 60 µA and AC_{rms} = 0.1 mA.

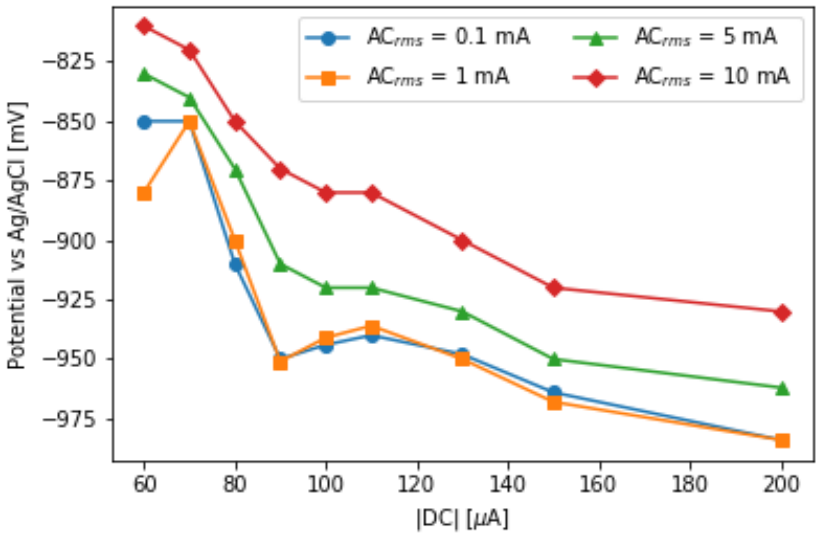

Figure 4.4: Lab: Mean potential of carbon steel at various combinations of DC and AC impressed to the carbon steel electrode. The frequency of the AC signal was (50 ± 1) Hz.

As mentioned previously, a potential in the range [-1050, -900] mV vs. Ag/AgCl is necessary to protect carbon steel from corroding in seawater. With a negligible AC magnitude, the laboratory experiments show that a DC within the range [80, 200] µA sufficiently protects the carbon steel. However, if an alternating current is introduced, the potential generally increases, meaning that the DC magnitude has to increase in order to still protect the carbon steel from corroding. In Figure 4.4, the green curve indicates the potential when AC_{rms} is equal to 5 mA. It shows that the DC must be increased to at least 90 µA in order to reduce the potential below -900 mV vs. Ag/AgCl. The most extreme case, in which AC_{rms} is equal to 10 mA, reveals a large increase in potential. Hence, to achieve protection of carbon steel in this scenario, the required DC is greater than 130 µA.

Generally, there is a clear qualitative trend, despite some exceptions. Impressing a larger DC (absolute value) decreases the potential, whereas impressing a larger AC increases the potential. Measurements at DC = 70 µA and low ACs deviate the most from this trend, with some increase in potential compared with measurements at 60 µA DC. However, Figure B.1 and Figure B.2 show relatively large uncertainty in these measurements.

According to the plot in Figure 4.4, the potential remains relatively unchanged when adjusting between small AC magnitudes at a constant DC. For 0.1 mA and 1 mA AC_{rms}, the corresponding potentials are quite similar. For some DC magnitudes, such as 60 µA and 150 µA, it appears that increasing AC_{rms} from 0.1 mA to 1 mA actually decreases the potential. By looking at the plots in Figure B.1 and Figure B.2 at DC = 60 µA and DC = 150 µA, it can be observed that the size of the error bars is larger than the potential difference. Therefore, it is hard to determine whether these measurements follow the trend (increasing potential with increasing AC) or not. However, by comparing this with the modeling results, for example in Figure 4.2, it can be observed that increasing the AC at small magnitudes may actually decrease the mean potential.

It should also be mentioned that the phase angle was obtained in each measured points, and that this varied between about -40° and -62°. The phase angle was largest (i.e. -40°) when the AC and DC impressed were both large, and smallest (i.e. -62°) when the AC and DC impressed were both small. However, when the AC was small and DC large, or vice versa, the phase angle was measured to be about -50°.

4.2 Direct and alternating currents impressed to mixed metal oxide (MMO) anode in COMSOL

To further explore the effect of AC on a galvanic couple in seawater, the platinum electrode was replaced with an industrial MMO anode in the modeling. The geometry was maintained as before, but some reactions and their kinetics were altered for this case. Potentials and corrosion rates will be presented here for different variations of parameters such as DC, AC_{rms}, C_{dl}, f, in addition to altering the area ratios. The effect of removing copper from the system will also be presented.

Most of the presented values (i.e. potential and corrosion rate) are calculated using the built-in "Average" operator in COMSOL. To gain an estimate of the uncertainty, each scenario is computed three times by varying the input parameters randomly within a $\pm$ 10% range. The plotted potentials and corrosion rates are the mean values from these three computations.

4.2.1 Potentials and corrosion rates vs. impressed currents

Initially, the steel in the galvanic couple was cathodically protected by impression of various DCs. The DC magnitudes were in the range 0.4 mA to 1.2 mA, which kept the potential of carbon steel between -840 mV and -1010 mV vs. Ag/AgCl. Then, similar to the procedure showcased in Figure 4.1, various AC_{rms} were impressed. Keeping C_{dl} and f constant at 0.1 F/m^2 and 50 Hz respectively, eight different AC_{rms} were studied: 0, 1, 5, 10, 20, 50, 100 and 200 mA. The resulting potentials are presented in Figure 4.5. Tabulated mean values and uncertainties are presented in Table C.3

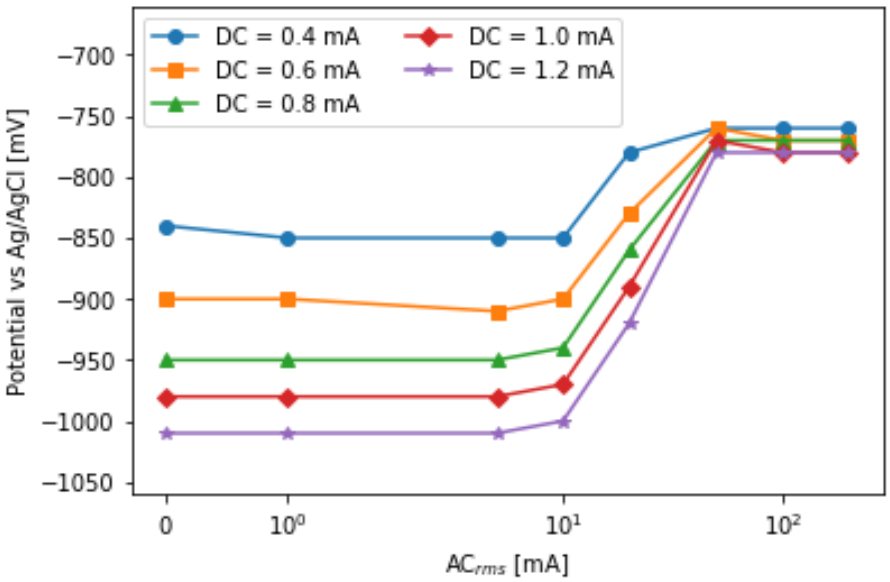

Figure 4.5: Model: Mean potential of carbon steel at various combinations of DC and AC impressed to the MMO electrode. C_{dl} and f were maintained at 0.1 F/m^2 and 50 Hz, respectively.

Left in Figure 4.5, the AC_{rms} is small. At these points, the total current is determined by the time-independent direct currents. Generally, increasing the AC_{rms} to about 10 mA has no effect on the mean potentials, as these are quite stable. When the AC_{rms} reaches above 20 mA, however, a large increase in potential is observed. According to the figure, the increase continues until AC_{rms} reaches 50 mA. Beyond 50 mA AC_{rms}, the mean potential once again stabilizes.

To better visualize how the impressed ACs affect the corrosion of carbon steel in the galvanic couple, the corrosion rates are plotted for the same data points, as shown in Figure 4.6. It should be noted that to obtain these corrosion rates, it has been assumed uniform corrosion of carbon steel. At small AC_{rms}, the corrosion rates are low for all variations of DC. Similar trends are observed as compared to the potential plot in Figure 4.5. When AC_{rms} is larger than 10 mA, the corrosion rates increase greatly. Despite increasing from the previous data point, the corrosion rates at $AC_{rms} = 20$ mA are still acceptable (≤ 0.02 mm/year). However, an AC_{rms} equal to 50, 100, and 200 mA yield a high corrosion rate, and the carbon steel is not sufficiently protected at these AC magnitudes. Mean corrosion rates with uncertainties are tabulated in Table C.4.

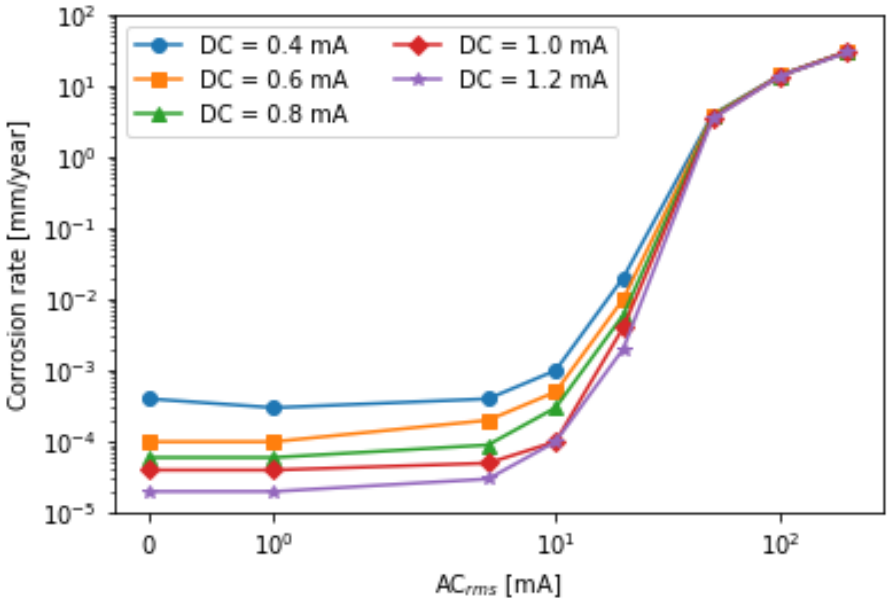

Figure 4.6: Model: Uniform corrosion rate of carbon steel at various combinations of DC and AC impressed to the MMO electrode. C_{dl} and f were maintained at 0.1 F/m^2 and 50 Hz, respectively.

It was attempted to compute the potentials and corrosion rates when impressing an AC_{rms} equal to 500 mA. However, the model solution would not converge for this case. The reader is referred to Section 5.2 for a discussion on this.

4.2.2 Effect of double layer capacitance

To study the effect of the double layer capacitance on the AC corrosion, C_{dl} was varied between 0.01 F/m^2 and 1 F/m^2. Realistic values for the double layer capacitance were hard to find in literature, but Yang et al. [35] calculated it to be about 0.3 F/m^2 for cathodically protected mild steel in artificial seawater. AC_{rms} and DC were varied similarly as above - within the range [0, 200] mA and [0.4, 1.2] mA, respectively. Resulting potentials and corrosion rates are presented in Figure 4.7 for DC = 0.8 mA. Similar plots for DC = 0.4, 0.6, 1.0 and 1.2 mA are included in Section B.2. Tabulated means and their respective uncertainties are stated in Table C.5 and Table C.6 for DC = 0.8 mA.

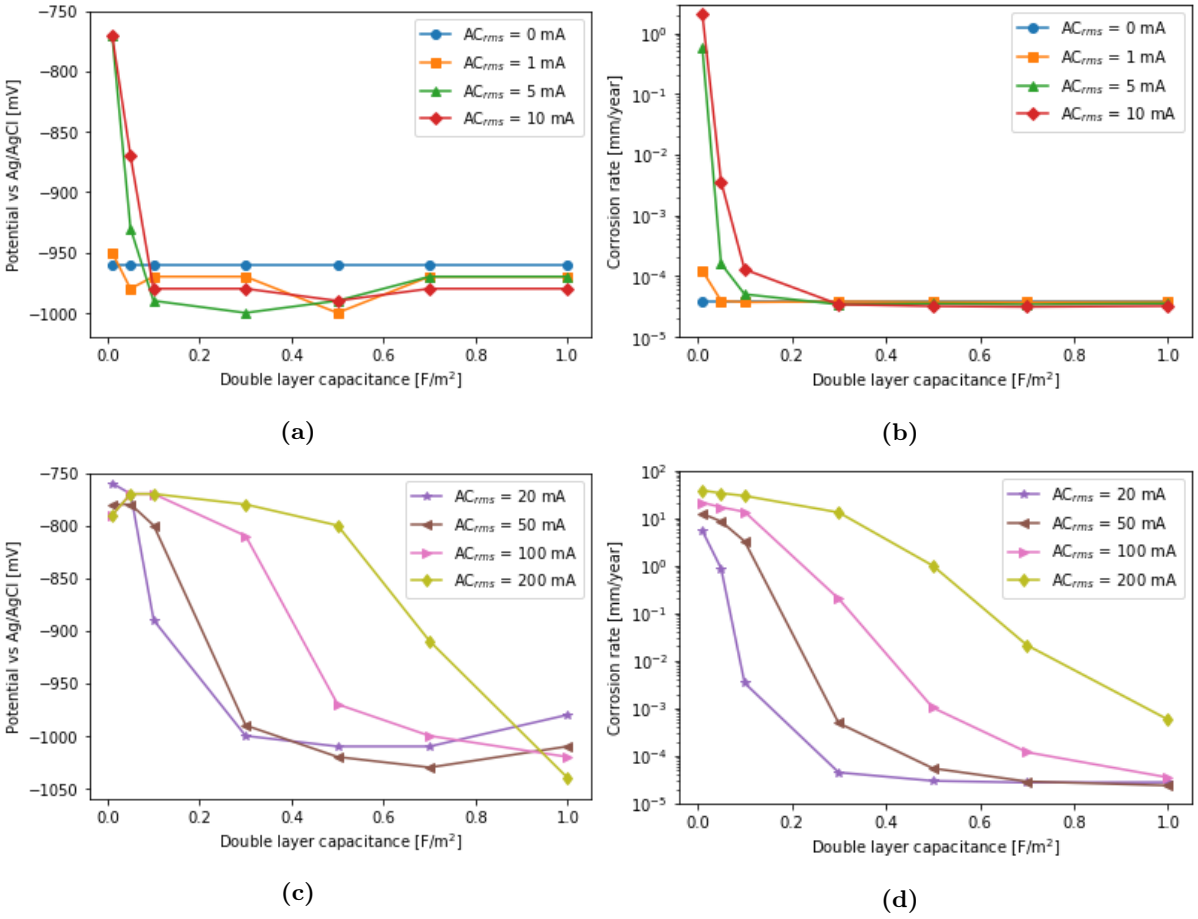

Figure 4.7: Model: Potentials and uniform corrosion rates of carbon steel as a function of C_{dl}, for various ACs impressed to the MMO electrode. The impressed DC is equal to 0.8 mA. Frequency of the AC signal is set to 50 Hz. (a) Potential vs. C_{dl} for small AC magnitudes. (b) Corrosion rate vs. C_{dl} for small AC magnitudes. (c) Potential vs. C_{dl} for large AC magnitudes. (d) Corrosion rate vs. C_{dl} for large AC magnitudes.

From Figure 4.7, it appears that the value of the double layer capacitance has a strong influence on the potential. Subplot (a) in Figure 4.7 shows the potential-dependence of the capacitance value for small AC magnitudes. At $AC_{rms} = 0$, the potential is constant and independent of C_{dl}. When AC_{rms} is increased to 1 mA, the potential still remains fairly constant. Similar potentials are observed for $AC_{rms} = 5$ mA and 10 mA, with an exception for very small values of C_{dl}. Here, the potential is considerably higher. Small capacitance values at these currents do also lead to significant corrosion rates, as showcased in subplot (b).

Similar trends can be observed in subplot (c) in Figure 4.7. At small capacitance values, i.e. far to the left, the potential of carbon steel is quite high. Increasing the capacitance generally decreases the potential, thus protecting the carbon steel. However, the capacitance in which the carbon steel changes from unprotected to protected vary greatly on the AC magnitude. To achieve a potential below -900 mV vs. Ag/AgCl, the necessary capacitance (minimum) is 0.1 F/m^2 for the case where AC_{rms} = 20 mA. When AC_{rms} increases from 20 mA to 100 mA, the minimum capacitance is also increased: from 0.1 F/m^2 to about 0.5 F/m^2. According to subplot (c) and (d), carbon steel exposed to 200 mA AC_{rms} is protected from corroding in seawater at a double layer capacitance of about 0.7 F/m^2. However, carbon steel will corrode at just 20 mA AC_{rms} if the double layer capacitance is only 0.01 F/m^2. Hence, the value of the double layer capacitance affects the AC corrosion strongly.

4.2.3 Effect of frequency

Effect of frequency was investigated by varying f from 30 Hz to 75 Hz. To obtain 15 periods for each case, as pointed out in Section 3.1.4, the total time for the AC application was altered depending on the frequency value. Plots of potentials and corrosion rates are presented in Figure 4.8 for different values of f and AC_{rms}. The DC in this figure is set to 0.8 mA. Similar plots for the other DC values are included in Section B.3. Tabulated means and their respective uncertainties are stated in Table C.7 and Table C.8 for DC = 0.8 mA.

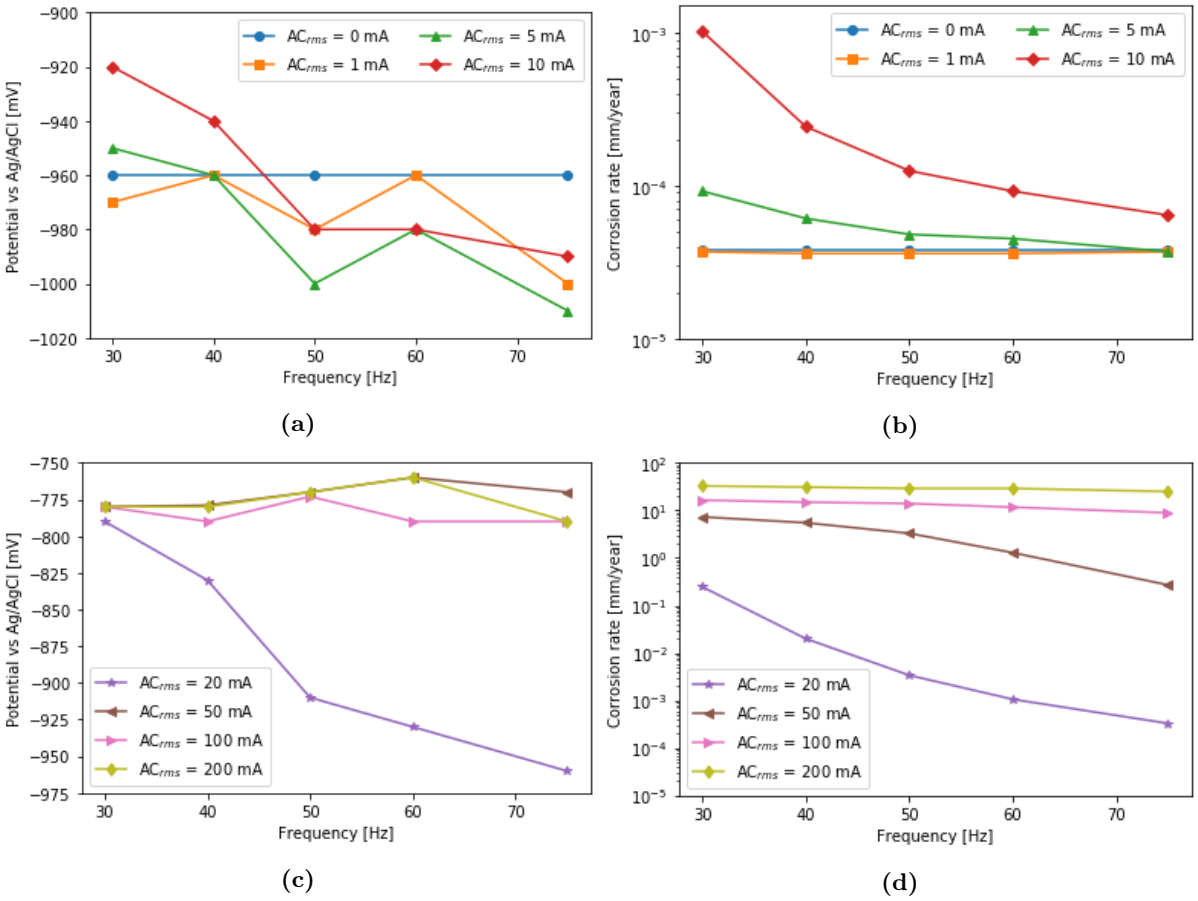

Figure 4.8: Model: Potentials and uniform corrosion rates of carbon steel as a function of f, for various ACs impressed to the MMO electrode. The impressed DC is equal to 0.8 mA, while the double layer capacitance is set to 0.1 F/m^2. (a) Potential vs. f for small AC magnitudes. (b) Corrosion rate vs. f for small AC magnitudes. (c) Potential vs. f for large AC magnitudes. (d) Corrosion rate vs. f for large AC magnitudes.

Figure 4.8 shows that the frequency influences the potential of carbon steel when alternating currents are present. Generally, the potential decreases when the frequency increases. Similarly, the uniform corrosion rate decreases when the frequency increases, as can be seen in subplots (b) and (d). There is especially a noticeable difference in corrosion rate at different frequencies when AC_{rms} = 20 mA. Increasing the frequency of the AC signal from 30 Hz to 75 Hz at this AC magnitude leads to a decrease in the corrosion rate, from $2.46 \cdot 10^{-1}$ mm/year to $3.30 \cdot 10^{-4}$ mm/year. In the same range, the potential decreases with about 170 mV. Similar behavior is observed for an AC_{rms} of 10 mA. According to subplot (b), the corrosion rate decreases by more than one order of magnitude when increasing the frequency from 30 Hz to 75 Hz.

4.2.4 Effect of area and separation distance

Until this point, the surface areas of carbon steel and copper have been equal (4 x 4 cm each). Varying the surface area ratio r_A, i.e. the steel/copper ratio, gave the potentials shown in Figure 4.9 at DC = 0.8 mA, for different magnitudes of AC. For each variation of the surface areas, the surface area of either copper or steel was kept constant, while the other surface area was reduced in the x-direction. The mean potentials and $2s$ are tabulated in Table C.9, together with the dimensions (in x-direction) of steel and copper in each case.

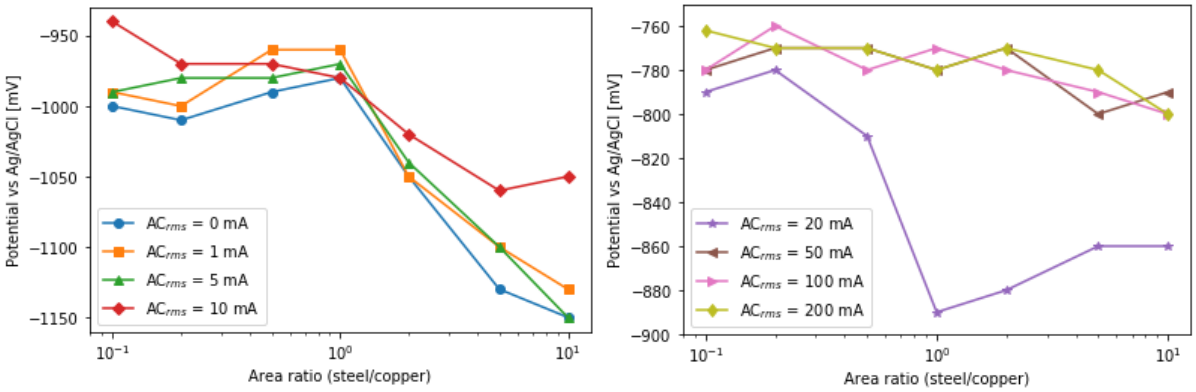

(a) **(b)**

Figure 4.9: Model: Potential of carbon steel as a function of the area ratio steel/copper, for various ACs impressed to the MMO electrode. The impressed DC is equal to 0.8 mA. Frequency of the AC signal and the double layer capacitance is kept constant and equal to 50 Hz and 0.1 F/m^2, respectively. Note that the y-axes are scaled differently in the two subplots.

According to Figure 4.9, an area ratio of 1 gives the least protection (i.e. highest potential) at small AC magnitudes. This area ratio does also result in the highest total surface area. When AC_{rms} increases to about 10 mA, another trend is observed. Here, the potential decreases with increasing area ratio, meaning that the carbon steel is least protected when there is excess copper. Consequently, an area ratio equal to 10 gives the highest protection.

Further increase of the AC_{rms}, up to 20 mA, shows a new dependence on the area ratio. At this AC level, it appears that the carbon steel is most protected at an area ratio of 1. This dependency is the exact opposite of the dependency at small ACs, where $r_A = 1$ gave the least protection. At even higher AC levels, the trend is unclear. If anything, an AC_{rms} above 50 mA suggest that the steel is more protected at a high area ratio. However, the uncertainty in the values are larger than the potential difference, so it is difficult to conclude. Regardless of the area ratio, the protection of steel is still limited for ACs above 50 mA, as the potential is significantly higher than the upper protection limit of -900 mV vs. Ag/AgCl.

So far, the potential difference between steel and copper has not been reviewed. Figure 4.10 shows two new geometries created; one where the copper and steel are placed closer to each other, and one where they are placed in separate ends of the electrolyte. The potential difference between copper and steel is plotted in Figure 4.11 for these two geometries, in addition to the original geometry in Figure 3.1. These are also tabulated in Table C.10, together with the uncertainty of the computations. For small ACs, the potential difference is only 1-2 mV, where the furthest distance leads to the largest potential drop. When the AC surpasses 20 mA, the potential drop increases greatly, followed by a large and negative potential difference at the highest AC level. Generally, the larger the distance between the electrodes, the larger (absolute) potential drop.

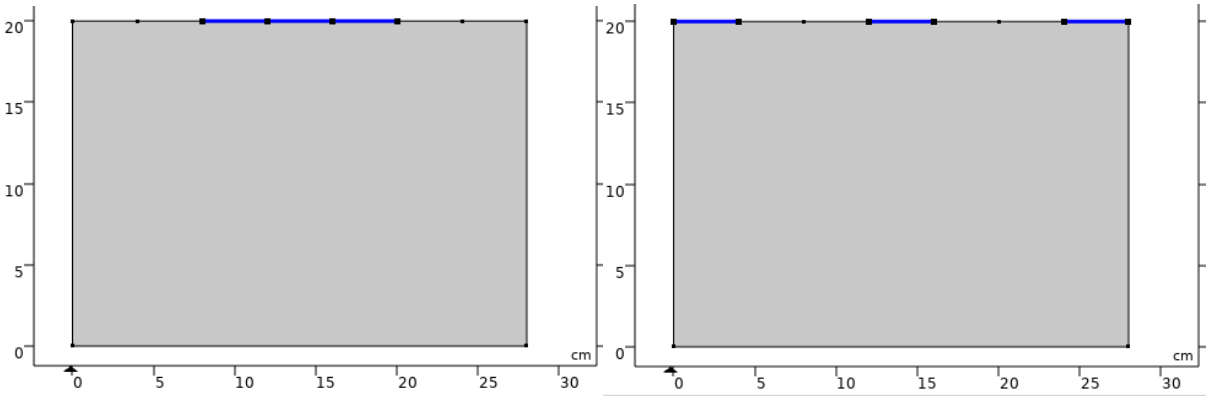

(a) (b)

Figure 4.10: Model: Geometry when the copper and steel are (a) placed closer (in contact with MMO), and (b) placed further away from each other. In (a), the distance copper-MMO and steel-MMO are both 0 cm. In (b), these distances are both 8 cm.

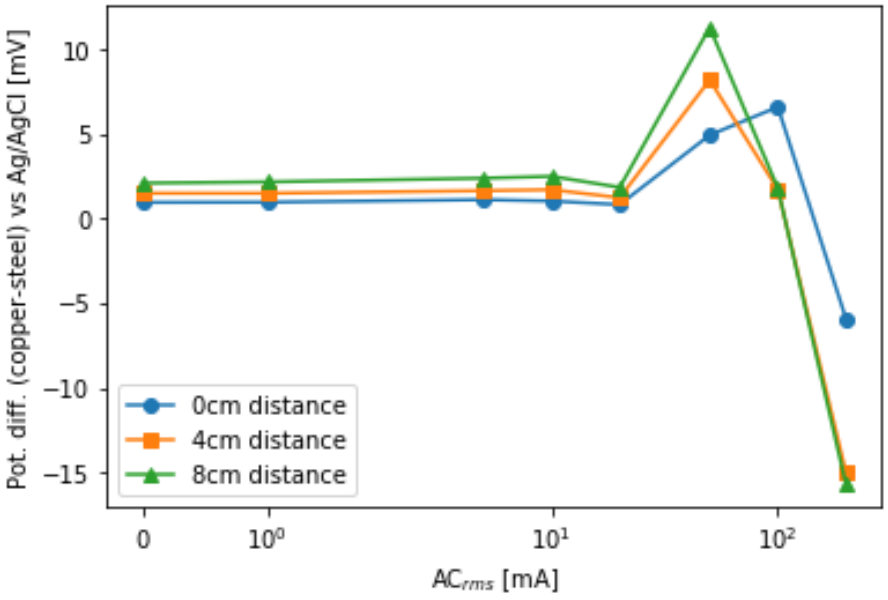

Figure 4.11: Model: The potential difference between copper and steel at various distances between the electrodes, and with impressing various ACs to the MMO electrode. Impressed DC is 0.8 mA. The specified distance is the distance between steel (or copper) and MMO. For the actual total distance between steel and copper, these can be observed in Figure 3.1 and Figure 4.10.

4.2.5 Removal of copper

The effect of copper on the system was investigated by removing copper from the system. Resulting potentials and corrosion rates are plotted in Figure 4.12 and tabulated in Table C.11 and Table C.12. It can be observed that the steel is now overprotected when impressing the same DC as in previous cases, and while impressing small ACs. Increasing the AC_{rms} up to 20 mA suggests that the corrosion rate increases to between 0.27 and 0.58 mm/year. The corrosion rate increases greatly at ACs above 20 mA; for 50 mA, the corrosion rate of carbon steel increases to an order of magnitude of 10^1 mm/year.

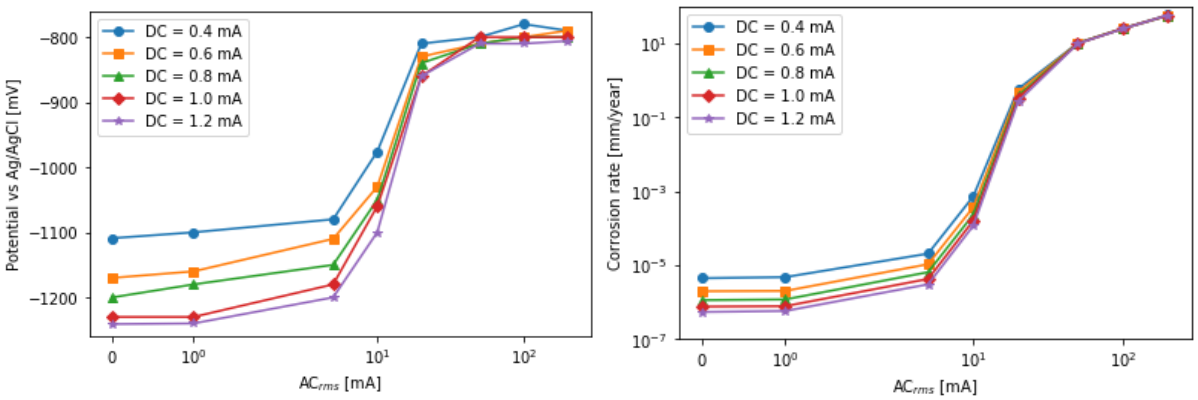

(a) (b)

Figure 4.12: Model: Potentials and uniform corrosion rates of carbon steel at various combinations of DC and AC impressed to the MMO anode. In this computation, the copper was removed from the system. C_{dl} and f were maintained at 0.1 F/m^2 and 50 Hz, respectively.

Figure 4.13 shows a comparison of the potentials and corrosion rates of carbon steel when copper is present vs. absent. It appears that, at low levels of AC, inclusion of copper reduces the protection of carbon steel. There is a shift in behavior for AC_{rms} = 20 mA, in which the potential and corrosion rate are higher when the copper is absent. According to this, the risk of AC corrosion can be reduced by connecting the carbon steel to copper at this AC magnitude.

At high AC levels, subplot (a) and (b) in Figure 4.13 contradict each other. Based on the potential plot, the absence of copper lowers the potential of carbon steel, yielding a potential closer to the protection potential range. However, the corrosion rate plot suggests that the corrosion rate increases in absence of copper. It should be noted that the corrosion rates are still extremely high at high ACs, so the presence or absence of copper has little effect in this specific case.

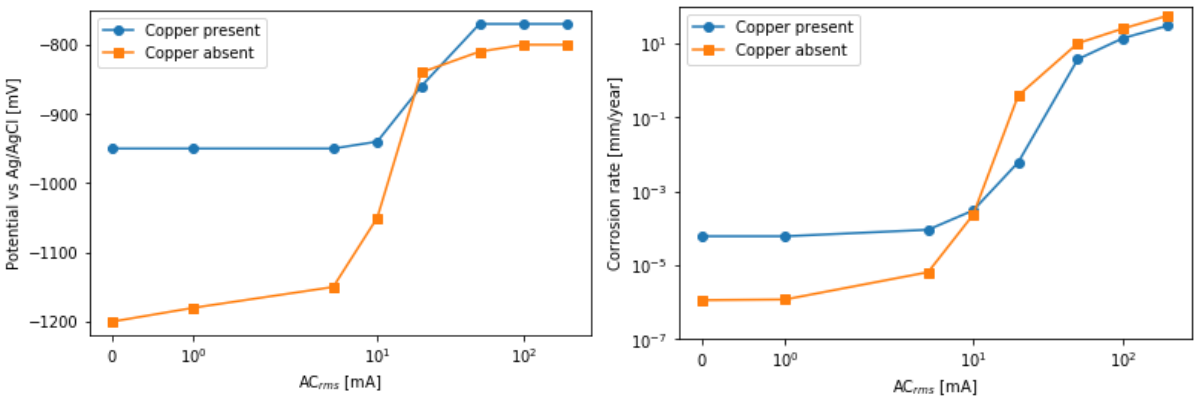

(a) **(b)**

Figure 4.13: Model: Potentials and uniform corrosion rates of carbon steel at various ACs impressed to the MMO electrode, both in absence and presence of copper. DC, C_{dl} and f were maintained at 0.8 mA, 0.1 F/m^2 and 50 Hz, respectively.

4.3 Cyclic polarizations

4.3.1 Copper

A cyclic polarization scan of copper in synthetic seawater is presented in Figure 4.14. As the anodic regime has been analyzed in an earlier work [7], only the cathodic regime was investigated in this work. Starting from the open circuit potential (OCP), the copper was polarized down to -1200 mV vs. OCP, and then polarized back up to the OCP. Due to the surface oxides that were initially present on the copper, the first scan (from OCP to -1200 mV vs. OCP) contributed to the reduction of these oxides, as indicated by a positive slope just below 1 A/m^2. However, it is also clear that ORR occurs around this current density, as the polarization curve becomes vertical at a certain point - a typical feature of the diffusion-limited ORR. Therefore, it was necessary to polarize the copper back to OCP in order to get a better measure of the ORR. Using the polarization curve, two regions were further analyzed.

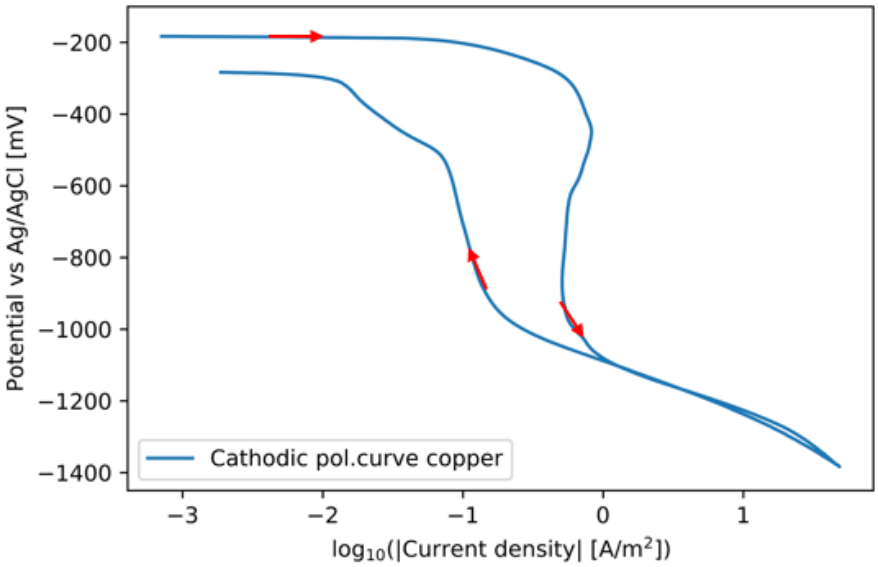

Figure 4.14: The results of a cyclic polarization scan of copper in synthetic seawater. The red arrows indicate the scan direction.

Various linear regimes can be observed at potentials below the OCP in Figure 4.14. Just below the open circuit potentials, it can be assumed that oxygen reduction is the dominant reaction. In Figure 4.15, a linear regression was performed in this area. The slope of this curve gave the cathodic Tafel slope of ORR on copper, which was found to be -285 mV/dec. Extrapolation of the Tafel curve to the reversible potential of ORR gave an estimate of the exchange current density. As the reversible potential of ORR in the given environment was 558 mV vs. Ag/AgCl, i_0 was estimated to be about $1.1 \cdot 10^{-5}$ A/m^2.

When the potential of copper starts to drop below -1000 mV vs. Ag/AgCl, the dominant reaction will typically be hydrogen evolution. The extrapolated Tafel curve of HER on copper is presented in Figure 4.16. Calculations showed that the reversible potential of HER was -556 mV vs. Ag/AgCl here, giving an exchange current density of $1.9 \cdot 10^{-4}$ A/m^2. From the slope, b_c was estimated to -143 mV/dec.

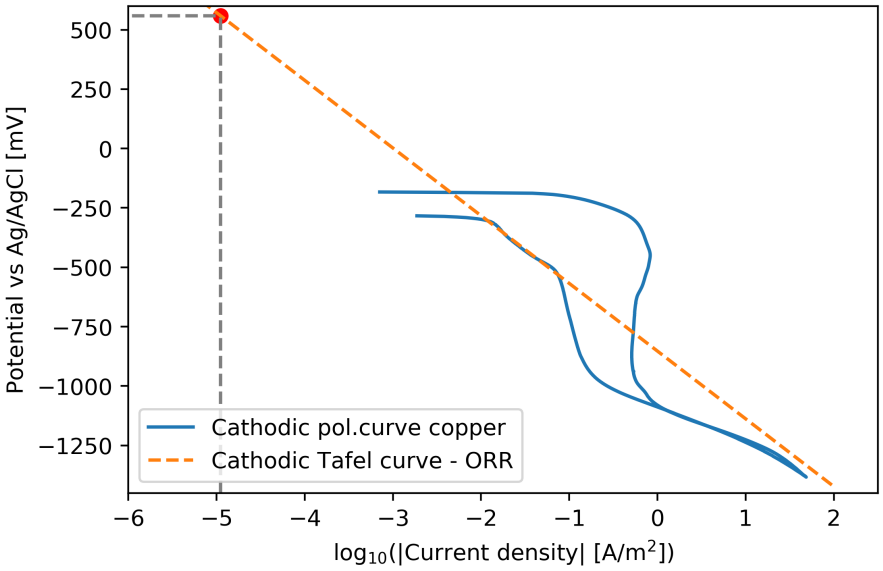

Figure 4.15: The cathodic polarization curve of copper in synthetic seawater, including the Tafel extrapolation of ORR. The cathodic Tafel slope and exchange current density were determined to be -285 mV/dec and $1.1 \cdot 10^{-5}$ A/m^2, respectively.

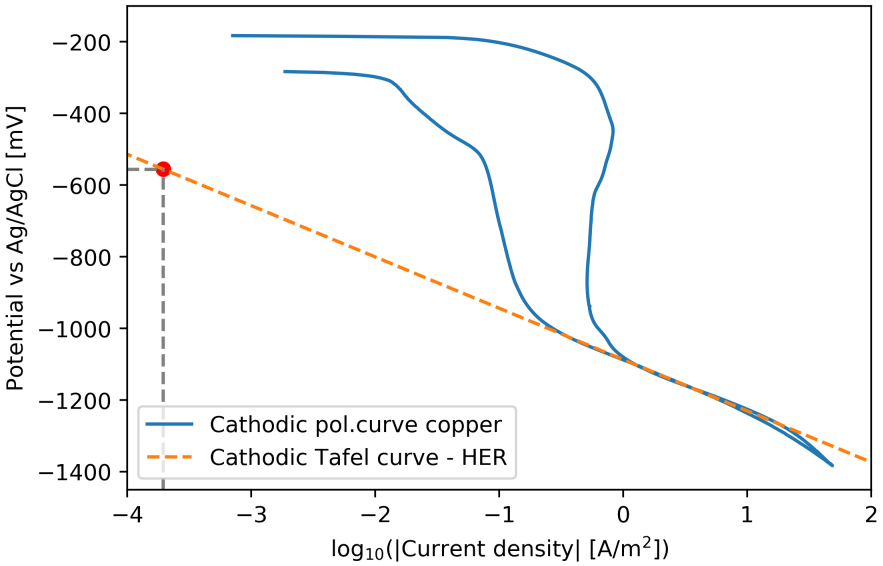

Figure 4.16: The cathodic polarization curve of copper in synthetic seawater, including the Tafel extrapolation of HER. The cathodic Tafel slope and exchange current density were determined to be -143 mV/dec and $1.9 \cdot 10^{-4}$ A/m^2, respectively.

4.3.2 Platinum

Similarly, cyclic polarization scans were carried out for platinum, both in anodic and cathodic direction. The polarization curves for platinum in synthetic seawater are shown in Figure 4.17. In both cases, the potential started off at the OCP-level, followed by polarizing the platinum ± 1200 mV vs. OCP.

Ideally, the anodic Tafel curve of two reactions (OER and CER) should be determined by the obtained anodic polarization curve. As the reversible potential of O_2/OH^- is lower than the reversible potential of Cl_2/Cl^- in the system, it was assumed that oxygen evolution would

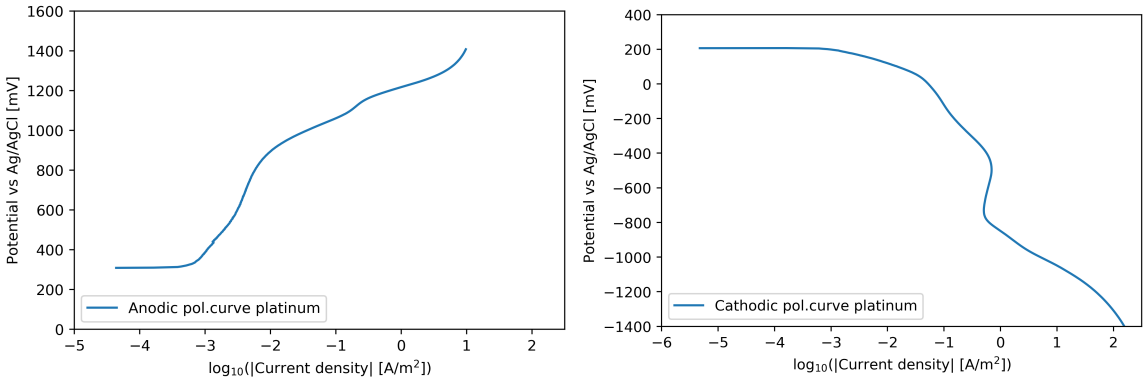

(a) Anodic polarization curve.

(b) Cathodic polarization curve.

Figure 4.17: Polarization curves for platinum in synthetic seawater, separated into an anodic (a) and a cathodic (b) polarization curve.

dominate in the lower potential region. This gave the Tafel curve in Figure 4.18, with b_a = 146 mV/dec and $i_0 = 3.4 \cdot 10^{-5}$ A/m^2 for OER on platinum.

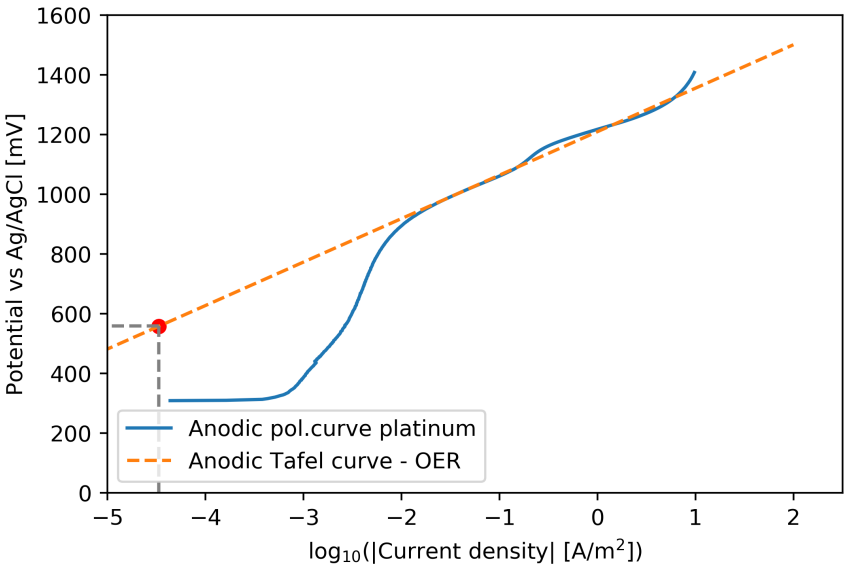

Figure 4.18: The anodic polarization curve of platinum in synthetic seawater, including the Tafel extrapolation of OER. The anodic Tafel slope and exchange current density were estimated to be 146 mV/dec and $3.4 \cdot 10^{-5}$ A/m^2, respectively.

At higher potentials, evolution of chlorine dominated on the anode. The anodic Tafel curve suggested a slope of 98 mV/dec for CER on platinum. With the reversible potential of Cl_2/Cl^- being equal to about 1034 mV vs. Ag/AgCl, extrapolation of the Tafel curve to this potential gave the exchange current density, $i_0 = 1.4 \cdot 10^{-2}$ A/m^2, as demonstrated in Figure 4.19.

Possible reduction reactions at the platinum are considered to be HER and ORR. Using similar reasoning as for copper, ORR is considered as the dominant reaction in the upper region of the cathodic polarization curve. Extrapolation of the cathodic Tafel curve is shown in Figure 4.20. This gave an exchange current density of $1.4 \cdot 10^{-3}$ A/m^2, with the slope equal to -374 mV/dec.

At potentials around -1000 mV vs. Ag/AgCl, hydrogen evolution dominates at the cathode. Hence, the cathodic Tafel curve of HER on platinum can be extrapolated as shown in Figure 4.21. Calculations showed that $i0$ was as high as $2.3 \cdot 10^{-2}$ A/m^2, with b_c equal to -187 mV/dec.

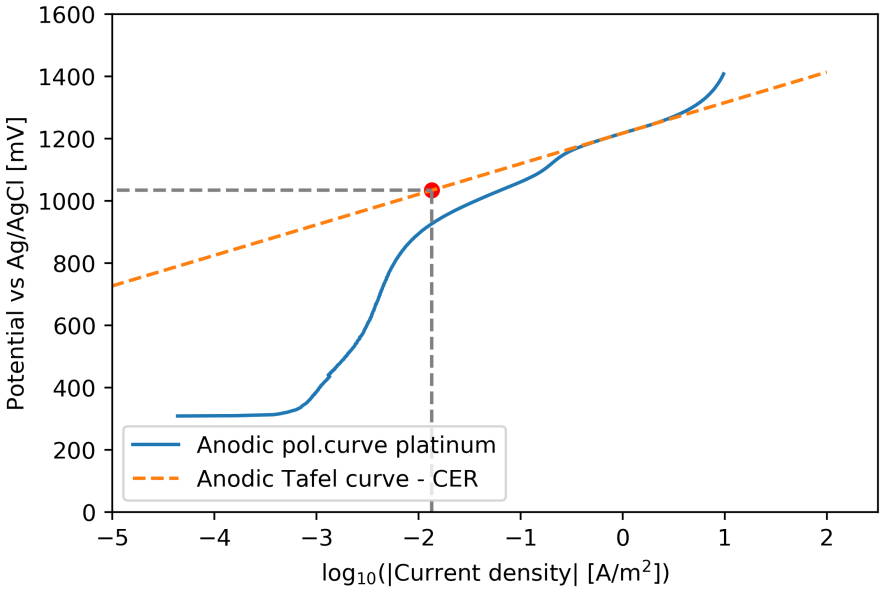

Figure 4.19: The anodic polarization curve of platinum in synthetic seawater, including the Tafel extrapolation of CER. The anodic Tafel slope and exchange current density were estimated to be 98 mV/dec and $1.4 \cdot 10^{-2}$ A/m^2, respectively.

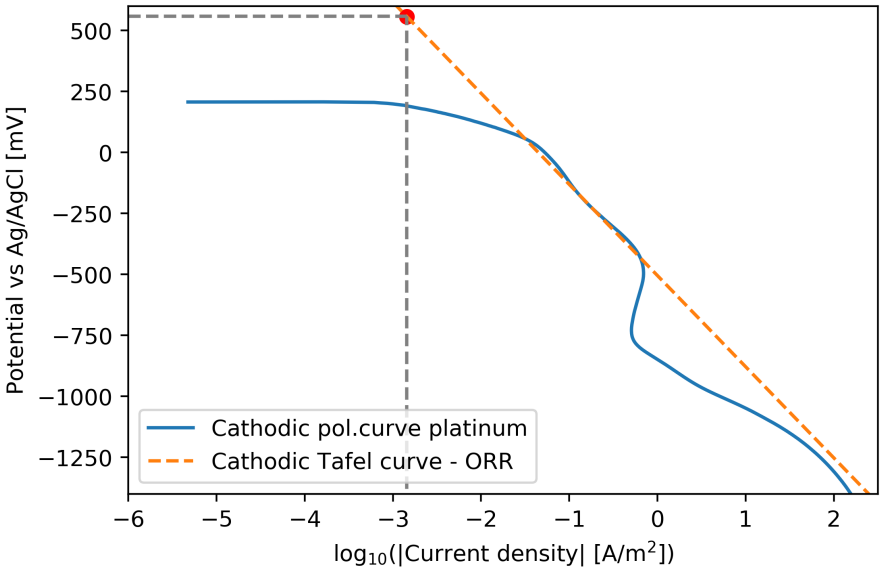

Figure 4.20: The cathodic polarization curve of platinum in synthetic seawater, including the Tafel extrapolation of ORR. The cathodic Tafel slope and exchange current density were determined to -374 mV/dec and $1.4 \cdot 10^{-3}$ A/m^2, respectively.

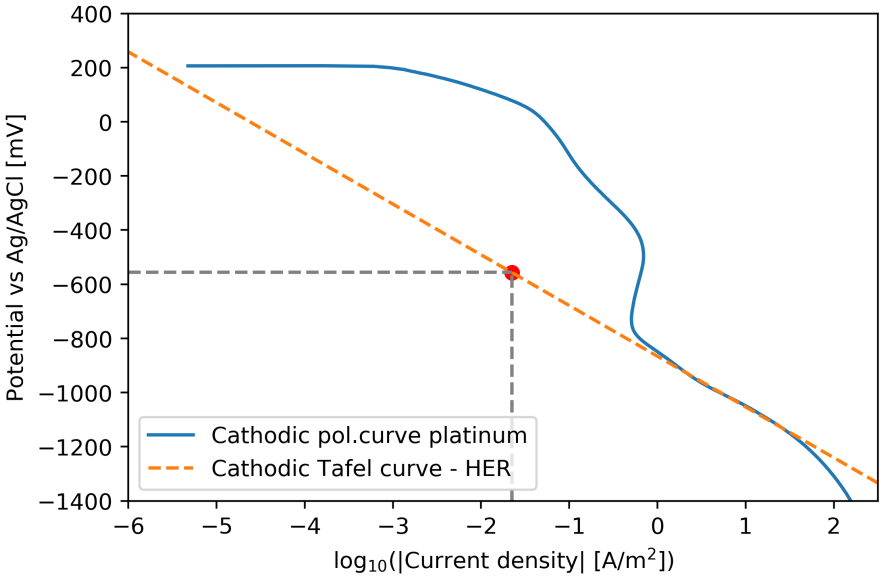

Figure 4.21: The cathodic polarization curve of platinum in synthetic seawater, including the Tafel extrapolation of HER. The cathodic Tafel slope and exchange current density were estimated to be -187 mV/dec and $2.3 \cdot 10^{-2}$ A/m^2, respectively.

5 Discussion

5.1 AC corrosion on steel - with platinum as inert anode

Comparing the modeling and experimental results in Section 4.1, similar trends can be observed. Increasing AC generally increases the potential, and increasing DC generally decreases the potential. However, in the experimental results, the case of a high AC consistently results in a higher potential compared to the other AC magnitudes. These results are not found in the modeling results: for small DCs, a larger AC appears to lead to a more negative potential, which is particularly noticeable for the case where the double layer capacitance is large (= 0.5 F/m^2).

Of course, it is difficult to quantitatively compare the modeling with the experimental work since the geometries are not identical. However, the results also differ qualitatively. According to Figure 4.2, obtained from modeling, increasing AC beyond a certain limit leads to stabilization of the potential. To obtain a working model, several assumptions must be made. In particular, the oxidation reactions are simplified in the model, since the only oxidation reaction defined on carbon steel is $Fe \longrightarrow Fe^{2+}$. Since the formation of precipitates and oxides is excluded from the modeling, this could lead to unrealistic results. When steel dissolves in laboratory experiments, a type of oxide layer is formed, which reduces the overall corrosion as well as lowering the potential of carbon steel. Comparing Figure 4.4 with Figure 4.2, increasing AC to the highest value gives a higher potential. However, the increase in potential according to the modeling is much larger than the experimental increase. At higher AC values, the steel is polarized longer in the anodic direction, and the dissolution of the steel increases. This underlines the importance of correctly describing the anodic reactions and passivation when large ACs are impressed to the system.

5.2 AC corrosion on steel - with mixed metal oxide (MMO) as inert anode

When a DC was impressed for 10 000 seconds before applying AC, the steel was cathodically protected. It is known that when carbon steel is cathodically protected in seawater, calcareous deposits form near the steel surface due to the local increase in pH. The formation of these deposits reduces the corrosion rate, because they impede the diffusion of O_2, thus reducing the reaction rate of ORR. Since the precipitation of these deposits ($Mg(OH)_2$ and $CaCO_3$) is not implemented in the modeling, they will not affect the modeling results. Therefore, the calculated corrosion rates could be high compared to a real scenario if the steel is cathodically protected. Calcareous deposits will also reduce the active surface area of steel, meaning the AC current density could become higher in reality. Of course, when AC is applied, the potential will change. If the applied AC is relatively high, the protective effect of the calcareous deposits deteriorates because 1) hydrogen evolves at low potentials, which could reduce the adhesion of the deposits, and 2) the formation of $CaCO_3$ is inhibited, making oxygen diffusion less hindered [36, 37, 38, 39].

Exposure of AC to a galvanic steel-copper-MMO couple resulted in an increase in both the potential and the corrosion rate. This relationship is also supported by several studies [6, 24, 25, 40]. For cathodically protected carbon steel exposed to AC, an AC_{rms} of 20 mA and below appears to be acceptable, as shown in Figure 4.6. This current corresponds to a current density of i_{AC} = 12.5 A/m^2. Fuchs et al. [41] estimated that an AC current density greater than 20 A/m^2 is unacceptable for steel in seawater, where the corrosion rate exceeded 0.2 mm/year. Similarly, Wakelin et al. [42] found that no corrosion was observed on steel at current densities i_{AC} below 20 A/m^2 and that corrosion was unpredictable in the range 20-100 A/m^2. Ideally, the modeling in this work should have explored even more ACs to get a better idea of what the actual acceptable i_{AC} are. However, it is clear from Figure 4.6 that the corrosion rate is unacceptable

when AC_{rms} reaches 50 mA - which corresponds to 31.25 A/m^2. This result contradicts the work of Wakelin et al. [42]. On the other hand, it must be emphasized that their work was on steel alone, and not steel electrically connected to copper.

Goidanich et al. [25, 43] found that in the positive (anodic) half cycle of AC interference, the corrosion rate increased with anodic polarization on the carbon steel. In the negative (cathodic) half cycle, they observed that the corrosion rate decreased with cathodic polarization, but not to the same extent as the increase during the positive half cycle. They reasoned that this was due to the non-linear relationship between potential and current density for the anodic polarization curve. Therefore, the anodic half cycle increased the corrosion rate more than the cathodic half cycle decreased it, resulting in a net positive increase in corrosion rate when AC is applied.

Bosch and Bogaerts [24] reported an exponential relationship between corrosion rate and applied AC voltage. In this work, a similar relationship is found, with the corrosion rate in Figure 4.6 increasing exponentially with the applied AC. However, when the AC becomes too high, i.e., higher than 50 mA, this relationship is no longer applicable. At these AC values, it also appears that the mean potential converges towards a limit - between -800 and -750 mV vs. Ag/AgCl, as shown in Figure 4.5. Overall, this is a behavior that has not been justified in the literature.

As mentioned in the results, an attempt was made to impress an AC_{rms} = 500 mA, but the solution did not converge. Neglecting the DC magnitude, since it is much smaller than the AC magnitude, the maximum current demand is equal to the amplitude of the current signal, i.e., 500 mA $\cdot \sqrt{2}$ = 707 mA. For the model geometry, this corresponds to 442 A/m^2. The only oxidation reaction implemented on the MMO anode is CER. Because of the diffusion of Cl^-, there is a limit to the current density achieved by this reaction alone. According to the literature, the typical limiting current density of CER in seawater is 1000-10000 A/m^2, but this depends on parameters such as salinity and flow [44]. In the modeled system, the limiting current density for CER is probably lower than the literature value because convection is not implemented [45]. When the fluid flow rate is low, the thickness of the Nernst diffusion layer δ increases, which means that the limiting current density decreases, as shown by equation (19). Therefore, when 500 mA AC_{rms} is impressed, the (maximum) current demand could be higher than the limiting value, causing the solution to diverge.

5.2.1 Effect of double layer capacitance

The effect of double layer capacitance on AC corrosion was studied by varying C_{dl} between 0.01 and 1 F/m^2, as presented in Section 4.2.2. It was found that this parameter strongly influences the behavior of the electrochemical system. According to subplot (d) in Figure 4.7, it appears that carbon steel is adequately protected up to 30 A/m^2 when doubling the C_{dl} from 0.1 F/m^2 to 0.2 F/m^2. From equation (45), it can be seen that the non-Faradaic current density is proportional to the value of the double layer capacitance. The total impressed current, both AC and DC, consists of a Faradaic and non-Faradaic term that contribute equally to the total current. An increase in C_{dl} means that i_{nf} increases and consequently i_f decreases. Since the current density in the Butler-Volmer equation (7) is the Faradaic current density, it is clear that C_{dl} affects the potential-current relationship. Considering equation (47), the impedance of the double layer capacitance is inversely proportional to the double layer capacitance. Hence, the increase of i_{nf} and the decrease of corrosion rate with increasing C_{dl} follow the trends typically observed with the impedance of the system. This trend was also validated by Ibrahim et al. [46].

In the modeling, the total interfacial capacitance was set equal to the capacitance of the double layer. Since oxide layers were not considered in the modeling, the capacitive effects of oxide layers on a metal surface were also ignored. Overall, if this had been modeled, the actual

capacitance would have increased, effectively resulting in a capacitance equal to the sum of the double layer capacitance and the dielectric capacitance. As mentioned earlier, an increase in capacitance results in a decrease in the corrosion rate because the capacitors act as a drain for AC [47]. There is a possibility that the capacitance changes during the application of AC, or that it depends on the AC magnitude. In the experimental work (on Pt), the phase angle ϕ was found to vary between -62° (at low AC) and -40° (at high AC). Thus, it appears that the fraction of non-Faradaic currents is smaller when AC is large, because a phase shift closer to 0 indicates that the electrical circuit element is more like a resistor (i.e., Faradaic). Such behavior could promote corrosion of steel at high AC levels. However, these results do not necessarily mean that the capacitance decreases. Ibrahim et al. [46] suggested that the total capacitance at an electrode surface increases with time and AC voltage. Since the amount of corrosion products increase with time and AC voltage (as discussed previously), the steel surface area increases, meaning the total charge stored by the capacitor could increase with time. Thus, the corrosion rate decreases. The increase in capacitance could explain why the model gave significantly higher corrosion rates at high AC magnitudes, as corrosion products were not included in the modeling and the capacitance was set constant during the computations.

5.2.2 Effect of frequency

The modeling results generally suggest that both the potential and the corrosion rate decrease with increasing frequency of the applied AC signal, as shown in Figure 4.8. Similar to the increase in double layer capacitance, equation (47) shows that increasing the frequency decreases the impedance of the double layer capacitance. Since the impedance of the charge-transfer resistance is independent of the frequency signal, increasing the frequency increases means that the current will go through the capacitor more. Hence, i_{nf} increases and the corrosion rate decreases. The relationship between the frequency of the AC signal and the corrosion rate of steel has been investigated in several studies [48, 49, 50]. There is a consensus that increasing the frequency decreases the corrosion rate of steel. Guo et al. [49] studied the corrosion of carbon steel in a simulated soil solution when the frequency varied from 10 Hz to 200 Hz during application of AC. In this frequency range, they found that the corrosion rate decreased by a factor of 3, from 1.2 mm/year to 0.4 mm/year, when the applied AC current density was 50 A/m^2.

Fernandes et al. [48] proposed an explanation for the relationship between frequency and corrosion rate based on kinetics - when the frequency is high, the time between anodic and cathodic polarization is short. When steel dissolves into Fe^{2+} and Fe^{3+} in the anodic half cycle, these ions begin to diffuse away from the surface. However, in the cathodic half cycle, there is a possibility that the metal ions will be deposited on the electrode surface. If the time between successive anodic and cathodic half cycles is short, the probability of immediate redeposition in the cathodic half cycle increases. Therefore, the corrosion rate is reduced. However, this does not explain the behavior in the model, since the concentration of Fe^{2+} is assumed to be constant at all times, and redeposition of the dissolved metal is not implemented.

5.2.3 Effect of area and separation distance

To better understand how the galvanic couple is affected by the application of AC, an attempt was made to change the area ratios between steel and copper. The two extremes are when the steel area is relatively small (1.6 cm^2) compared to the copper area (16 cm^2), and when steel (16 cm^2) is significantly larger than copper (1.6 cm^2). For these extremes, the area ratio r_A ($= A_{\text{steel}}/A_{\text{copper}}$) is 0.1 and 10, respectively. For the case of $r_A = 1$, the area ratio in all other results, the areas of steel and copper are both equal to 16 cm^2. Figure 4.9 shows how the

potential relates to the area ratio in the model.

At low AC levels, an area ratio of 1 is the least protective because the potential is highest here. Note that this is also the case for the largest total area. Connecting the steel to a large copper electrode, the galvanic effect will be large and the corrosion of the steel will be enhanced. If the steel area is large as well, the total current demand will also increase. Increasing the level of AC to a medium or high level, an area ratio of 0.1 provides the least protection. At this area ratio, the steel area is small compared to the copper area. It appears that the application of AC has a greater impact on protection here, as this area of steel effectively gives the highest AC current density. Also, for all AC levels except AC_{rms} = 20 mA, a large area ratio gives the higehst protection. At this area ratio, the steel area is large, meaning the AC current density at the steel electrode is low, and the copper area is small (the galvanic effect is minimal). However, it must be emphasized that the potentials at high AC and different area ratios are all quite similar. Moreover, the uncertainties in the calculated potentials shown in Table C.9 are larger than the potential differences at different area ratios.

It is well known from potential theory that when there is a large distance between two electrodes, there is typically a potential difference between the two electrodes. The potential difference increases with both the distance and the conductivity of the electrolyte. Mixed potential theory states that the more noble metal will have a higher potential if there is a potential drop. In this case, that is copper. Figure 4.11 shows how the potential difference varies in the model, while Figure 4.10 shows the different geometries analyzed. Although the distances studied are all quite small, it still shows how dependent the potential drop is on the separation distance. In a real scenario where ships are docked, the distance between the ship hull and the ground electrode could be several meters, resulting in much higher potential drops. At high AC levels, the potential of steel actually appears to be higher than the potential of copper. It is difficult to justify this behavior, but it has already been shown that the model is flawed at relatively high ACs because the anodic processes on steel and copper are not correctly defined.

5.2.4 Effect of copper

The removal of copper from the electrochemical system shows how the copper affects the overall protection of the carbon steel. A comparison of the presence or absence of copper can be seen in Figure 4.13. At negligible AC magnitudes, the theory expects the steel to be better protected when copper is not present. This expectation is confirmed by the model computations. However, when the AC reaches beyond 20 mA, the potentials and corrosion rates no longer correlate. Removing copper at such high AC levels, the potential appears to decrease, but the corrosion rate increases. A likely reason for this behavior is the effect of area. Consider the positive half cycle of the applied AC, that is, when the metals are polarized in the anodic direction. By applying 100 mA AC_{rms} to a steel-copper couple, the current will be distributed between the two metals in the couple. This results in the potentials and corrosion rates as presented in Figure 4.13. When disconnecting or isolating the copper from the system, the AC current density on the steel will be higher because all the current will flow to the steel. One proposed explanation is that the effect of the increased AC current density on the steel cancels out the galvanic effect of connecting the steel to copper, thus increasing the corrosion rate of the steel. Another possibility is that the capacitance decreases when copper is removed, as shown by equation (46). Since capacitance is proportional to area, and the total area decreases when copper is removed, the total charge stored by the capacitor also decreases. Consequently, i_{nf} decreases and i_f increases, leading to an increase in the corrosion rate.

Despite the increase in corrosion rate when copper is removed, the potential appears to decrease. Since copper has a higher (less negative) open circuit potential, copper contributes to an increase in the average potential of steel when they are electrically connected. In summary, for the potential behavior, the increase in potential due to connection with copper is more significant than the increase in average potential due to increased AC current density. Therefore, the potential for the galvanic couple is higher when an equal AC magnitude is impressed. In contrast, the corrosion rate (proportional to the partial current density for metal dissolution) is more dependent on the AC current density.

5.3 Kinetics

In the modeling, it was assumed that the electrochemical system is governed by Tafel kinetics, i.e. that equation (15) and (17) are obeyed. Most of the relevant Tafel parameters were found experimentally, either in this work (Section 4.3) or in a previous work [7]. The kinetics parameters were assumed constant throughout the modeling, meaning they were independent of the applied AC. Goidanich et al. [25] reported, however, that for carbon steel exposed to AC, i_0 increases and b_c decreases in absolute value with increasing AC. Since the exchange current density increases, this could mean that the corrosion rate increases due to the increase in the partial current density of metal dissolution. Goidanich et al. [25] also showed that the steel became less noble when large AC densities were impressed. However, it is not easy to draw conclusions from this alone because the AC dependence for the kinetics of copper is unknown. For example, if copper becomes significantly less noble as AC increases, it could help lowering the corrosion rate of steel when electrically connected.

In some cases it proved difficult to extract linear slopes from the polarization curves gathered experimentally. This problem is clear in Figure 4.15, where it was necessary to polarize the copper sample back to the OCP level in order to obtain a linear relationship for ORR. One could argue that the same procedure should have been executed for the extraction of ORR on Pt. Despite not doing so, Figure 4.20 indicates a distinct linear regime when polarizing platinum in cathodic direction. A possible explanation here is that the OCP level of platinum is significantly higher than for copper, giving the ORR more time before reaching the diffusion limiting current density (indicated by a vertical slope). Also, the amount of oxides on the platinum surface is probably more limited, as platinum generally does not dissolve (at least not to the same extent as copper), meaning oxygen will be the dominant reduction reaction at these potentials. A possibility was to add the experimental curves directly into the model. However, it was challenging to relate the experimental curve to one specific reaction, as there were several reactions occurring per polarization curve.

A limiting current density for ORR in seawater was set to 5 A/m^2 in the COMSOL model. Based on the laboratory experiments, the current reaches a limit at just below 1 A/m^2, which can be observed in Figure 4.14 and in the cathodic part of Figure 4.17. This could in turn yield a more negative potential experimentally compared to the modeling, as the limiting current for ORR appears lower, meaning more hydrogen must be evolved at a lower current density.

There are several issues related to obtaining kinetics parameters at electrodes experimentally. Electrochemical properties of electrode surfaces are, to a large extent, influenced by specific adsorption of anions [51]. In seawater, the concentration of chloride anions is quite high. Hence, the number of surface sites on the electrode could be reduced, effectively decreasing the active surface area of the electrode. Kinetics parameters, in particular the exchange current density, is strongly dependent on the active surface area. The decrease in area will in turn make the actual exchange current density higher than the calculated exchange current density.

In literature, it is more common to study polarization curves in a strongly acidic or alkaline environment. Because of the low (or high) pH, the concentration of H^+ (or OH^-) is large. When investigating e.g. HER on carbon steel in this environment, the concentration of H^+ (or OH^-) is relatively stable, which removes the concentration effect on the final polarization curves. In seawater at pH=8, the concentration of OH^- is 10^{-6} mol/L. By polarizing the carbon steel in cathodic direction, the concentration of OH^- increase greatly with time, and by the end of the polarization scan, the relative change in OH^- is large near the carbon steel. From equation (9), it is clear that i_0 is dependent on the concentration of the species involved in the reaction, making it beneficial to keep the concentrations relatively stable throughout the measurement.

As mentioned, anodic Tafel parameters on MMO were obtained from literature. Work by Yeo et al. [52] suggested that the exchange current density of OER on $RuIrO_x$ anodes was $4 \cdot 10^{-10}$ A/m^2 at pH=0. Reksten et al. [53] showed that the reaction order with respect to H^+ for OER was -1.3 between pH=0 and pH=3 on $Ir_{0.3}Ru_{0.7}O_2$. Assuming a constant reaction order up to pH=8, and assuming that the chlorides will not affect the kinetics of OER, i_0 in seawater (at pH=8) was calculated as 10 A/m^2 on MMO using equation (11). This i_0 of OER is 10 times the magnitude of the i_0 of CER at the same anode. Knowing that the oxygen efficiency of MMO anodes typically are low [21], it was determined that the extrapolation was incorrect. To avoid oxygen evolution dominating on the MMO anode, the possibility of OER on MMO was excluded in the model. Practically, this means that the oxygen efficiency was set to 0, which could have some implications on the overall system. Since OER is not defined on MMO, steel, or copper, there are no sources for O_2 in this case. To ensure that the modeled seawater had access to oxygen at all times, the oxygen concentration at the electrolyte-air interface was set constant. This also ensures that oxygen diffuses from the electrolyte surface and spreads throughout the electrolyte as oxygen is reduced at the cathode(s).

5.4 Further work

To be able to use the results from this work in a practical manner, some things need to be modified. Overall, the model gives good and reasonable results for both potential and corrosion rate upon application of AC. Also, the model's dependency on variables such as double layer capacitance and frequency are in-line with both theory and literature. However, the model struggles when the AC level gets too high. With that in mind, the following points are proposed to be worked on further:

- **Chemical reactions and oxide formations:** To better model the reality, more chemical reactions need to be added in the system. As the developed model mainly consider electrochemical reactions, the formation of oxides and deposits on the electrode surfaces are not modeled. For problems involving cathodic protection, the formation of e.g. calcareous deposits on the electrode surfaces will affect the results greatly, though to a less extent when AC is applied. Precipitations could be implemented by use of the "quasiparticle model" - a model developed by Clark et al. [54].
- **Several alternating currents:** In the current work, alternating currents ranging from 1 mA to 200 mA were investigated. However, it was found that currents in the range 20-50 mA were most interesting, as the steel went from being protected to corroding significantly in this range. It is suggested to include several alternating currents in this range, to better understand the effect of AC on the protection of carbon steel.

- **Current distribution:** Other interesting results that could be obtained from the current model is how the current distributes on the two electrodes (steel and copper). The current distribution could help understanding the effect of the applied AC, and perhaps explain certain phenomena - e.g. why the potential of steel is higher than the potential of copper at high AC levels.
- **Modeling of ships in 3D:** To better understand the effect of connecting ships to onshore power, it is suggested to modify the geometry to a ship geometry in three dimensions. Inclusion of more realistic ship hull materials (i.e. specific carbon steel or aluminum alloys) and substituting the current geometry with a ship geometry would be an option. However, this will require larger computational resources.
- **Coating:** Implementing coating and its deterioration could be interesting to include in the model. Coating can be included by defining the thickness of the initial coating, type of coating, and breakdown factors.
- **Application in other industries:** Later down the line, the model could be expanded and perhaps utilized in other industries where AC corrosion is a threat to a system consisting of one or several electrode materials. For example marine structures that are cathodically protected, either by ICCP or by sacrificial anodes.

6 Conclusion

Finite element modeling in COMSOL Multiphysics® was carried out to investigate how external alternating and direct currents affected the corrosion of carbon steel connected to copper. The modeling was done by impressing various currents to an inert anode and computing the potential and corrosion rate of the steel. The main conclusions of the work are summarized below:

- The application of AC to a galvanic couple of steel and copper generally increases both the potential and the corrosion rate of the steel. Using MMO as an inert anode in the system, it was found that applying $AC_{rms} = 20$ mA to a cathodically protected steel-copper couple was acceptable ($\sim 10^{-3} - 10^{-2}$ mm/year), but increasing the AC to 50 mA resulted in severe corrosion rates ($\sim$4 mm/year). These currents were equivalent to 12.5 A/m^2 and 31.25 A/m^2, respectively. An exponential relationship was observed between the corrosion rate and the applied AC up till 50 mA. The exponential relationship agrees with the literature. At AC levels $\geq$ 50 mA, the model suggested that the mean potential converged toward an upper limit. Here, the computed corrosion rates were extremely high - about 4 mm/year ($AC_{rms} = 50$ mA), 14 mm/year ($AC_{rms} = 100$ mA), and 30 mm/year ($AC_{rms} = 200$ mA). This behavior was attributed to major simplifications in the modeled dissolution reactions and a lack of chemical reactions (e.g., formation of corrosion products and precipitates) in the modeling.

- The effect of the double layer capacitance on AC corrosion was investigated. It was found that the corrosion rates are strongly dependent on this parameter. Increasing the double layer capacitance from 0.1 F/m^2 to 0.7 F/m^2 decreased the corrosion rate (at $AC_{rms} =$ 200 mA) by about three orders of magnitude - from 29 mm/year to $2.12 \cdot 10^{-2}$ mm/year. The decrease in potential and corrosion rate with increasing double layer capacitance was confirmed by literature and explained by impedance theory.

- Modeling results suggest that frequency affects the potential and corrosion rate when AC is applied. It was found that both potential and corrosion rate decreased when frequency was increased. At $AC_{rms} = 50$ mA, the corrosion rate decreased from 7.3 to 0.27 mm/year when the frequency was increased from 30 Hz to 75 Hz. The relationship between frequency and corrosion rate was attributed to the dependence between frequency and impedance of the capacitance. An increase in frequency leads to a decrease in impedance and thus an increase in non-Faradaic current and a decrease in Faradaic current.

- Altering the area ratios of steel/copper between 0.1 and 10 proved that the electrochemical system was dependent on the area ratio. However, it was observed that the effect of area ratio depended on the magnitude of the impressed AC as well. At low AC levels, it was discovered that an area ratio of 1 gave the least protection. However, this was also the case with the largest total surface area, and a probable reason as to why it showed a relatively high potential (although still protected). At elevated AC levels, it appeared that the low area ratio (0.1) gave the least protection, i.e. where the steel area is small compared to the copper area. This behavior was explained by the increase in AC current density on the steel (due to the relatively low area), and the copper contributing to a galvanic effect.

- To get a measure on the potential drop in the system, the potential difference between copper and steel was plotted vs. various AC magnitudes, at three different separation distances. As expected, the potential drop increased when the separation distance increased. At high ACs the potential of steel was found to be higher than the potential of copper, which was surprising.

- By removing copper from the system, it was clear that the potential of the carbon steel changed. At low AC levels ($0 - 5$ mA), the effect of copper negatively contributed to the protection of carbon steel - when copper was present, the potential increased by $200 - 250$ mV, while the corrosion rate (of the steel) increased with a factor of $10^1 - 10^2$. Thus, isolating copper from the system increased the protection of steel at low AC levels. At higher AC levels, the absence of copper proved to have a negative effect on the protection of steel. At 200 mA AC_{rms}, removing copper increased the corrosion rate from 30 mm/year to 56 mm/year (at a DC level of 0.8 mA). This behavior was explained by the area effect, since the total area was halved when copper was removed. It was concluded that the reduction in total area, i.e., the increase in AC current density on steel and the reduction in capacitance, was more significant than the galvanic effect of the steel-copper couple.

- The accuracy of extracting kinetic parameters from polarization curves in seawater was discussed. It was highlighted that the high concentration of chloride anions could affect the behavior of the electrochemical system by specific adsorption on the electrode surfaces. Furthermore, it was noted that polarization curves typically are obtained in either strongly acidic or alkaline solutions, since the concentration of H^+ or OH^- is high here. In neutral seawater, it might be difficult to maintain a stable concentration of these species throughout the polarization scan, which would affect the results.

- Finally, the developed model successfully describes the effects of AC on a steel-copper coupling based on experiments, theory, and literature at low ACs. When the ACs are too large, i.e., when corrosion is expected, the model fails (especially) quantitatively. Nevertheless, it is clear that AC-assisted galvanic corrosion is a threat to ships connected to onshore power, but this is strongly dependent on the AC magnitude.

References

[1] E. B. Mehammer, O. E. Kongstein, and A. P. Brede, "Grounding Strategies for High Voltage Shore Connection of Large Passenger Vessels," in *2018 IEEE International Conference on Environment and Electrical Engineering*, Institute of Electrical and Electronics Engineers Inc., 2018.

[2] G. Parise, L. Parise, P. B. Chavdarian, S. Sabatini, and C.-L. Su, "2015 IEEE Industry Applications Society Annual Meeting," in *The TN-island system for cold ironing*, pp. 1–6, 2015.

[3] European Commission, "Roadmap to a Single European Transport Area - Towards a Competitive and Resource Effective System," tech. rep., 2011.

[4] Norwegian Government's Expert Committee for Green Competitiveness, "Green Competitiveness," tech. rep., 2016.

[5] E. B. Mehammer and S. Laedre, "Landstrøm i Bergen-fare for korrosjon? Resultater av feltmålinger," tech. rep., 2019.

[6] D. K. Kim, S. Muralidharan, T. H. Ha, J. H. Bae, Y. C. Ha, H. G. Lee, and J. D. Scantlebury, "Electrochemical studies on the alternating current corrosion of mild steel under cathodic protection condition in marine environments," *Electrochimica Acta*, vol. 51, no. 25, pp. 5259–5267, 2006.

[7] F. A. Wessel, "Modeling of Galvanic Corrosion in Presence of External Currents," tech. rep., NTNU, 2021.

[8] COMSOL Multiphysics® v. 6.0. www.comsol.com., *COMSOL AB.* 2022.

[9] A. J. Bard and L. R. Faulkner, *Electrochemical Methods : Fundamentals and Applications.* Hoboken, NJ: John Wiley & Sons, 2nd ed., 2001.

[10] V. S. Bagotsky, *Fundamentals of Electrochemistry.* John Wiley & Sons, 2nd ed., 2005.

[11] K. B. Oldham, J. C. Myland, and A. M. Bond, *Electrochemical Science and Technology: Fundamentals and Applications.* John Wiley & Sons, 1st ed., 2012.

[12] J. Newman and K. E. Thomas-Alyea, *Electrochemical Systems.* Hoboken, New Jersey: John Wiley & Sons, Inc., third edition ed., 2004.

[13] V. C. Srivastava, I. M. Mishra, and S. Suresh, "Oxygen Mass Transfer in Bioreactors," in *Comprehensive Biotechnology, Second Edition*, vol. 2, pp. 947–956, Elsevier Inc., 2011.

[14] C. F. Clarke, D. Hardie, and B. M. Ikeda, "The effect of hydrogen content on the fracture of pre-cracked titanium specimens," *Corrosion Science*, vol. 36, no. 3, pp. 487–509, 1994.

[15] K. Nisancioglu, "Corrosion Basics and Engineering," 1994.

[16] Det Norske Veritas, "Recommended Practice: Cathodic Protection Design," tech. rep., 2010.

[17] D. P. Riemer and M. E. Orazem, "A mathematical model for the cathodic protection of tank bottoms," in *Corrosion Science*, vol. 47, pp. 849–868, Elsevier Ltd, 2005.

[18] E. Diaz and R. Adey, "Optimising the location of anodes in cathodic protection systems to smooth potential distribution," *Advances in engineering software*, vol. 36, no. 9, pp. 591–598, 2005.

[19] L. Xu, Y. Xin, L. Ma, H. Zhang, Z. Lin, and X. Li, "Challenges and solutions of cathodic protection for marine ships," *Corrosion Communications*, vol. 2, pp. 33–40, 2021.

[20] T. Krebs, "ICCP System for Internal Protection of Monopiles for Offshore Wind Farms," in *CORROSION 2018*, (Phoenix, Arizona), 2018.

[21] D. H. Kroon and L. M. Ernes, "MMO Coated Titanium Anodes for Cathodic Protection," in *CORROSION 2017*, (Nashville, Tennessee), 2007.

[22] Evoqua Water Technologies, "Impressed Current Cathodic Protection," 2022.

[23] J. E. B. Randles, "Kinetics of rapid electrode reactions." 1947.

[24] R. W. Bosch and W. F. Bogaerts, "A theoretical study of AC-induced corrosion considering diffusion phenomena," Tech. Rep. 3, 1998.

[25] S. Goidanich, L. Lazzari, and M. Ormellese, "AC corrosion - Part 1: Effects on overpotentials of anodic and cathodic processes," *Corrosion Science*, vol. 52, no. 2, pp. 491–497, 2010.

[26] C. Liu and R. G. Kelly, "A Review of the Application of Finite Element Method (FEM) to Localized Corrosion Modeling," *Corrosion - The Journal of Science and Engineering*, vol. 75, no. 11, pp. 1285–1299, 2019.

[27] T. Nann and J. Heinze, "Simulation in electrochemistry using the finite element method: Part 1: The algorithm," *Electrochemistry Communications*, vol. 1, no. 7, pp. 289–294, 1999.

[28] N. Sridhar, C. S. Brossia, D. S. Dunn, and A. Anderko, "Predicting Localized Corrosion in Seawater," Tech. Rep. 10, Southwest Research Institute, San Antonio, TX, 2002.

[29] G. Kaye and T. Laby, *Tables of Physical and Chemical Constants*. New York: Longman, 15th ed., 1986.

[30] J. R. Rumble, *"Thermo, Electro & Solution Chemistry" in CRC Handbook of Chemistry and Physics*. Boca Raton, Florida: CRC Press/Taylor & Francis, 102 ed., 2021.

[31] D. L. Wise and G. Houghton, *The diffusion coefficients of ten slightly soluble gases in water at 10-60° C*, vol. 21. Pergamon Press Ltd, 1966.

[32] A. Tang and O. C. Sandall, "Diffusion Coefficient of Chlorine in Water at 25-60°C," *Journal of Chemical and Engineering Data*, vol. 30, no. 2, pp. 189–191, 1985.

[33] M. Goudarzi and M. Ghorbani, "A study on ternary mixed oxide coatings containing Ti, Ru, Ir by sol–gel method on titanium," *Journal of Sol-Gel Science and Technology*, vol. 73, no. 2, pp. 332–340, 2015.

[34] ASTM International, "Standard Practice for Preparation of Substitute Ocean Water," 2021.

[35] Y. Yang, J. D. Scantlebury, and E. V. Koroleva, "A study of calcareous deposits on cathodically protected mild steel in artificial seawater," *Metals*, vol. 5, pp. 439–456, 3 2015.

[36] S. Rossi, P. L. Bonora, R. Pasinetti, L. Benedetti, M. Draghetti, and E. Sacco, "Laboratory and Field Characterization of a New Sacrificial Anode for Cathodic Protection of Offshore Structures," *Corrosion*, vol. 54, pp. 1018–1025, 12 1998.

[37] T. Okstad, O. Rannestad, R. Johnsen, and K. Nisancioglu, "Significance of Hydrogen Evolution during Cathodic Protection of Carbon Steel in Seawater," *Corrosion*, vol. 63, no. 9, pp. 857–865, 2007.

[38] K. Forthun, "Alternating Current Corrosion of Aluminium Sacrificial Anodes," tech. rep., NTNU, 2013.

[39] L. S. Lilleby, "Effect of AC current on calcareous deposits," tech. rep., NTNU, 2009.

[40] S. Muralidharan, D.-K. Kim, T.-H. Ha, J.-H. Bae, Y.-C. Ha, H.-G. Lee, and J. D. Scantlebury, "Influence of alternating, direct and superimposed alternating and direct current on the corrosion of mild steel in marine environments," *Desalination*, vol. 216, no. 1, pp. 103–115, 2007.

[41] W. Fuchs, H. Steinwrath, and H. Ternes, "Corrosion of Iron by Alternating Current with Relation Current Density and Frequency," tech. rep., Das Gas-Und Wasserfach, 1958.

[42] R. G. Wakelin, R. A. Gummow, and S. M. Segall, "AC Corrosion - Case Histories, Test Procedures, & Mitigation," tech. rep., NACE, 1998.

[43] S. Goidanich, L. Lazzari, and M. Ormellese, "AC corrosion. Part 2: Parameters influencing corrosion rate," *Corrosion Science*, vol. 52, no. 3, pp. 916–922, 2010.

[44] J. E. Bennett, "Electrodes for generation of hydrogen and oxygen from seawater," *International Journal of Hydrogen Energy*, vol. 5, no. 4, pp. 401–408, 1980.

[45] Y. Tanaka, "Chapter 11 Limiting Current Density," in *Membrane Science and Technology* (Y. Tanaka, ed.), vol. 12, pp. 245–270, Elsevier, 2007.

[46] I. Ibrahim, M. Meyer, H. Takenouti, and B. Tribollet, "AC Induced Corrosion of Underground Steel Pipelines. Faradaic Rectification under Cathodic Protection: II. Theoretical Approach with Electrolyte Resistance and Double Layer Capacitance for Bi-Tafelian Corrosion Mechanism," *Journal of the Brazilian Chemical Society*, vol. 27, pp. 605–615, 2015.

[47] L. Nielsen and P. Cohn, "AC-Corrosion and Electrical Equivalent Diagrams," tech. rep., 2000.

[48] S. Z. Fernandes, S. G. Mehendale, and S. Venkatachalam, "Influence of frequency of alternating current on the electrochemical dissolution of mild steel and nickel," *Journal of Applied Electrochemistry*, vol. 10, no. 5, pp. 649–654, 1980.

[49] Y.-B. Guo, C. Liu, D.-G. Wang, and S.-H. Liu, "Effects of alternating current interference on corrosion of X60 pipeline steel," *Petroleum Science*, vol. 12, no. 2, pp. 316–324, 2015.

[50] S. B. Lalvani and G. Zhang, "The corrosion of carbon steel in a chloride environment due to periodic voltage modulation: Part I," *Corrosion Science*, vol. 37, no. 10, pp. 1567–1582, 1995.

[51] P. Broekmann, M. Wilms, M. Kruft, C. Stuhlmann, and K. Wandelt, "In-situ STM investigation of specific anion adsorption on Cu(111)," *Journal of Electroanalytical Chemistry*, vol. 467, no. 1, pp. 307–324, 1999.

[52] R. S. Yeo, J. Orehotsky, W. Visscher, and S. Srinivasan, "Ruthenium-Based Mixed Oxides as Electrocatalysts for Oxygen Evolution in Acid Electrolytes," *Journal of The Electrochemical Society*, vol. 128, no. 9, pp. 1900–1904, 1981.

[53] A. H. Reksten, H. Thuv, F. Seland, and S. Sunde, "The oxygen evolution reaction mechanism at IrxRu1-xO2 powders produced by hydrolysis synthesis," *Journal of Electroanalytical Chemistry*, vol. 819, pp. 547–561, 2018.

[54] S. Clark, A. Latz, and B. Horstmann, "Rational Development of Neutral Aqueous Electrolytes for Zinc–Air Batteries," *ChemSusChem*, vol. 10, no. 23, pp. 4735–4747, 2017.

A Uncertainty

A.1 Mean and standard deviation

When extracting one value from a set of values, one often calculates the mean (average) value. In statistical theory, the mean $\bar{x}$ of a set of values (x_1, x_2, ..., x_N) is the sum divided by the number of values:

$$\bar{x} = \frac{1}{N}\sum_{i=1}^{N} x_i, \tag{A.1}$$

where N is the total number of values in the set. From the mean value, the sample standard deviation s_N can be calculated by the following equation:

$$s_N = \sqrt{\frac{1}{N}\sum_{i=1}^{N}(x_i - \bar{x})^2}. \tag{A.2}$$

However, if the number of values in the set N is quite small, equation (A.2) could prove incorrect. To reduce bias, as the actual mean (population mean) for a set of values is rarely known, the equation can be modified by Bessel's correction:

$$s = \sqrt{\frac{1}{N-1}\sum_{i=1}^{N}(x_i - \bar{x})^2}. \tag{A.3}$$

Assuming that the values in the set are normally distributed, doubling the standard deviation s is used to obtain a 95% confidence interval of the parameter value. The value $2s$ was used to denote the uncertainty of the mean parameters found in this work. Still, it is difficult to conclude whether the values are actually normally distributed or not. Nevertheless, the value $2s$ serves as an indicator of the uncertainty of the mean value, even though it does not indicate the actual range of the parameter value with 95% confidence.

A.2 Uncertainty-calculations for galvanostatic EIS scans at lab

Here is an example of how the mean and standard deviation of the potential were calculated from the experimental data. For DC = 60 µA and $\mathrm{AC_{rms}}$ = 0.1 mA, a total of 175 potentials were obtained at a frequency of (50 ± 1) Hz. These values were merged into one list, and the mean value was calculated as

$$\bar{x} = \frac{1}{175}\sum_{i=1}^{175} x_i = -852.52 \text{ mV}. \tag{A.4}$$

Uncertainty in this variable can then be calculated. As the number of values N is quite large in this case, both equation (A.2) and (A.3) practically give the same standard deviation. Utilizing equation (A.3) gives the standard deviation s:

$$s = \sqrt{\frac{1}{175-1}\sum_{i=1}^{175}(x_i - \bar{x})^2} = 22.25 \text{ mV}. \tag{A.5}$$

As stated in Section A.1, the potential within 95% confidence can be found by doubling the standard deviation, and assuming that the values are normally distributed. This gives

$$E(\mathrm{DC}{=}60\mu\mathrm{A},\ \mathrm{AC_{rms}}{=}0.1 \text{ mA}) = -850 \text{ mV} \pm 40 \text{ mV}. \tag{A.6}$$

The calculated E is here the potential vs. Ag/AgCl on the carbon steel electrode when 60 µA DC and 0.1 mA AC_{rms} are impressed to the counter electrode. Similar calculations are done for the different combinations of DC and AC.

A.3 Uncertainty-calculations for results obtained from model

Here is an example of how the mean and standard deviation of the modeling results were calculated. For this example, AC_{rms} is equal to 10 mA and DC equal to 0.8 mA. The double layer capacitance and frequency of the AC signal were kept constant at 0.1 F/m^2 and 50 Hz, respectively. Three computations were made, where the input parameters varied within a $\pm$ 10% range. The following potentials were obtained at the carbon steel electrode:

1. -0.965294290 V
2. -0.908677788 V
3. -0.932847288 V

Then, the mean potential (vs. Ag/AgCl) was calculated according to equation (A.1):

$$\bar{x} = \frac{1}{3}\sum_{i=1}^{3} x_i = -0.93561 \text{ V} = -935.61 \text{ mV}. \tag{A.7}$$

As the number of samples is quite low ($N = 3$), the Bessel's correction in equation (A.3) is utilized to obtain the standard deviation s of these computations:

$$s = \sqrt{\frac{1}{3-1}\sum_{i=1}^{3}(x_i - \bar{x})^2} = 0.02841 \text{ V} = 28.41 \text{ mV}. \tag{A.8}$$

Then, stating the mean potential with $2s$ uncertainty, this gives

$$E(\text{DC=0.8 mA, } AC_{rms}\text{=10 mA}) = -940 \text{ mV} \pm 60 \text{ mV}, \tag{A.9}$$

which also is tabulated in Table C.3. Similar calculations were done for all computed values in this work. It should be noted that the values are not normally distributed, as the sample size (3) is quite small.

B Plots and figures

B.1 Lab: Direct and alternating currents impressed to Pt

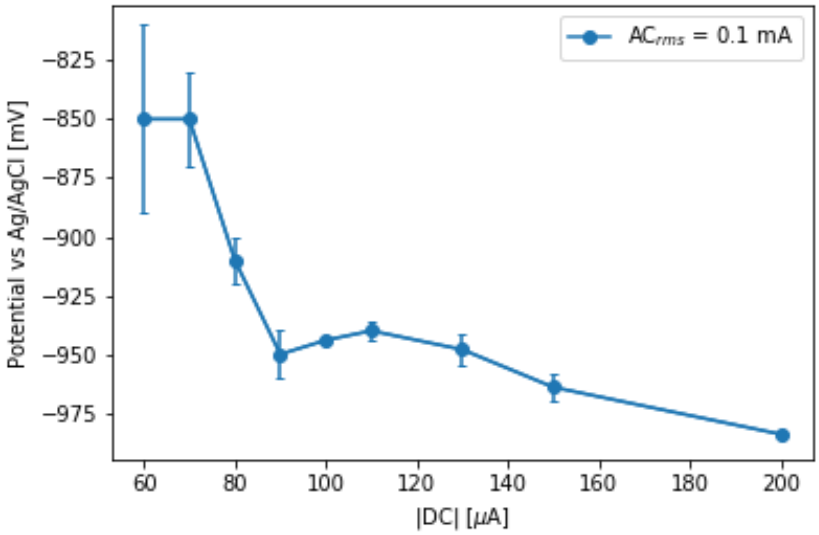

Figure B.1: Lab: Calculated mean potential of carbon steel vs. DC current impressed at AC_{rms} = 0.1 mA. Error bars represent two standard deviations of uncertainty.

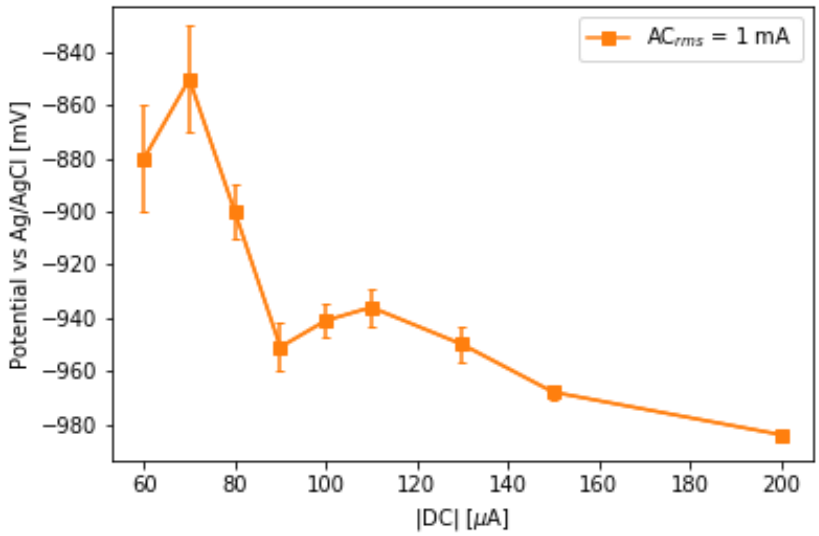

Figure B.2: Lab: Calculated mean potential of carbon steel vs. DC current impressed at AC_{rms} = 1 mA. Error bars represent two standard deviations of uncertainty.

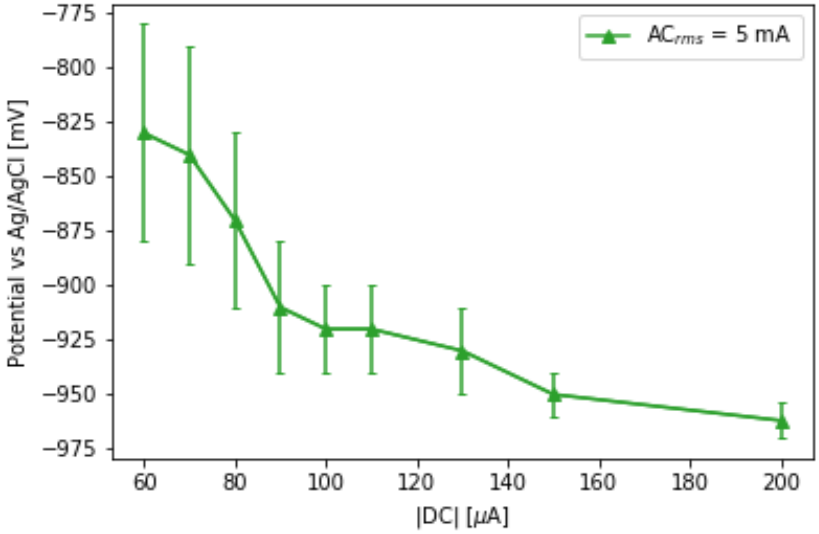

Figure B.3: Lab: Calculated mean potential of carbon steel vs. DC current impressed at $AC_{rms} = 5$ mA. Error bars represent two standard deviations of uncertainty.

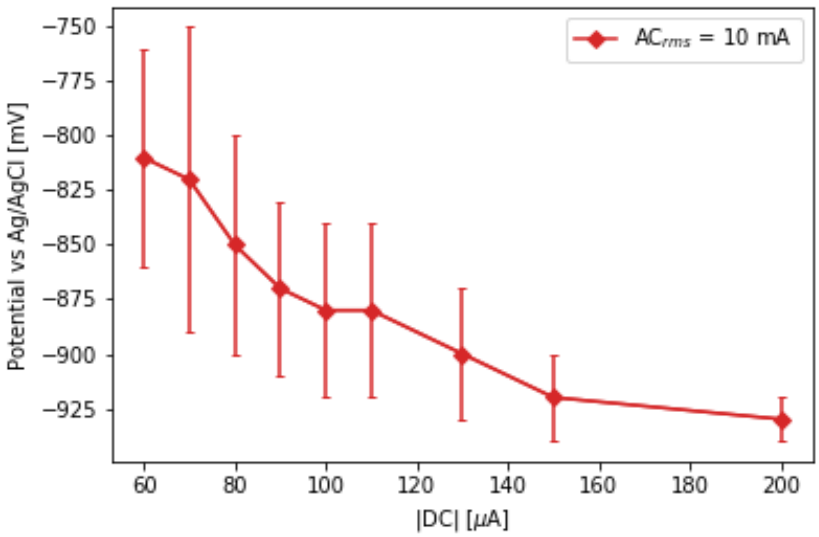

Figure B.4: Lab: Calculated mean potential of carbon steel vs. DC current impressed at $AC_{rms} = 10$ mA. Error bars represent two standard deviations of uncertainty.

B.2 Model: Direct and alternating currents impressed to MMO anode while varying the double layer capacitance

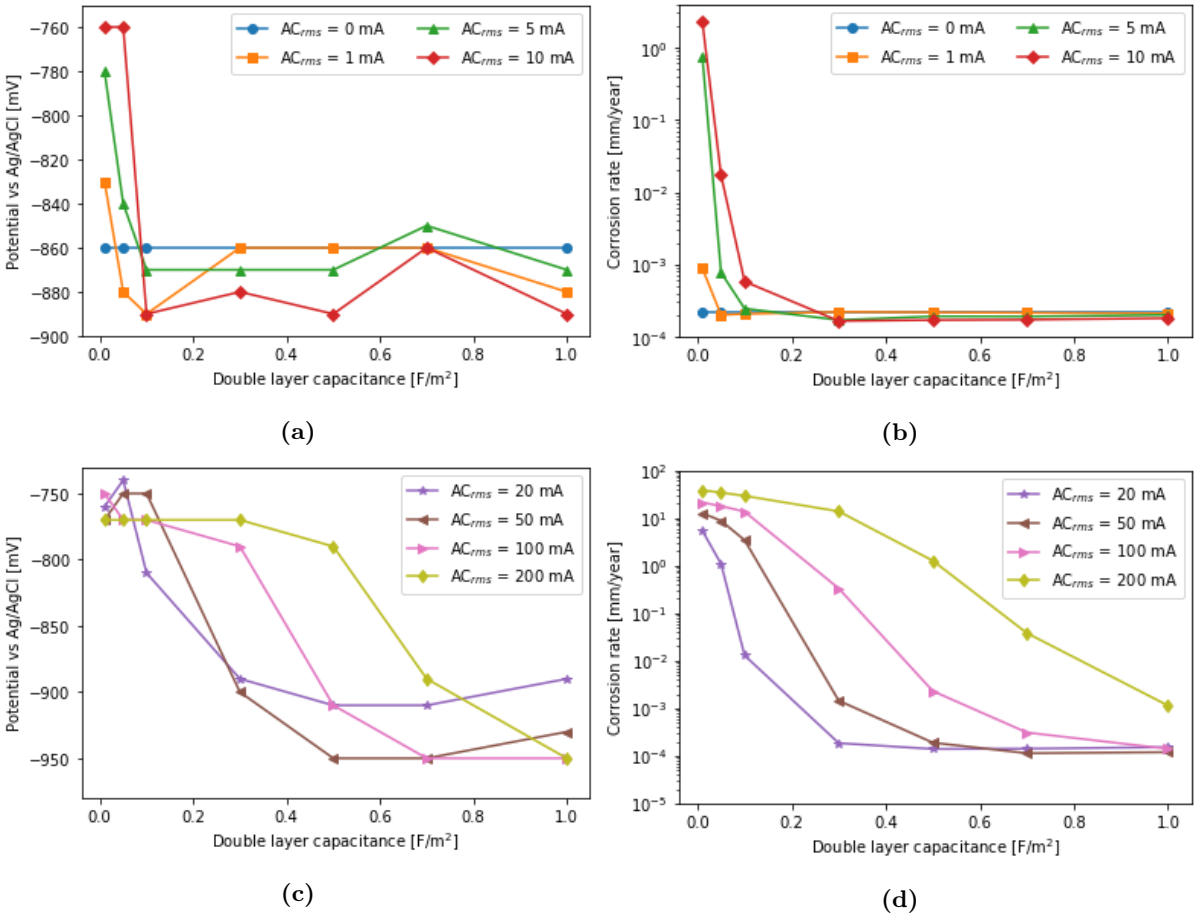

Figure B.5: DC = 0.4 mA. Potentials and uniform corrosion rates of carbon steel as a function of C_{dl}, for various ACs impressed to the MMO electrode in COMSOL. Frequency of the AC signal is set to 50 Hz. (a) Potential vs. C_{dl} for small AC magnitudes. (b) Corrosion rate vs. C_{dl} for small AC magnitudes. (c) Potential vs. C_{dl} for large AC magnitudes. (d) Corrosion rate vs. C_{dl} for large AC magnitudes.

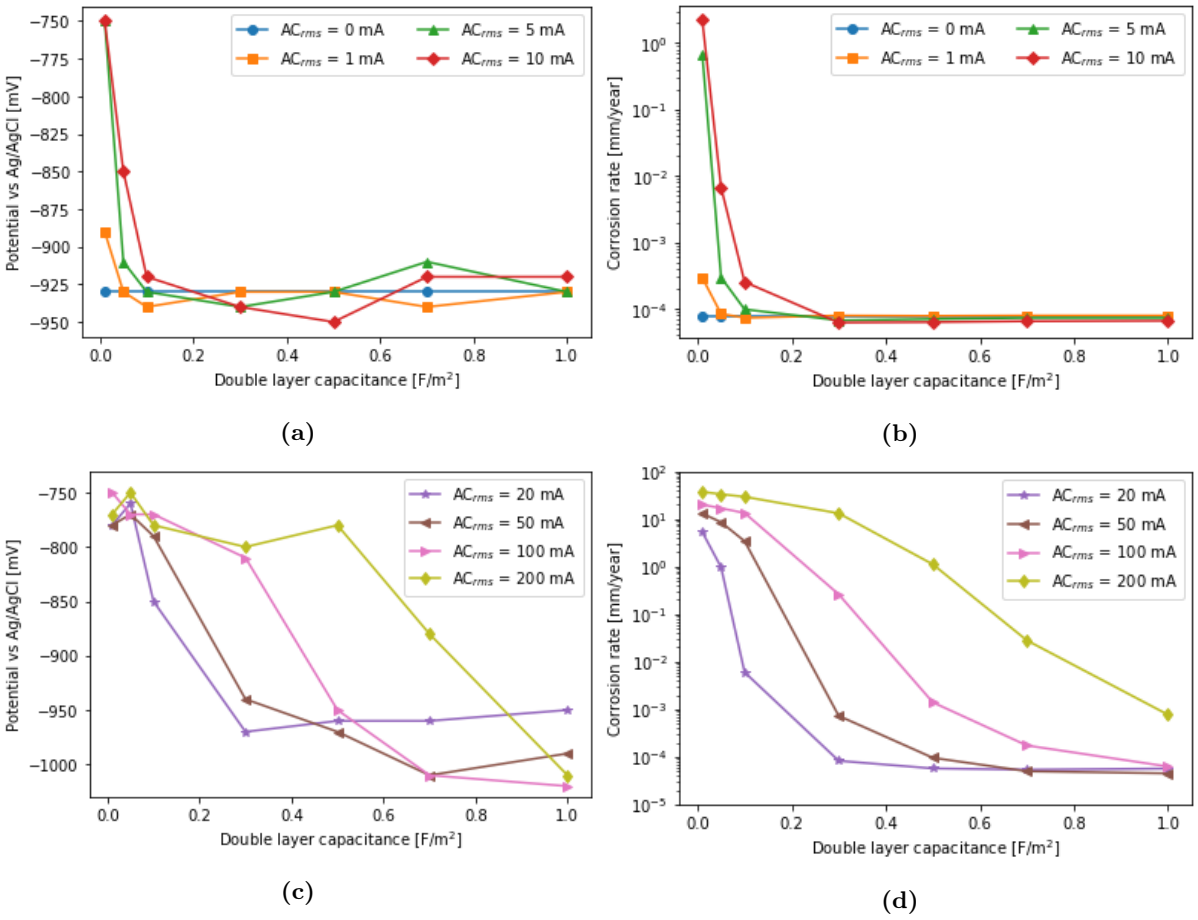

Figure B.6: DC = 0.6 mA. Potentials and uniform corrosion rates of carbon steel as a function of C_{dl}, for various ACs impressed to the MMO electrode in COMSOL. Frequency of the AC signal is set to 50 Hz. (a) Potential vs. C_{dl} for small AC magnitudes. (b) Corrosion rate vs. C_{dl} for small AC magnitudes. (c) Potential vs. C_{dl} for large AC magnitudes. (d) Corrosion rate vs. C_{dl} for large AC magnitudes.

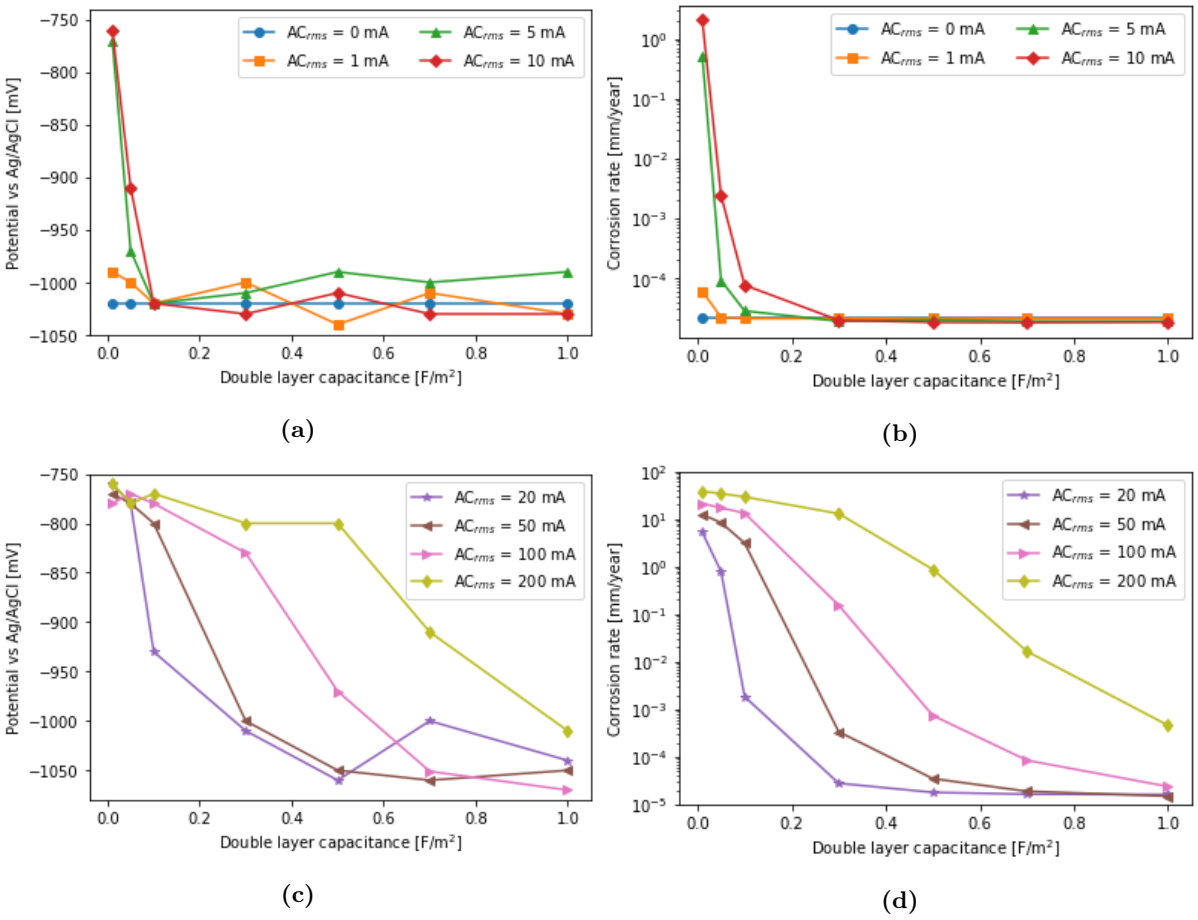

Figure B.7: DC = 1.0 mA. Potentials and uniform corrosion rates of carbon steel as a function of C_{dl}, for various ACs impressed to the MMO electrode in COMSOL. Frequency of the AC signal is set to 50 Hz. (a) Potential vs. C_{dl} for small AC magnitudes. (b) Corrosion rate vs. C_{dl} for small AC magnitudes. (c) Potential vs. C_{dl} for large AC magnitudes. (d) Corrosion rate vs. C_{dl} for large AC magnitudes.

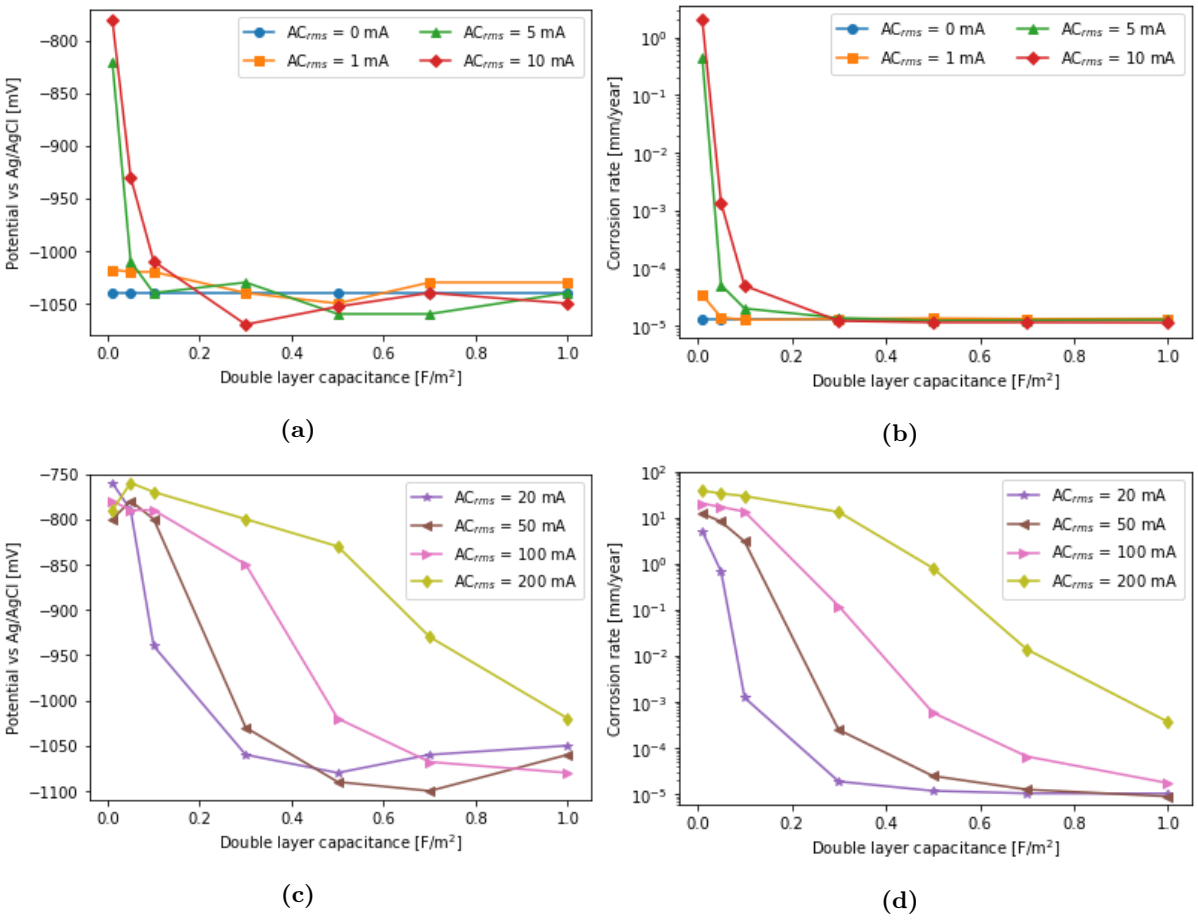

Figure B.8: DC = 1.2 mA. Potentials and uniform corrosion rates of carbon steel as a function of C_{dl}, for various ACs impressed to the MMO electrode in COMSOL. Frequency of the AC signal is set to 50 Hz. (a) Potential vs. C_{dl} for small AC magnitudes. (b) Corrosion rate vs. C_{dl} for small AC magnitudes. (c) Potential vs. C_{dl} for large AC magnitudes. (d) Corrosion rate vs. C_{dl} for large AC magnitudes.

B.3 Model: Direct and alternating currents impressed to MMO anode while varying the frequency of the AC signal

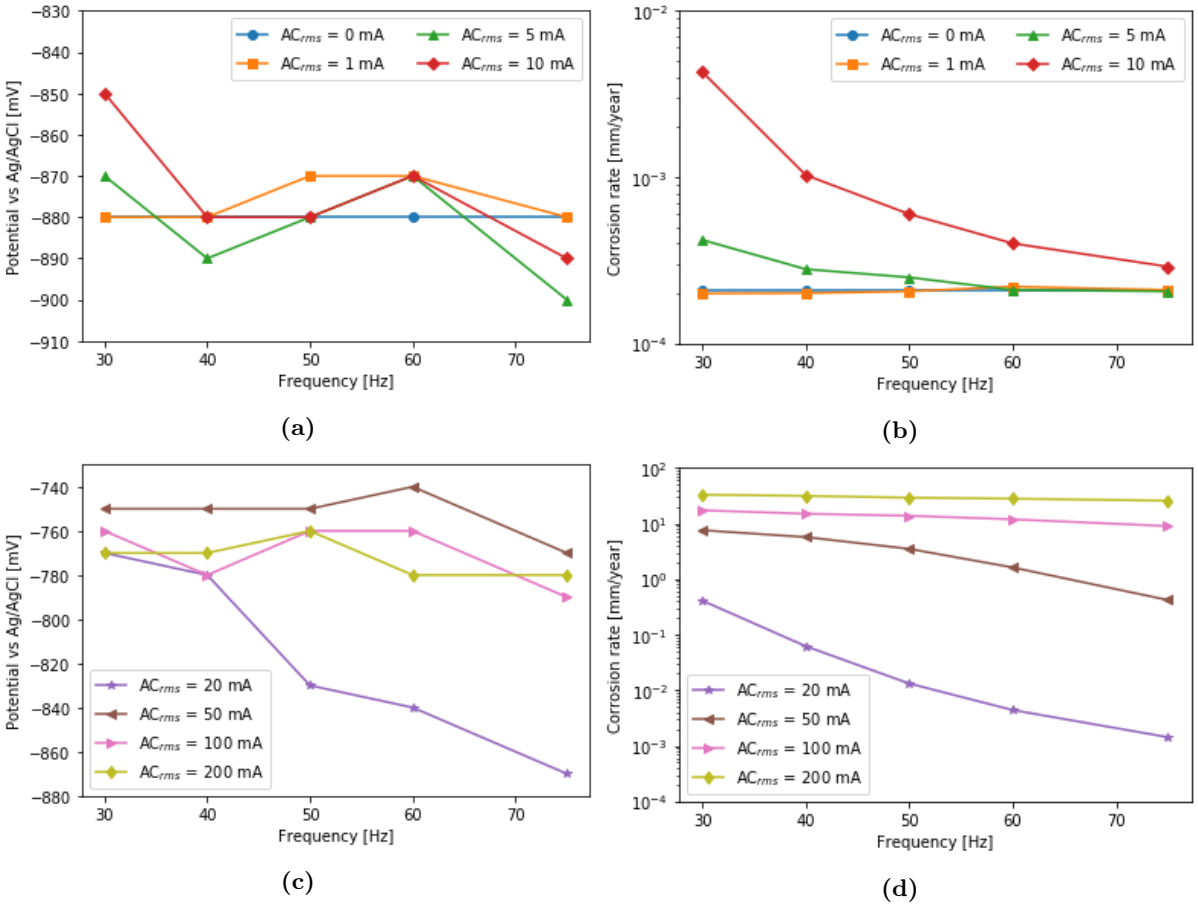

Figure B.9: DC = 0.4 mA. Potentials and uniform corrosion rates of carbon steel as a function of f, for various ACs impressed to the MMO electrode in COMSOL. The double layer capacitance is set to 0.1 $\mathrm{F/m^2}$. (a) Potential vs. f for small AC magnitudes. (b) Corrosion rate vs. f for small AC magnitudes. (c) Potential vs. f for large AC magnitudes. (d) Corrosion rate vs. f for large AC magnitudes.

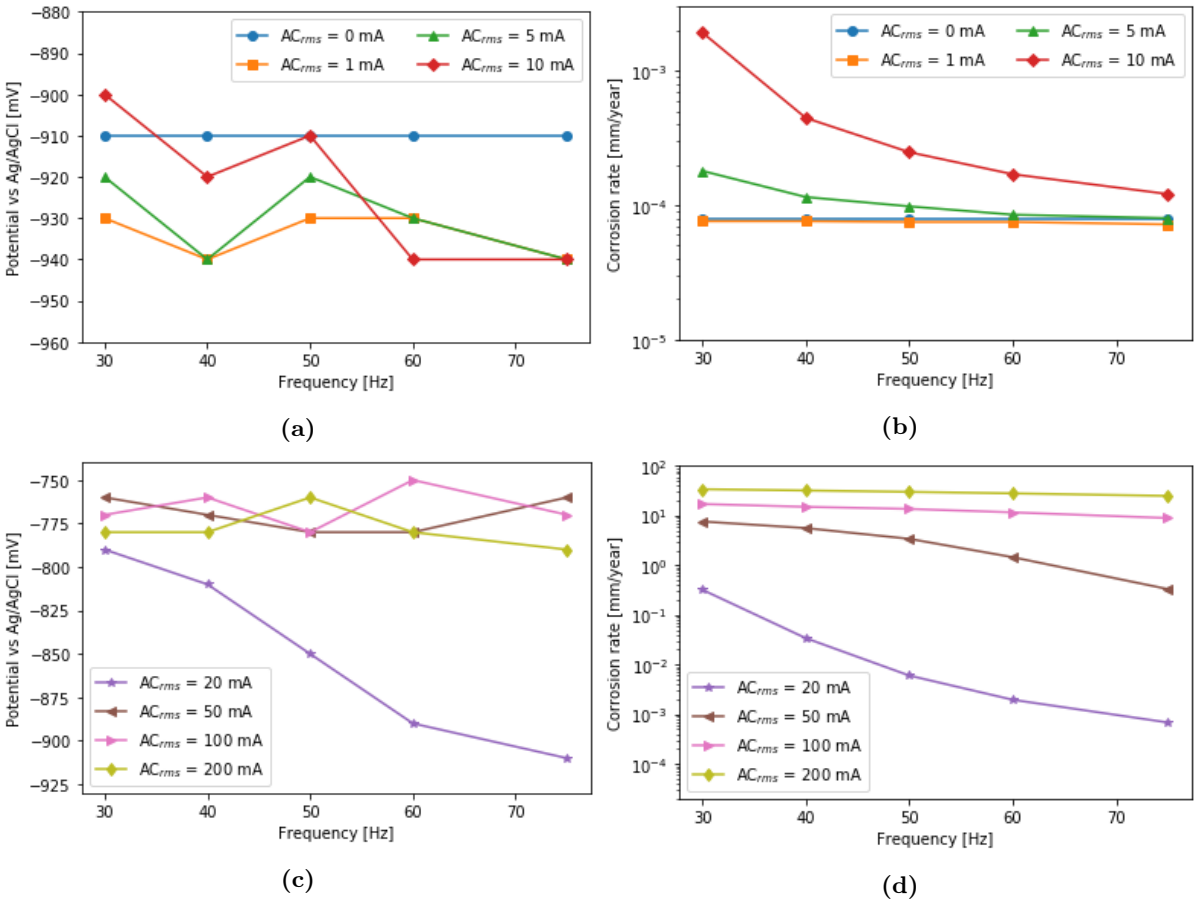

Figure B.10: DC = 0.6 mA. Potentials and uniform corrosion rates of carbon steel as a function of f, for various ACs impressed to the MMO electrode in COMSOL. The double layer capacitance is set to 0.1 $\mathrm{F/m^2}$. (a) Potential vs. f for small AC magnitudes. (b) Corrosion rate vs. f for small AC magnitudes. (c) Potential vs. f for large AC magnitudes. (d) Corrosion rate vs. f for large AC magnitudes.

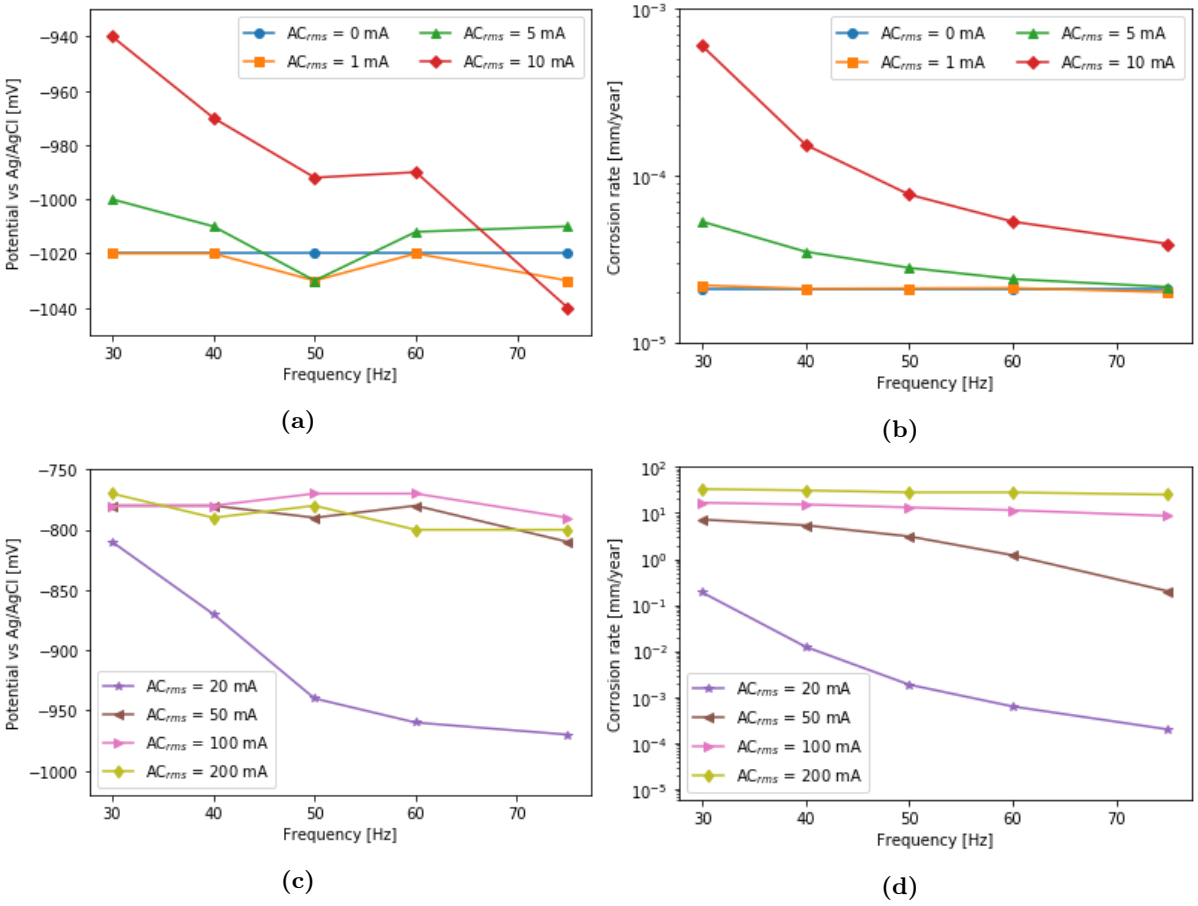

Figure B.11: DC = 1.0 mA. Potentials and uniform corrosion rates of carbon steel as a function of f, for various ACs impressed to the MMO electrode in COMSOL. The double layer capacitance is set to 0.1 $\mathrm{F/m^2}$. (a) Potential vs. f for small AC magnitudes. (b) Corrosion rate vs. f for small AC magnitudes. (c) Potential vs. f for large AC magnitudes. (d) Corrosion rate vs. f for large AC magnitudes.

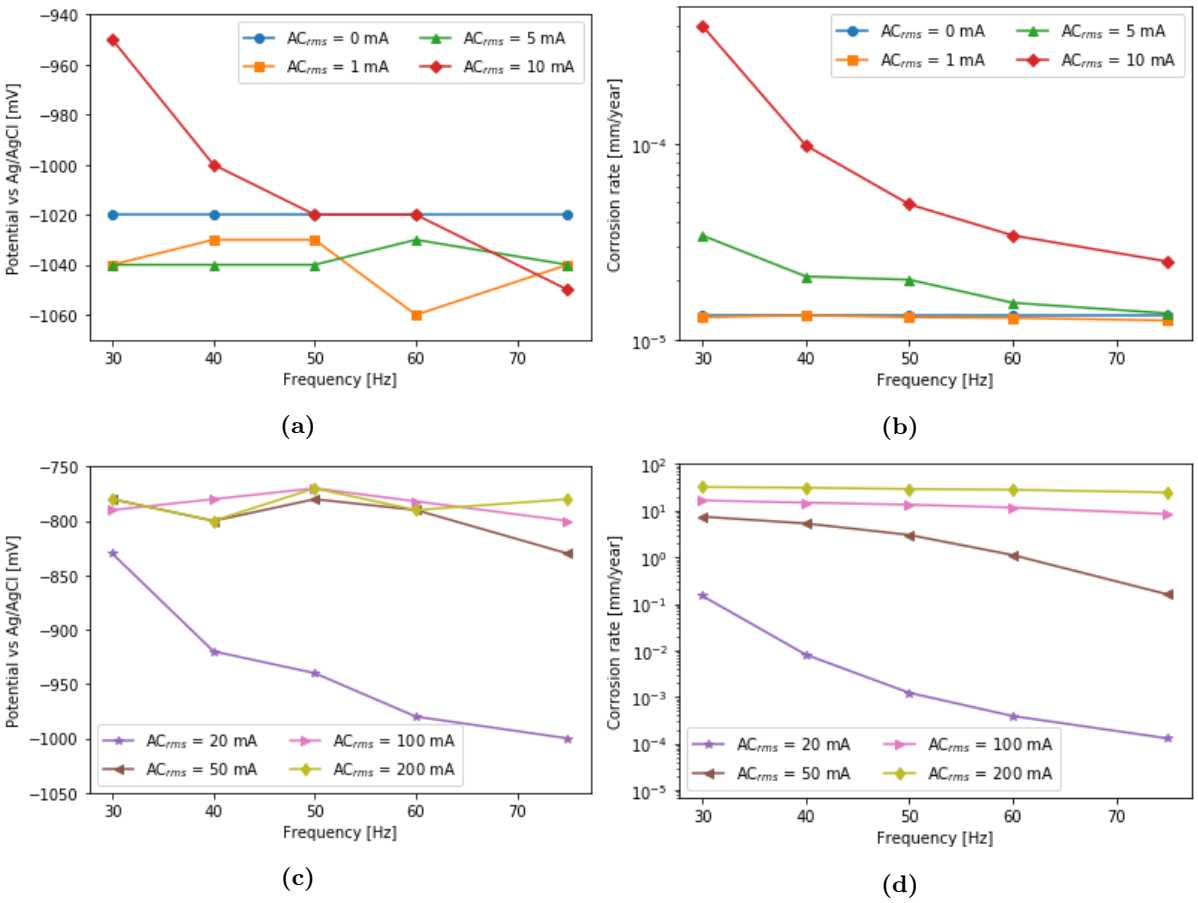

Figure B.12: DC = 1.2 mA. Potentials and uniform corrosion rates of carbon steel as a function of f, for various ACs impressed to the MMO electrode in COMSOL. The double layer capacitance is set to 0.1 $\mathrm{F/m^2}$. (a) Potential vs. f for small AC magnitudes. (b) Corrosion rate vs. f for small AC magnitudes. (c) Potential vs. f for large AC magnitudes. (d) Corrosion rate vs. f for large AC magnitudes.

C Tabulated values and uncertainties

C.1 Model: Direct and alternating currents impressed to Pt

Table C.1: Model: Potential of carbon steel at various combinations of AC_{rms} [mA] and DC [mA] impressed to Pt at C_{dl} = 0.1 F/m^2. The values are stated as the mean value ± 2s [mV]. The frequency is 50 Hz.

DC \ AC$_{rms}$	**0.5**	**5**	**25**	**100**
0.3	-822 ± 7	-837 ± 8	-751 ± 4	-763 ± 6
0.4	-866 ± 6	-876 ± 7	-766 ± 6	-767 ± 6
0.5	-900 ± 8	-908 ± 3	-784 ± 3	-771 ± 8
0.6	-929 ± 9	-935 ± 8	-801 ± 5	-773 ± 8
0.7	-953 ± 5	-957 ± 5	-818 ± 9	-776 ± 3
0.8	-974 ± 6	-977 ± 6	-833 ± 4	-778 ± 4
0.9	-992 ± 5	-998 ± 4	-849 ± 5	-780 ± 7
1.0	-1009 ± 6	-1014 ± 5	-862 ± 6	-782 ± 4
1.1	-1025 ± 7	-1028 ± 4	-875 ± 8	-784 ± 5
1.2	-1039 ± 6	-1041 ± 8	-887 ± 5	-786 ± 4

Table C.2: Model: Potential of carbon steel at various combinations of AC_{rms} [mA] and DC [mA] impressed to Pt at C_{dl} = 0.5 F/m^2. The values are stated as the mean value ± 2s [mV]. The frequency is 50 Hz.

DC \ AC$_{rms}$	**0.5**	**5**	**25**	**100**
0.3	-821 ± 2	-831 ± 6	-873 ± 7	-911 ± 7
0.4	-866 ± 4	-875 ± 5	-913 ± 6	-929 ± 5
0.5	-900 ± 7	-909 ± 6	-943 ± 6	-944 ± 5
0.6	-929 ± 6	-936 ± 7	-967 ± 7	-955 ± 9
0.7	-953 ± 4	-960 ± 8	-988 ± 7	-965 ± 8
0.8	-974 ± 8	-981 ± 4	-1006 ± 6	-974 ± 8
0.9	-993 ± 5	-999 ± 8	-1023 ± 8	-982 ± 8
1.0	-1009 ± 7	-1016 ± 8	-1038 ± 4	-990 ± 7
1.1	-1025 ± 8	-1031 ± 7	-1051 ± 7	-998 ± 7
1.2	-1039 ± 6	-1044 ± 7	-1063 ± 9	-1005 ± 9

C.2 Model: Direct and alternating currents impressed to MMO anode

Table C.3: Model: Potential of carbon steel at various combinations of AC_{rms} [mA] and DC [mA] impressed to MMO. The values are stated as the mean value ± $2s$ [mV]. C_{dl} and f are held at 0.1 F/m^2 and 50 Hz, respectively.

AC_{rms} \ DC	**0.4**	**0.6**	**0.8**	**1.0**	**1.2**
0	-840 ± 50	-900 ± 50	-950 ± 60	-980 ± 50	-1010 ± 50
1	-850 ± 50	-900 ± 60	-950 ± 60	-980 ± 60	-1010 ± 60
5	-850 ± 60	-910 ± 50	-950 ± 60	-980 ± 50	-1010 ± 50
10	-850 ± 60	-900 ± 60	-940 ± 60	-970 ± 60	-1000 ± 50
20	-780 ± 50	-830 ± 50	-860 ± 60	-890 ± 60	-920 ± 50
50	-760 ± 20	-760 ± 20	-770 ± 20	-770 ± 20	-780 ± 20
100	-760 ± 10	-770 ± 10	-770 ± 10	-780 ± 10	-780 ± 10
200	-760 ± 10	-770 ± 10	-770 ± 10	-780 ± 10	-780 ± 10

Table C.4: Model: Uniform corrosion rate of carbon steel at various combinations of AC_{rms} [mA] and DC [mA] impressed to MMO. The values are stated as the mean value ± $2s$ [mm/year]. C_{dl} and f are held at 0.1 F/m^2 and 50 Hz, respectively.

AC_{rms} \ DC	**0.4**	**0.6**	**0.8**	**1.0**	**1.2**
0	$(4 \pm 3)\cdot10^{-4}$	$(1 \pm 1)\cdot10^{-4}$	$(6 \pm 5)\cdot10^{-5}$	$(4 \pm 3)\cdot10^{-5}$	$(2 \pm 2)\cdot10^{-5}$
1	$(3 \pm 3)\cdot10^{-4}$	$(1 \pm 1)\cdot10^{-4}$	$(6 \pm 5)\cdot10^{-5}$	$(4 \pm 3)\cdot10^{-5}$	$(2 \pm 2)\cdot10^{-5}$
5	$(4 \pm 4)\cdot10^{-4}$	$(2 \pm 1)\cdot10^{-4}$	$(9 \pm 8)\cdot10^{-5}$	$(5 \pm 4)\cdot10^{-5}$	$(3 \pm 2)\cdot10^{-5}$
10	$(1 \pm 1)\cdot10^{-3}$	$(5 \pm 5)\cdot10^{-4}$	$(3 \pm 2)\cdot10^{-4}$	$(1 \pm 1)\cdot10^{-4}$	$(1.0 \pm 0.9)\cdot10^{-4}$
20	$(2 \pm 2)\cdot10^{-2}$	$(1 \pm 1)\cdot10^{-2}$	$(6 \pm 7)\cdot10^{-3}$	$(4 \pm 4)\cdot10^{-3}$	$(2 \pm 3)\cdot10^{-3}$
50	3.9 ± 0.8	3.8 ± 0.9	3.7 ± 0.9	3.5 ± 0.9	3.4 ± 0.9
100	13.9 ± 0.5	13.8 ± 0.4	13.7 ± 0.4	13.7 ± 0.4	13.6 ± 0.4
200	30 ± 1	30 ± 1	30 ± 1	30 ± 2	29 ± 1

C.3 Model: Direct and alternating currents impressed to MMO anode while varying the double layer capacitance

Table C.5: Model: Potential of carbon steel as a function of C_{dl} [F/m^2], for various ACs [mA] impressed to MMO. The impressed DC is equal to 0.8 mA, while f is held at 50 Hz. All values are stated as the mean value ± 2s [mV].

$\mathbf{C_{dl}}$ \ $\mathbf{AC_{rms}}$	**0**	**1**	**5**	**10**
0.01	-960 ± 30	-950 ± 20	-770 ± 10	-770 ± 10
0.05	-960 ± 30	-980 ± 50	-930 ± 40	-870 ± 20
0.1	-960 ± 30	-970 ± 10	-990 ± 20	-980 ± 60
0.3	-960 ± 30	-970 ± 30	-1000 ± 40	-980 ± 50
0.5	-960 ± 30	-1000 ± 40	-990 ± 40	-990 ± 70
0.7	-960 ± 30	-970 ± 40	-970 ± 50	-980 ± 90
1.0	-960 ± 30	-970 ± 30	-970 ± 10	-980 ± 80

$\mathbf{C_{dl}}$ \ $\mathbf{AC_{rms}}$	**20**	**50**	**100**	**200**
0.01	-760 ± 20	-780 ± 30	-790 ± 30	-790 ± 30
0.05	-770 ± 20	-780 ± 40	-770 ± 50	-770 ± 40
0.1	-890 ± 60	-800 ± 40	-770 ± 60	-770 ± 20
0.3	-1000 ± 30	-990 ± 50	-810 ± 10	-780 ± 50
0.5	-1010 ± 60	-1020 ± 90	-970 ± 60	-800 ± 70
0.7	-1010 ± 60	-1030 ± 80	-1000 ± 50	-910 ± 50
1.0	-980 ± 40	-1010 ± 10	-1020 ± 50	-1040 ± 50

Table C.6: Model: Uniform corrosion rate of carbon steel as a function of C_{dl} [F/m^2], for various ACs [mA] impressed to MMO. The impressed DC is equal to 0.8 mA, while f is held at 50 Hz. All values are stated as the mean value ± 2s [mm/year].

$\mathbf{C_{dl}}$ \ $\mathbf{AC_{rms}}$	**0**	**1**	**5**	**10**
0.01	$(3.8 \pm 0.2)\cdot10^{-5}$	$(1.23 \pm 0.07)\cdot10^{-4}$	$(5.8 \pm 0.5)\cdot10^{-1}$	2.1 ± 0.1
0.05	$(3.8 \pm 0.2)\cdot10^{-5}$	$(3.9 \pm 0.1)\cdot10^{-5}$	$(1.59 \pm 0.06)\cdot10^{-4}$	$(3.58 \pm 0.01)\cdot10^{-3}$
0.1	$(3.8 \pm 0.2)\cdot10^{-5}$	$(3.7 \pm 0.2)\cdot10^{-5}$	$(5.0 \pm 0.3)\cdot10^{-5}$	$(1.28 \pm 0.06)\cdot10^{-4}$
0.3	$(3.8 \pm 0.2)\cdot10^{-5}$	$(3.8 \pm 0.2)\cdot10^{-5}$	$(3.4 \pm 0.1)\cdot10^{-5}$	$(3.4 \pm 0.1)\cdot10^{-5}$
0.5	$(3.8 \pm 0.2)\cdot10^{-5}$	$(3.73 \pm 0.05)\cdot10^{-5}$	$(3.5 \pm 0.1)\cdot10^{-5}$	$(3.18 \pm 0.07)\cdot10^{-5}$
0.7	$(3.8 \pm 0.2)\cdot10^{-5}$	$(3.7 \pm 0.3)\cdot10^{-5}$	$(3.4 \pm 0.2)\cdot10^{-5}$	$(3.1 \pm 0.2)\cdot10^{-5}$
1.0	$(3.8 \pm 0.2)\cdot10^{-5}$	$(3.745 \pm 0.001)\cdot10^{-5}$	$(3.53 \pm 0.05)\cdot10^{-5}$	$(3.2 \pm 0.2)\cdot10^{-5}$

$\mathbf{C_{dl}}$ \ $\mathbf{AC_{rms}}$	**20**	**50**	**100**	**200**
0.01	5.4 ± 0.2	12.3 ± 0.6	21 ± 2	37.7 ± 0.6
0.05	$(8.7 \pm 0.5)\cdot10^{-1}$	8.4 ± 0.5	16.7 ± 0.9	33 ± 2
0.1	$(3.4 \pm 0.2)\cdot10^{-3}$	3.22 ± 0.06	13.4 ± 0.5	29 ± 2
0.3	$(4.5 \pm 0.2)\cdot10^{-5}$	$(4.9 \pm 0.2)\cdot10^{-4}$	$(2.0 \pm 0.1)\cdot10^{-1}$	13 ± 1
0.5	$(3.0 \pm 0.1)\cdot10^{-5}$	$(5.5 \pm 0.2)\cdot10^{-5}$	$(1.03 \pm 0.06)\cdot10^{-3}$	$(9.9 \pm 0.3)\cdot10^{-1}$
0.7	$(2.76 \pm 0.07)\cdot10^{-5}$	$(2.91 \pm 0.08)\cdot10^{-5}$	$(1.2 \pm 0.1)\cdot10^{-4}$	$(2.12 \pm 0.09)\cdot10^{-2}$
1.0	$(2.8 \pm 0.2)\cdot10^{-5}$	$(2.4 \pm 0.1)\cdot10^{-5}$	$(3.53 \pm 0.09)\cdot10^{-5}$	$(5.8 \pm 0.3)\cdot10^{-4}$

C.4 Model: Direct and alternating currents impressed to MMO anode while varying the frequency of the AC signal

Table C.7: Model: Potential of carbon steel as a function of f [Hz], for various ACs [mA] impressed to MMO. The impressed DC is equal to 0.8 mA, while C_{dl} is held at 0.1 F/m^2. All values are stated as the mean value ± $2s$ [mV].

f \ AC$_{rms}$	**0**	**1**	**5**	**10**
30	-960 ± 60	-970 ± 40	-950 ± 30	-920 ± 20
40	-960 ± 60	-960 ± 40	-960 ± 60	-940 ± 40
50	-960 ± 60	-980 ± 70	-1000 ± 40	-980 ± 30
60	-960 ± 60	-960 ± 30	-980 ± 80	-980 ± 70
75	-960 ± 60	-1000 ± 50	-1010 ± 40	-990 ± 40

f \ AC$_{rms}$	**20**	**50**	**100**	**200**
30	-790 ± 50	-780 ± 10	-780 ± 70	-780 ± 50
40	-830 ± 40	-779 ± 4	-790 ± 40	-780 ± 50
50	-910 ± 40	-770 ± 40	-773 ± 8	-770 ± 30
60	-930 ± 30	-760 ± 30	-790 ± 20	-760 ± 30
75	-960 ± 50	-770 ± 20	-790 ± 20	-790 ± 50

Table C.8: Model: Uniform corrosion rate of carbon steel as a function of f [Hz], for various ACs [mA] impressed to MMO. The impressed DC is equal to 0.8 mA, while C_{dl} is held at 0.1 F/m^2. All values are stated as the mean value ± $2s$ [mm/year].

f \ AC$_{rms}$	**0**	**1**	**5**	**10**
30	$(3.83 \pm 0.06)\cdot10^{-5}$	$(3.7 \pm 0.2)\cdot10^{-5}$	$(9.2 \pm 0.2)\cdot10^{-5}$	$(1.02 \pm 0.03)\cdot10^{-3}$
40	$(3.83 \pm 0.06)\cdot10^{-5}$	$(3.6 \pm 0.3)\cdot10^{-5}$	$(6.1 \pm 0.3)\cdot10^{-5}$	$(2.43 \pm 0.07)\cdot10^{-4}$
50	$(3.83 \pm 0.06)\cdot10^{-5}$	$(3.6 \pm 0.2)\cdot10^{-5}$	$(4.8 \pm 0.3)\cdot10^{-5}$	$(1.25 \pm 0.06)\cdot10^{-4}$
60	$(3.83 \pm 0.06)\cdot10^{-5}$	$(3.6 \pm 0.2)\cdot10^{-5}$	$(4.5 \pm 0.3)\cdot10^{-5}$	$(9.2 \pm 0.5)\cdot10^{-5}$
75	$(3.83 \pm 0.06)\cdot10^{-5}$	$(3.7 \pm 0.3)\cdot10^{-5}$	$(3.70 \pm 0.04)\cdot10^{-5}$	$(6.4 \pm 0.3)\cdot10^{-5}$

f \ AC$_{rms}$	**20**	**50**	**100**	**200**
30	$(2.46 \pm 0.04)\cdot10^{-1}$	7.3 ± 0.4	16.5 ± 0.8	32.8 ± 0.8
40	$(2.00 \pm 0.09)\cdot10^{-2}$	5.5 ± 0.1	14.9 ± 0.6	31 ± 2
50	$(3.4 \pm 0.1)\cdot10^{-3}$	3.3 ± 0.1	14 ± 1	29 ± 1
60	$(1.06 \pm 0.06)\cdot10^{-3}$	1.29 ± 0.06	11.7 ± 0.6	29 ± 2
75	$(3.30 \pm 0.04)\cdot10^{-4}$	$(2.7 \pm 0.1)\cdot10^{-1}$	8.9 ± 0.4	25 ± 2

C.5 Model: Direct and alternating currents impressed to MMO anode while varying the area and placement of steel and copper

Table C.9: Model: Potential of carbon steel as a function of the area ratio r_A ($A_{\text{steel}}/A_{\text{copper}}$), for various ACs [mA] impressed to MMO. The impressed DC is equal to 0.8 mA. Dimensions (in x-direction) of the steel/copper areas are given in parenthesis. All values are stated as the mean value ± 2s [mV]. C_{dl} and f are held at 0.1 F/m^2 and 50 Hz, respectively.

$\mathbf{r_A}$ \ $\mathbf{AC_{rms}}$	**0**	**1**	**5**	**10**
0.1 (0.4x4 cm)	-1000 ± 40	-990 ± 40	-990 ± 70	-940 ± 20
0.2 (0.8x4 cm)	-1010 ± 40	-1000 ± 20	-980 ± 40	-970 ± 40
0.5 (2x4 cm)	-990 ± 70	-960 ± 50	-980 ± 10	-970 ± 40
1 (4x4 cm)	-980 ± 60	-960 ± 50	-970 ± 30	-980 ± 30
2 (4x2 cm)	-1050 ± 30	-1050 ± 60	-1040 ± 10	-1020 ± 60
5 (4x0.8 cm)	-1130 ± 80	-1100 ± 100	-1100 ± 20	-1060 ± 50
10 (4x0.4 cm)	-1150 ± 10	-1130 ± 60	-1150 ± 50	-1050 ± 20

$\mathbf{r_A}$ \ $\mathbf{AC_{rms}}$	**20**	**50**	**100**	**200**
0.1 (0.4x4 cm)	-790 ± 30	-780 ± 40	-780 ± 40	-762 ± 9
0.2 (0.8x4 cm)	-780 ± 40	-770 ± 60	-760 ± 60	-770 ± 20
0.5 (2x4 cm)	-810 ± 40	-770 ± 60	-780 ± 50	-770 ± 10
1 (4x4 cm)	-890 ± 70	-780 ± 60	-770 ± 40	-780 ± 10
2 (4x2 cm)	-880 ± 20	-770 ± 30	-780 ± 30	-770 ± 20
5 (4x0.8 cm)	-860 ± 30	-800 ± 50	-790 ± 20	-780 ± 40
10 (4x0.4 cm)	-860 ± 30	-790 ± 40	-800 ± 70	-800 ± 30

Table C.10: Model: The potential difference between copper and steel at various distances between the electrodes [cm], and with impressing various ACs [mA] to MMO. A DC is held at 0.8 mA. The values are stated as the mean value ± 2s [mV]. C_{dl} and f are held at 0.1 F/m^2 and 50 Hz, respectively.

$\mathbf{AC_{rms}}$ \ **Distance**	**0**	**4**	**8**
0	$(9.6 \pm 0.2)\cdot 10^{-1}$	2.1 ± 0.1	1.50 ± 0.05
1	$(9.7 \pm 0.1)\cdot 10^{-1}$	2.17 ± 0.09	1.50 ± 0.07
5	1.12 ± 0.03	2.39 ± 0.07	1.65 ± 0.07
10	1.04 ± 0.03	2.5 ± 0.1	1.71 ± 0.03
20	$(8.3 \pm 0.1)\cdot 10^{-1}$	1.85 ± 0.08	1.24 ± 0.03
50	4.94 ± 0.07	11.3 ± 0.4	8.2 ± 0.2
100	6.6 ± 0.3	1.8 ± 0.1	1.72 ± 0.09
200	-5.9 ± 0.2	-15.7 ± 0.7	-15 ± 1

C.6 Model: Direct and alternating currents impressed to MMO anode in absence of copper

Table C.11: Model: Potential of carbon steel at various combinations of AC_{rms} [mA] and DC [mA] impressed to MMO in absence of copper. The values are stated as the mean value ± 2s [mV]. C_{dl} and f are held at 0.1 F/m^2 and 50 Hz, respectively.

AC_{rms} \ DC	**0.4**	**0.6**	**0.8**	**1.0**	**1.2**
0	-1109 ± 5	-1170 ± 20	-1200 ± 10	-1230 ± 20	-1241 ± 7
1	-1100 ± 20	-1160 ± 20	-1180 ± 20	-1230 ± 30	-1240 ± 20
5	-1080 ± 30	-1110 ± 30	-1150 ± 30	-1180 ± 20	-1200 ± 30
10	-976 ± 5	-1030 ± 20	-1050 ± 50	-1060 ± 20	-1100 ± 20
20	-810 ± 30	-830 ± 30	-840 ± 30	-860 ± 30	-860 ± 40
50	-800 ± 40	-810 ± 20	-810 ± 10	-800 ± 20	-810 ± 20
100	-780 ± 20	-800 ± 20	-800 ± 10	-800 ± 20	-810 ± 30
200	-790 ± 10	-790 ± 20	-800 ± 10	-800 ± 10	-806 ± 4

Table C.12: Model: Uniform corrosion rate of carbon steel at various combinations of AC_{rms} [mA] and DC [mA] impressed to MMO. The values are stated as the mean value ± 2s [mm/year]. C_{dl} and f are held at 0.1 F/m^2 and 50 Hz, respectively.

AC_{rms} \ DC	**0.4**	**0.6**	**0.8**
0	$(4.4 \pm 0.1)\cdot10^{-6}$	$(1.95 \pm 0.07)\cdot10^{-6}$	$(1.12 \pm 0.05)\cdot10^{-6}$
1	$(4.7 \pm 0.1)\cdot10^{-6}$	$(1.99 \pm 0.02)\cdot10^{-6}$	$(1.17 \pm 0.01)\cdot10^{-6}$
5	$(2.03 \pm 0.06)\cdot10^{-5}$	$(1.05 \pm 0.02)\cdot10^{-5}$	$(6.4 \pm 0.1)\cdot10^{-6}$
10	$(7.1 \pm 0.1)\cdot10^{-4}$	$(3.62 \pm 0.08)\cdot10^{-4}$	$(2.29 \pm 0.06)\cdot10^{-4}$
20	$(5.82 \pm 0.08)\cdot10^{-1}$	$(4.80 \pm 0.09)\cdot10^{-1}$	$(3.83 \pm 0.05)\cdot10^{-1}$
50	10.1 ± 0.5	10.1 ± 0.3	10.0 ± 0.1
100	25.1 ± 0.2	25.1 ± 0.3	25 ± 1
200	58 ± 2	56 ± 2	56 ± 2

AC_{rms} \ DC	**1.0**	**1.2**
0	$(7.5 \pm 0.2)\cdot10^{-7}$	$(5.36 \pm 0.07)\cdot10^{-7}$
1	$(7.7 \pm 0.2)\cdot10^{-7}$	$(5.7 \pm 0.2)\cdot10^{-7}$
5	$(4.2 \pm 0.1)\cdot10^{-6}$	$(3.00 \pm 0.08)\cdot10^{-6}$
10	$(1.57 \pm 0.03)\cdot10^{-4}$	$(1.14 \pm 0.04)\cdot10^{-4}$
20	$(3.33 \pm 0.06)\cdot10^{-1}$	$(2.7 \pm 0.1)\cdot10^{-1}$
50	9.8 ± 0.4	9.8 ± 0.3
100	25 ± 1	24.6 ± 0.9
200	57 ± 2	57 ± 1

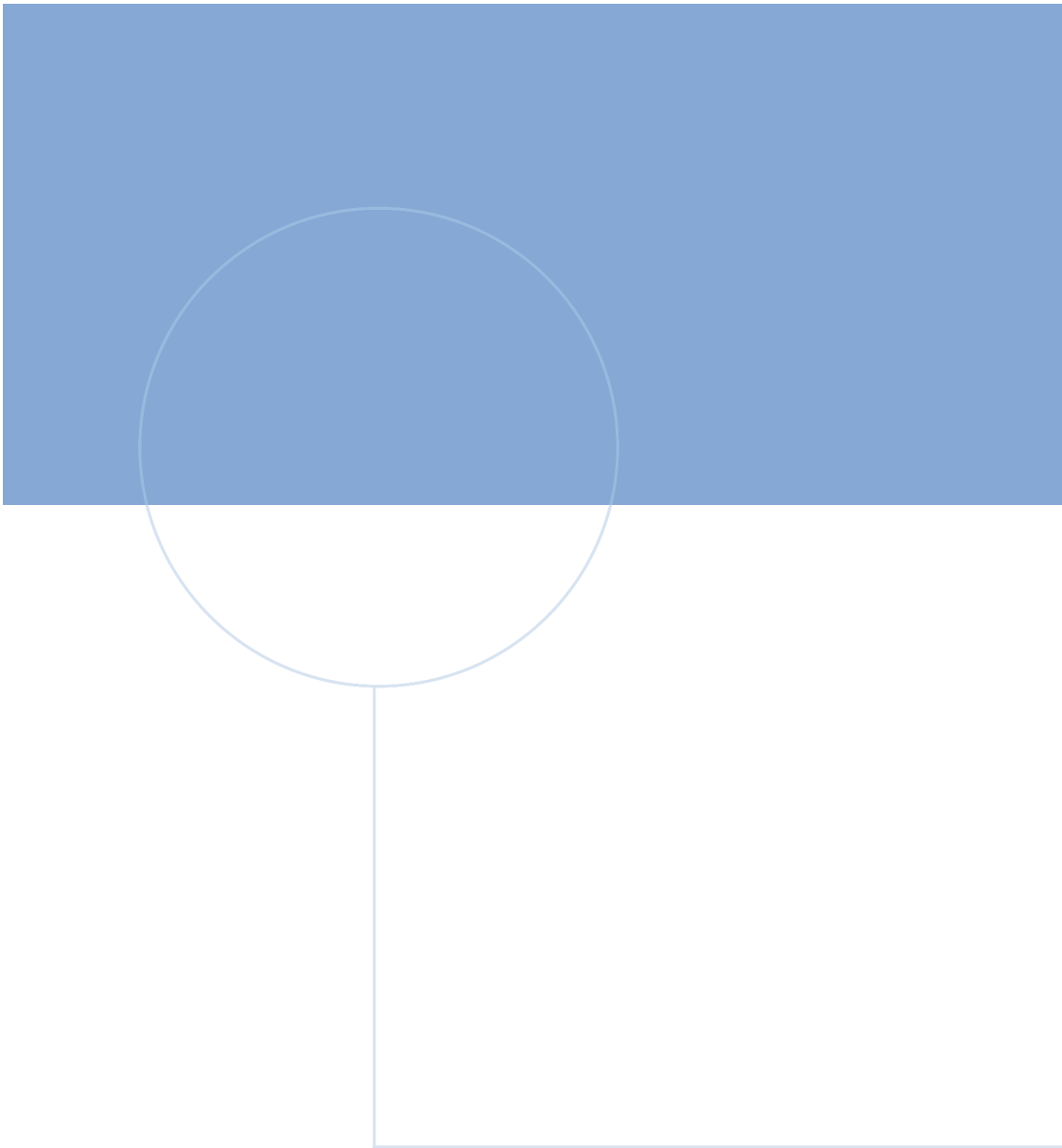

NTNU

Norwegian University of
Science and Technology